# *HYPERFINE INTERACTIONS IN AMORPHOUS AND CRYSTALLINE ALLOYS CONTAINING RARE EARTH METALS*

NADIM JONI SHAH

A thesis submitted to the Victoria University of Manchester
for the degree of Doctor of Philosophy
in the Faculty of Science

January 1987

*DECLARATION*

None of the work described in this thesis has been presented in support of any other degree at this university or elsewhere.

To my mother, father, and grandfather

*ACKNOWLEDGEMENTS*

I should like to express my gratitude to Jeff Ross for his supervision throughout my period of study. The sacrifice of his time at weekends in showing me how to operate the Mössbauer spectrometer during the "early days" and subsequent help with nmr experiments has been greatly appreciated. It is a pleasure to acknowledge many useful discussions with Iain Mackenzie, Peter Mitchell and Malcolm McCausland; in particular I should like to thank Iain and Peter for reading substantial parts of the typescript and offering constructive advice. (Sorry about the "flashy" control panel, Iain, it eluded us both!) I also wish to convey my thanks to Peter for my forthcoming introduction to neutron scattering, the "Grenoble boondoggle". On the matter of boondoggles, I can but thank Henry Hall for introducing the word into my vocabulary. Needless to say, such expert opinion is always welcomed!

It has indeed been a pleasure to be part of the Low Temperature Group and as such I wish to thank all the members for making my time an interesting and enjoyable one. More specifically, thanks are due to Des McMorrow for his "comradeship" and sincere friendship, extending back to our undergraduate days, and Carlo Carboni for his friendship during the last three years. To Gil West and Stan Gillott, "Eddie" would like to thank you for providing such excellent technical advice and innumerable litres of that volatile liquid.

During the course of this work a number of collaborations have been undertaken. I should like to take this opportunity to thank all my collaborators, especially Dr Yamamoto.

Last but by no means least, I wish to extend my gratitude to Claire Ryalls for assistance with matters grammatical, words wot I can't spell, proof-reading and for t$^{y}_{p}$ing the manuscript. I should like to thank my family for their support and encouragement over the years.

*ABSTR ACT*

The hyperfine interaction in amorphous rare earth and crystalline systems has been studied. $^{155}Gd$ Mössbauer spectroscopy and spin-echo nmr techniques, where the probe ion is Ho, Tb or Pr, have been used to investigate amorphous, ferromagnetic alloys of the form R:(Gd,Y,Cu) and R:(Gd,Ag). The amorphous series $Tb_xLa_5(Fe_{82}B_{18})_{95-x}$ and the crystalline compounds $R_2Fe_{14}B$, where R = Ho, Tb and Pr have been studied by nmr only. High frequency measurements were carried out in zero and applied fields of up to 8 T at 4.2 and 1.3 K, in the frequency range 3 to 7.5 GHz. All Mössbauer spectra were taken in zero and 6 T applied fields at 4.2 K, except one; a spectrum was taken for $Gd_{30}Ag_{70}$, above its Curie temperature, at 46 K.

The nmr results on R:(Gd,Y,Cu) and R:(Gd,Ag), together with a value of $|V_{zz}|$ obtained from the high temperature Mössbauer spectrum, have been shown to agree qualitatively with the HPZ model for random magnetic anisotropy.

Tb nmr results in $Tb_xLa_5(Fe_{82}B_{18})_{95-x}$ clearly indicate an antiferromagnetic coupling of the Tb and Fe moments. Measurements of the gyromagnetic shift due to applied fields and spin-spin relaxation suggest that the composition with x = 30 is not homogeneous and probably consists of several amorphous phases.

The generally agreed spin-canted structure of $Ho_2Fe_{14}B$ results in four magnetically inequivalent sites. The nmr results presented here lead to an identification of only two sites, one of which has a fully polarized moment and the other is slightly quenched. Nuclear quadrupole measurements are shown to be consistent with a spin-reorientation. The Ho and Fe sublattices are antiferromagnetically coupled. In $Pr_2Fe_{14}B$, two sites are expected; both were identified and shown to be fully polarized. No gyromagnetic shift of the resonant lines, in applied fields of up to 8 T, was observed in this material. Despite a variety of experimental conditions, a Tb resonance was not detected in $Tb_2Fe_{14}B$.

CONTENTS

# CHAPTER 1: Introduction

## 1.1 HISTORICAL BACKGROUND

Metals have been in common use for the past 8000 years; with the exclusion of developments in this century, their structure has consisted of crystalline aggregates. Historically, the first report in which amorphous metallic alloys were claimed to have been fabricated was by Kramer (1934, 1937), using a method based on vapour deposition. Somewhat later Brenner *et al* (1950) claimed to have made amorphous alloys by electrodeposition; they observed only one broad diffuse peak in the X-ray diffraction pattern. It should, nonetheless, be noted that the preparation of amorphous alloys may be much older. There is evidence to suggest that amorphous alloys were prepared by electrodeless depostion as early as the 18th century (for a discussion see Buschow 1984, for example).

A major breakthrough took place in 1959 when Duwez *et al* (1960) succeeded in preparing amorphous alloys directly from the melt by a technique subsequently referred to as splat-quenching, much to the inventor's displeasure. Cooling rates close to $10^6$ K/s were achieved by forcing atomized droplets of a liquid alloy to impinge very rapidly onto a cold, highly thermally-conducting substrate. The first alloy to be prepared in this way consisted of a Au-Si composition close to the eutectic point (Klement *et al* 1960).

For a number of years the investigation of amorphous alloys was confined to the $Au_{1-x}Si_x$ and $Pd_{1-x}Si_x$ systems. The situation changed, however, when it became possible to make liquid-quenched amorphous alloys based on 3d transition metals. The interest in these alloys was primarily due to their magnetic properties and possible applications.

Gubanov (1960) predicted that the occurrence of ferromagnetism should extend to amorphous alloys, despite the lack of long-range

periodicity. This theorectically-predicted retention of ferromagnetism was first confirmed experimentally by Mader and Norwick (1965) on vapour-quenched $Au_{1-x}Co_x$ alloys. It was also expected that magnetocrystalline anisotropies would be absent in ferromagnetic amorphous alloys (Simpson and Brambley, 1971) giving these materials rather low coercive forces. However, many amorphous alloys were subsequently made which did have considerable coercive forces; these large coercive forces were demonstrated to arise from compositional inhomogeneity and the substantial strain frozen in during the quench process (Chi and Cargill 1976). It was demonstrated (Luborsky *et al* 1975 and Egami *et al* 1975) that very low coercivities could be obtained by annealing, thereby rendering such alloys eminently suitable in systems requiring low magnetic losses. Interestingly enough, by controlled recrystallization a wide variety of metastable phases can be accessed which lead to large coercive fores and hard magnetic properties (see chapter 7).

## 1.2 TYPES OF DISORDER

A variety of amorphous magnetic materials exhibit spontaneous long-range ordering of localized moments below a critical temperature which is characteristic of each substance. The types of order in amorphous alloys are more numerous than those found in crystalline systems; the additional spin-ordering arrangements are a direct consequence of topological disorder. It is topological disorder that is at the heart of amorphous magnetism, ensuring that no two atomic sites are equivalent whereas all macroscopic directions may be equivalent. A short discussion of disorder and a number of new concepts that result is presented below.

Conceptually, it is possible to distinguish three types of disorder in a solid; the distinctions are illustrated in figure (1.1) for two-dimensional networks. By distorting a perfect monatomic crystal

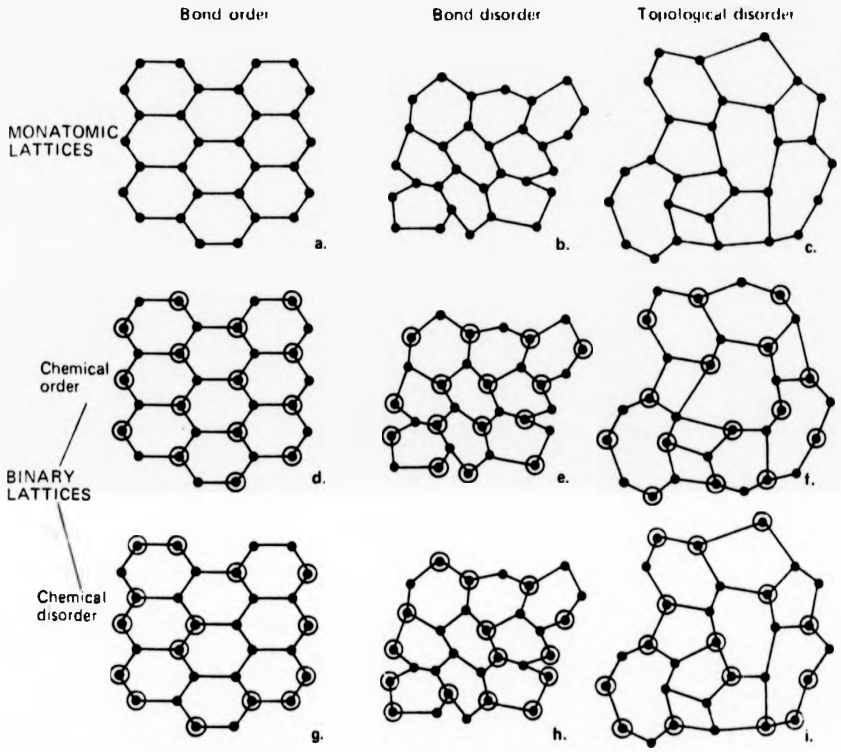


**Figure (1.1)** Types of disorder on two-dimensional monatomic and binary lattices.

(figure (1.1a), it is possible to introduce bonds of different lengths making different angles with each other, thereby destroying the periodicity of the structure (figure (1.1b). This is termed "bond disorder" and is the simplest variety since the bond-disordered network remains topologically equivalent to the crystal.

A more pronounced disruption of periodicity is that due to topological disorder (figure (1.1c)). The network includes rings with more and less members than six, the number in the starting structure, distributed at random among the six-membered ones. By necessity, topological disorder includes bond disorder but a topologically disordered network cannot be distorted back into a crystal. Some degree of topological disorder is probably essential in the formation of any glass.

The structure of a perfectly ordered binary AB alloy (figure (1.1d)) may be disordered while retaining its crystallinity (figure 1.1g); this constitutes chemical disorder. Metallic glasses are almost invariably multicomponent alloys of the type shown in figure (1.1h); they include bond, chemical and topological disorder.

### 1.2.1 EFFECTS OF DISORDER

In a binary alloy of the form $A_xB_{1-x}$, where the B atoms are non-magnetic, chemical disorder leads directly to the concept of percolation. At a certain critical concentration, $x_p$, there appear to be continuous infinite paths joining the magnetic atoms, many of which belong to the bulk cluster. The remainder of the magnetic atoms belong to small, isolated clusters. Symmetry-breaking, long-range magnetic order of any sort is only possible for $x > x_p$. It is clear that $x_p$ depends critically on the range of the interaction, but for nearest-neighbour coupling it is of the order $2/N$, where N is the effective coordination number for an amorphous composition of magnetic, A, atoms only.

By contrast to ferromagnetism, where disorder does not necessarily induce change in the phenomenon itself, antiferromagnetic interactions on a disordered lattice can produce results which differ dramatically from those in a crystal. In an amorphous solid there is a distribution of exchange interaction because of the dependence of the coupling constant on the separation of the moments. If the coupling between the spins is predominantly antiferromagnetic then different exchange paths favour different relative alignments of a pair. This effect is known as frustration (Toulouse 1977). Frustration is not restricted to topologically disordered systems but also arises when positive and negative exchange interactions are randomly distributed, even on a square lattice, for example (Toulouse 1977). Indeed, Simpson (1974) pointed out that it is impossible to make a consistent subdivision of a non-crystalline lattice into two sublattices. Antiferromagnetism cannot therefore be established over more than a few interatomic spacings because of the mismatch produced by topological disorder.

Site inequivalency in amorphous structures leads to a distribution in the magnitude of the atomic moments, even at the absolute zero of temperature. Moment distributions in rare-earth compounds and alloys, however, are narrow because the 4f shell is so well shielded from its environment. The delocalized nature of 3d moments, together with variations in type and number of nearest neighbours from site to site, ensures a broad moment distribution. The extent of the distribution can at times be large enough to contain transition-metal ions in both magnetic and non-magnetic states in the same material.

Topological disorder introduces large randomly varying electrostatic fields at the atomic sites. It has been shown (see chapter 3 and references therein for a fuller discussion) that second order "crystal field" terms, absent by symmetry in many crystalline structures, are dominant in amorphous structures. A local easy axis results at each

site and a simple model for treating these effects has been derived by Harris *et al* (1973); a detailed description is given in chapter 3.

## 1.3 THE HYPERFINE INTERACTION: A DIAGNOSTIC TOOL

The hyperfine interaction can be studied by a variety of techniques (see, for example, Freeman and Watson 1965) but when the microscopic probes are rare earths then certain unique advantages are conferred that make such studies a focus of interest. The R ions in the majority of rare-earth alloys are triply ionized and have a partly-filled 4f shell. The radius of the shell is much smaller than a typical interatomic separation and it is well-screened by the $5s^2$ and $5_p^6$ shells. For R ions in a solid, the electronic structure of the shell is therefore practically the same as for the free ion. In particular, the orbital contribution to the total magnetic moment retains most of its free-ion value. It is of importance to note that for rare-earth elements the spin-orbit interaction dominates the crystal-field and exchange interactions. As a consequence, J, the total angular momentum quantum number, is a constant of the motion; it is this feature that greatly simplifies the description of rare-earth magnetism.

In the present work, the hyperfine interaction has been studied by nmr and Mössbauer spectroscopies. It is therefore appropriate to draw attention to the information that can be obtained directly and indirectly by these methods. The parameters that can be measured (hyperfine fields, electric field gradients (e.f.g), isomer shifts and resonance linewidths) are extremely sensitive to local variations around the probe ions. Local structural information in an amorphous sample can be inferred by comparison of measured e.f.g.s with those found in its crystalline counterpart (Panissod *et al* 1980). Measurements of the e.f.g. probably represent the best source of local structural information. The sign of the principal component, $V_{zz}$, depends on the

character of the surrounding charge distribution and departures from spherical symmetry are manifest in the asymmetry parameter, $\eta$. In this respect, Mössbauer experiments in the paramagnetic region are limited since the quadrupolar splitting depends on the magnitude and not the direction of the e.f.g. (see chapter 4 for a more detailed account).

The hyperfine field reflects the magnitude of atomic moments. In principle the associated distributions can be obtained directly from spin-echo nmr. In practice, however, sensitivity of the spectrum to excitation conditions and the frequency response of the detection system are prohibitive. Nevertheless, limits can be placed on the extent of the distribution with impunity. Hyperfine field distributions derived from Mössbauer studies are plagued by difficulties arising from the adoption of complicated fitting procedures and the assumptions made therein; most fitting procedures treat the quadrupole interaction as a perturbation of the magnetic interaction. This assumption is not applicable to $^{155}$Gd Mössbauer and therefore data analysis to obtain field distibution has not been attempted throughout the course of the present work. The advantages of using $^{155}$Gd as a probe centre around the fact that it is an S-state ion resulting in negligible quenching effects and a quadrupole splitting that gives a direct measure of the extra-ionic e.f.g.

It should be stressed that nmr and Mössbauer techniques probe the local environment and can thus access information directly; this information can only be inferred from bulk measurements such as magnetization.

## 1.4 SCOPE OF THE WORK

The main body of this thesis is concerned with the hyperfine interaction of four rare-earth ions, namely Pr, Gd, Tb, and Ho in amorphous materials. The techniques alluded to in the preceeding section have been used to facilitate this study. In common with the

study of any material, a sample must exist and be available in the required phase; the problem is most acute when dealing with amorphous compositions. Relative ease of preparation and availability are therefore crucial factors which need to be taken into account. In this respect, a "simple" amorphous magnetic system, $Gd_xY_{63-x}Cu_{37}$, containing only one magnetic ion, was chosen for investigation. The system lends itself to doping with other rare-earths and thereby facilitates an nmr study of the rare-earth probe nuclei.

The consequences of two magnetic species in an amorphous structure pose a further challenge. The series $Tb_xLa_5(Fe_{82}B_8)$ was chosen primarily because it displays a compensation composition where the magnetization of the Tb and Fe subnetworks is equal and opposite, resulting in zero bulk magnetization, as well as two magnetic ions.

The polycrystalline materials $R_2Fe_{14}B$ were discovered partly because of investigations into the magnetic properties of amorphous $Tb_5La_5(Fe_{82}B_{18})_{90}$ (see chapters 6 and 7). A study of the hyperfine interaction in these relatively new materials is of fundamental interest because of the rich and varied magnetic properties that arise from the competition between exchange and crystal-field interactions.

# CHAPTER 2: The Hyperfine Interaction

## 2.1 INTRODUCTION

It is not the intention here to present a general review of the hyperfine interaction of rare-earth ions but merely to draw attention to some rather specific features thereof (for a detailed account see McCausland and Mackenzie 1979, for example). In particular, the influence of the hyperfine interaction on the nmr spectrum is illustrated.

The majority of rare-earth ions in a solid are triply ionized and have a partly filled 4f shell, the radius of which is approximately an order of magnitude smaller than a typical intra-ionic separation. A consequence of the small 4f shell radius is that its electronic structure is essentially the same in metals as in the isolated ion. The angular momenta of the 4f electrons couple according to the Russell-Saunders scheme where the spins first combine to give the largest possible spin quantum number S compatible with the Pauli exclusion principle, and then the orbital angular momenta combine to maximize L, the total orbital angular momentum number. The total orbital and spin angular momenta are then coupled by an effective spin orbit interaction of the form

$$H_{so} = \lambda \underline{L} \cdot \underline{S} \qquad (2.1)$$

to form the resultant electronic angular momentum operator $\underline{J}$. The spin orbit splitting, $\Delta_{so}$, is of the order of 1000 K for Ho, Tb and Pr and therefore the thermal population of excited J multiplets can safely be neglected at liquid helium temperatures, the temperatures at which all the experiments have been conducted. For rare-earth ions in a solid, $H_{so}$ is usually the dominant interaction and thus J is a "good" quantum

number as, of course, it is for the free ion.

Apart from the spin-orbit interaction, a magnetic, non-S-state R ion in a solid experiences a number of other important interactions: (a) the exchange interaction which arises out of the overlap of electronic wave functions (see Smart 1966, for example) and tends to align the spins parallel or antiparallel, (b) the crystal field interaction, $H_{cf}$, which is a result of the interaction of the aspherical charge distribution of the rare-earth ion with the electrostatic potential created by neighbouring charges, and (c) the hyperfine interaction, $H_{hf}$, which arises from the interaction of the rare-earth nucleus with its environment. Each of these interactions is discussed below but it should be noted that in general the following inequality holds:

$$H_{so} \gg H_{el} \gg H_{hf} \qquad (2.2)$$

where $$H_{el} = H_{ex} + H_{cf} \qquad (2.3)$$

The first of the inequalities (2.2) ensures that J remains a "good" quantum number for a rare-earth ion in a solid which leads to a considerable simplification of the theory. A consequence of the second inequality is that $H_{hf}$ may be treated as a perturbation on $H_{el}$.

## 2.2 HYPERFINE INTERACTION OF AN ISOLATED ION.

To an adequate degree of accuracy, the hyperfine interaction of an isolated ion may be represented as

$$H_{hf} = H_{hfd} + H_{hfq} \qquad (2.4)$$

The interaction of the nuclear magnetic dipole, $\mu_n$, with the effective

magnetic field $\underline{B}_{hf}$, due to the surrounding electron cloud is represented by $H_{hfd}$. $H_{hfq}$ represents the interaction of the nuclear electric quadrupole tensor with the electric field gradient (e.f.g.) arising from the aspherical charge distribution of the electron cloud.

$H_{hfd}$ is generally at least an order of magnitude greater than $H_{hfq}$, and can be written as

$$H_{hfd} = hA\underline{J}.\underline{I} = -\underline{B}_{hf}.\underline{\mu}_n \qquad (2.5)$$

where A, the magnetic hyperfine coupling constant, has been deduced from electron paramagnetic resonance by Bleaney (1972) and is customarily expressed in the form

$$a_0' = AJ \qquad (2.6)$$

The expression for $H_{hfq}$ is more involved than that for $H_{hfd}$ but, nevertheless, can be expressed in terms of $\underline{J}$ and $\underline{I}$. Following McCausland and Mackenzie (1979), $H_{hfq}$ can be written as

$$H_{hfq} = B\left[\frac{3(\underline{J}.\underline{I})^2 + 3/2(\underline{J}.\underline{I}) - J(J+1)I(I+1)}{2J(2J-1)I(2I-1)}\right] \qquad (2.7)$$

where $B$ absorbs the strength of the electronic e.f.g and the nuclear quadrupole moment $Q_n$ (Bleaney 1972)

Equation (2.7) may be rewritten, by use of angular momentum commutation rules, as

$$H_{hfq} = \frac{hP_o'}{J(2J-1)}\left[(3J_z^2-\underline{J}^2)(I_z^2-\underline{I}^2/3)+(J_x^2-J_y^2)(I_x^2-I_y^2)\right.$$
$$+(J_xJ_y+J_yJ_x)(I_xI_y+I_yI_x)+(J_yJ_z+J_zJ_y)(I_yI_z+I_zI_y)$$
$$\left.+(J_zJ_x+J_xJ_z)(I_zI_x+I_xI_z)\right] \qquad (2.8)$$

where $P_0'$ is a measure of the coupling and is given by

$$P_0' = \frac{3B}{4I(2I-1)h} \qquad (2.9)$$

Once again the parameter $P_0'$ has been deduced by Bleaney (1972) from experiment. The free ion parameters, along with others of interest, are listed in table (2.1) for the three rare-earth ions, namely Ho, Tb and Pr, which have been used as probe nuclei for the experiments described here.

| Isotope | I | $g_n$ | $\frac{Q_n}{I(2I-1)}$ ($m^2$) | $a_0'$ (MHz) | $P_0'$ (MHz) |
|---|---|---|---|---|---|
| $^{141}$Pr | 5/2 | 1.70 | -0.59 | 4372 (40) | -2.62 (0.13) |
| $^{159}$Tb | 3/2 | 1.329 | +45 | 3180 (30) | +386 (20) |
| $^{165}$Ho | 7/2 | 1.151 | +11.4 | 6497 (8) | +63 (3) |

TABLE 2.1 Nuclear data and intra-ionic hyperfine parameters for Pr, Tb and Ho. Units of $Q_n$: $m^2 \times 10^{-30}$.

The total free ion hyperfine interaction is a function of the operators $\underline{J}$ and $\underline{I}$ and may be written as:

$$H_{hf}(\underline{J},\underline{I}) = \sum_r E_r(\underline{J}) N_r(\underline{I}) \qquad (2.10)$$

where $E_r(\underline{J})$ are the elecronic operators and $N_r(\underline{I})$ the nuclear operators. By considering $H_{hf}$ as a perturbation on $H_{el}$, to first order, the hyperfine splitting is determined by an effective nuclear Hamiltonian of the form

$$H_{hf}(\underline{J},\underline{I}) = \sum_r \langle E_r(\underline{J}) \rangle N_r(\underline{I}) \qquad (2.11)$$

where $$\langle E_r \rangle = \langle E_0 | E_r(\underline{J}) | E_0 \rangle \qquad (2.12)$$

if the only significantly populated state is the ground state.

2.2.1 THE EXCHANGE INTERACTION

The exchange interaction is electrostatic in origin and arises as a direct consequence of the Pauli exclusion principle. The simple model developed here is sufficient for the interpretation of nmr data. For a detailed review of the theory the reader is referred to Freeman (1972).

In consideration of an assembly of lanthanide ions, the direct exchange interaction may be neglected given that the small radius of the 4f shell will ensure that there is no appreciable overlap of the 4f wave functions. Nevertheless, there is a significant exchange coupling between the localized 4f spins, $\underline{S}$, and the conduction electrons $\underline{s}$, which is referred to as the s-f interaction (Freeman 1972). It has already been noted that J is a good quantum number and therefore it is appropriate to project $\underline{S}$ onto $\underline{J}$ and write the interaction in terms of a projected spin $\underline{\sigma}$. The s-f interaction can thus be expressed as

$$H_{sf} = -J_{sf}(\underline{r})\underline{\sigma}.\underline{s} \qquad (2.13)$$

where $\underline{r}$ is measured from the centre of the R ion and the function $J_{sf}$ depends on conduction electron states in a rather complicated way.

The s-f interaction results in a spatially varying conduction electron polarization in the neighbourhood of the R ion which in turn interacts with the projected spin $\underline{\sigma}_j$ on a neighbouring ion $R_j$. The conduction electrons therefore mediate an indirect exchange coupling between R and its neighbours of the form

$$H^j_{ex} = -J(r_j)\underline{\sigma}_j.\underline{\sigma} \qquad (2.14)$$

The detailed form of the function $J(\underline{r})$ is a difficult problem, the simplest model of which is the so called Rudermann-Kittel-Kasuya-Yosida (RKKY) interaction (Rudermann and Kittel 1954, Kasuya 1956 and Yosida 1957). Despite its limitations (see McCausland and Mackenzie 1979, for example) the model indicates, in a qualitative way, the long-range oscillatory character of the conduction electron polarization and hence the inter-ionic exchange interaction.

Without prejudice to the form of $J(\underline{r})$, the total exchange interaction between R and its neighbours $R_j$ can be written as

$$H_{ex} = -\sum_j J(\underline{r}_j)\underline{s}_j \cdot \underline{S} \qquad (2.15)$$

2.2.2 THE CRYSTAL FIELD INTERACTION

As mentioned earlier, the crystal field interaction is an electrostatic coupling of the aspherical charge distribution of an R ion with the inhomogeneous electric field (the crystal field) which exists in a solid. On the basis of the point-charge model, determination of $H_{cf}$ is the evaluation of the electrostatic potential $V(r,\Theta,\Phi)$ at a point $(r,\Theta,\Phi)$ which is given by

$$V(r,\Theta,\varphi) = \sum_j \frac{q_j}{|(\underline{R}_j - \underline{r})|} \qquad (2.16)$$

where, following the notation of Hutchings (1964), $q_j$ is the charge of the jth neighbouring ion, a distance $R_j$ from the origin.

Suppose now that a magnetic ion of interest has charge $q_i$ at $(r_i,\Theta_i,\Phi_i)$, then the crystalline potential energy is

$$W_c = \Sigma\, q_i V_i = \sum_i \sum_j \frac{q_i q_j}{|\underline{R}_j - \underline{r}_i|} \qquad (2.17)$$

The crystal potential, equation (2.16), can be calculated directly in terms of tesseral harmonics (tesseral harmonics are real functions which are linear combinations of spherical harmonics); the method is based on the spherical harmonic addition theorem and gives the following expression for V:

$$V(r,\theta,\phi) = q_j \sum_{n=0}^{\infty} \frac{r^n}{R_j^{n+1}} \left[ \sum_{\alpha} \frac{4\pi}{2n+1} Z_{n\alpha}(\theta_j,\phi_j) Z_{n\alpha}(\theta,\phi) \right] \qquad (2.18)$$

For k charges,

$$V(r,\theta,\phi) = \sum_{n=0}^{\infty} \sum_{\alpha} r^n \gamma_{n\alpha} Z_{n\alpha}(\theta,\phi) \qquad (2.19)$$

where

$$\gamma_{n\alpha} = \sum_{j=1}^{k} \frac{4\pi}{(2n+1)} q_j \frac{Z_{n\alpha}(\theta_j,\phi_j)}{R_j^{n+1}} \qquad (2.20)$$

Hutchings (1964) has shown that most of the coefficients $\gamma_{n\alpha}$ in the expansion of the potential are zero for commonly occurring site symmetries. For example, if the site has four-fold cubic symmetry then the only non-vanishing coefficients are $\gamma_{40}$, $\gamma_{44}$, $\gamma_{60}$ and $\gamma_{64}$. In general the potential function must reflect the point symmetry of the lattice site. The less symmetric the site, the more terms occur in the expansion of the potential. It should be noted that not all non-zero terms in the expansion of the potential will affect the energy level of the magnetic ion; their matrix elements may yet be zero. Hutchings (1964) has listed the rules governing the occurrence of non-zero terms in the expansion of the potential and also the rules which limit the

number of non-zero matrix elements; of these rules, two are most prominent. Firstly, if there is an inversion centre at the site of interest then there will be no odd-n terms and secondly, all terms of n > 21, where l is the orbital quantum number of the single magnetic electrons, vanish.

Taking account of the above rules, the matrix elements are most readily evaluated using the operator-equivalent method (Stevens 1952) which is, in essence, an application of the Wigner-Eckart theorem (see Edmonds 1957, for example). By expressing the tesseral functions in Cartesian coordinates, and in the notation of Stevens (1952), Hutchings (1964) has demonstrated that $H_{cf}$ can be written as

$$H_{cf} = \sum_{nm} \left[A_n^m \theta_n \langle r^n \rangle\right] O_n^m \qquad (2.21)$$

where the quantities $A_n^m\langle r^n\rangle$ are known as the crystal field parameters and $\theta_n$ the Stevens' coefficients. Equation (2.21) can thus be expressed as

$$H_{cf} = \sum_{nm} B_n^m O_n^m \qquad (2.22)$$

where $$B_n^m = \theta_n A_n^m \langle r^n \rangle \qquad (2.23)$$

## 2.3 THE HYPERFINE INTERACTION

The hyperfine interaction of an isolated lanthanide ion has already been discussed in section (2.2.1). The interaction is dramatically altered when the ion is embedded in a solid:

the form of the Hamiltonian, which can be divided into an intra-ionic, $H'$, and an extra-ionic, $H''$, contribution is detailed below. Thus, the hyperfine interaction can be written as

$$H = H' + H'' \tag{2.24}$$

### 2.3.1 THE INTRA-IONIC HYPERFINE INTERACTION

The intra-ionic contribution to the hyperfine interaction can itself be divided into two components; magnetic dipolar and electric quadrupolar parts, $H'_d$ and $H'_q$, respectively. Thus

$$H' = H'_d + H'_q \tag{2.25}$$

and following McCausland and Mackenzie, the effective intra-ionic dipolar h.f.i. in a solid is

$$H'_d = h\underline{a}'.\underline{I} = -\underline{B}'.\underline{\mu}_n \tag{2.26}$$

where $$\underline{a}' = A\langle\underline{J}\rangle \tag{2.27}$$

and $$\underline{B}' = \left[\frac{-h}{g_n\beta_n}\right]\underline{a}' \tag{2.28}$$

If the z-axis is parallel to $\langle\underline{J}\rangle$ then

$$H'_d = ha'I_z \tag{2.29}$$

where $$a' = A\langle J_z\rangle = a'_0\frac{\langle J_z\rangle}{J} \tag{2.30}$$

The intra-ionic quadrupolar term can be written down in a straight-forward manner using equations (2.8) and (2.11), i.e.

$$H'_q = h\Big[P'\Big[I_z^2 - \frac{I(I+1)}{3}\Big] + P'_1[I_x^2 - I_y^2] + P'_2[I_xI_y + I_yI_x] + P'_3[I_yI_z + I_zI_y] + P'_4[I_zI_x + I_xI_z]\Big] \qquad (2.31)$$

where $$P' = \frac{\langle 3J_z^2 - J(J+1)\rangle}{J(2J-1)} P'_0 \qquad (2.32)$$

(For a definition of $P'_1$ etc the reader is referred to McCausland and Mackenzie 1979; only $P'$ is used in the analysis of data presented in this thesis.)

It should be noted that by comparing the leading term of equation (2.31) with the electronic quadrupolar interaction, the following expression is obtained for $P'$:

$$hP' = \frac{3eQ_nV'_{zz}}{4I(2I-1)} \qquad (2.33)$$

where $V'_{zz}$ is the z component of the intra-ionic e.f.g. at the nuclear site.

### 2.3.2 THE EXTRA-IONIC HYPERFINE INTERACTION

The extra-ionic part of the magnetic hyperfine interaction may be written as

$$H''_d = h\mathbf{a}''.\mathbf{I} = \mathbf{B}''.\boldsymbol{\mu}_n \qquad (2.34)$$

There are four contributions to the extra-ionic hyperfine field $B''$, namely

$$\underline{B}'' = \underline{B}_a + \underline{B}''_{dip} + \underline{B}''_{ce} + \underline{B}''_{orb} \qquad (2.35)$$

$B_a$ is the applied field, $\underline{B}''_{dip}$ is the classical extra-ionic dipolar field, $\underline{B}''_{ce}$ represents the Fermi contact interaction arising directly or indirectly from polarized conduction electrons and $\underline{B}''_{orb}$ is the field due to the orbital motion of conduction electrons in the immediate vicinity of the parent ion. With due regard to the error limits on the data being presented in later chapters, only $\underline{B}''_{ce}$ is of concern and takes the form

$$\underline{B}''_{ce} = K_o \underline{B}_a + \underline{B}''_p + \underline{B}''_n \qquad (2.36)$$

where $$\underline{B}''_p = K_p \langle \underline{\sigma}_p \rangle \qquad (2.37)$$

and $$\underline{B}''_n = \sum_j f(\underline{r}_j) \langle \underline{\sigma}_j \rangle \qquad (2.38)$$

$K_o$ and $K_p$ are constants, $f(\underline{r})$ is a function characteristic of the metal, $\underline{\sigma}_p$ and $\underline{\sigma}_j$ are the projected spins on the parent ion and its neighbours. $B''_n$ is usually referred to as the transferred hyperfine field (t.h.f).

The extra-ionic quadrupolar interaction takes the same form as equation (2.31), the intra-ionic quadrupolar interaction. If the hyperfine interaction is dominated by $H'_d$ , then $H''_q$ approximates to (see McCausland and Mackenzie 1979)

$$(H''_q)_{diag} = hP''(I_z^2 - (1/3)(I+1)I) \qquad (2.39)$$

where $$hP'' = \frac{3eQ_n V''_{zz}}{4I(2I-1)} \qquad (2.40)$$

## 2.4 THE NMR SPECTRUM

The total hyperfine interaction can be written, taking the magnetic dipole contribution first, as

$$H_d = H_d' + H_d'' = h\underline{a}_t \cdot \underline{I} = -\underline{B}_t \cdot \underline{\mu}_n \tag{2.41}$$

where $$\underline{a}_t = \underline{a}' + \underline{a}'' \tag{2.42}$$

and $$\underline{B}_t = \underline{B}' + \underline{B}'' = \frac{-h}{g_n \beta_n} \underline{a}_t \tag{2.43}$$

Similarly, the total quadrupole interaction

$$H_q = H_q' + H_q'' \tag{2.44}$$

can be expressed in the same form as (2.31) but with the total coupling parameter given by

$$P_t = P' + P'' \tag{2.45}$$

The complete nuclear spin Hamiltonian is then $H = H_d + H_q$, i.e

$$\begin{aligned} H = h\Big[ & a_t I_z + P_t\left[ I_z^2 - \frac{I(I+1)}{3} \right] + P_{1t}\left[ I_x^2 + I_y^2 \right] \\ & + P_{2t}\left[ I_x I_y + I_y I_x \right] + P_{3t}\left[ I_y I_z + I_z I_y \right] \\ & + P_{4t}\left[ I_z I_x + I_x I_z \right] \Big] \end{aligned} \tag{2.46}$$

The dominant feature of the hyperfine interaction in highly polarized non-S-state ions is a very large intra-ionic field $\underline{B}'$ which arises from the orbital motion of the 4f electrons. The resultant $a_t$

($a''$ is usually relatively small) is at least an order of magnitude greater than $P_t$. To a first approximation, the off-diagonal terms of equation (2.46) can be neglected (for detailed discussion see McCausland and Mackenzie 1979) and the energy levels, $E_m$, are

$$E_m = h\{a_t m + P_t[m^2 - (1/3)(I+1)I]\} \qquad (2.47)$$

where m is the eigenvalue of $I_z$. The resultant nmr frequencies are therefore

$$\nu_{m,m-1} = |a_t + (2m-1)P_t| \qquad (2.48)$$

An nmr spectrum therefore consists of 2I lines centred about $|a_t|$, with a line separation of $|2P_t|$.

## 2.5 AMORPHOUS MATERIALS AND NMR SPECTRA

A multiplicity of environments in the amorphous state will in general lead to a distribution of hyperfine parameters (see chapter 3 for a detailed discussion). Clearly, the extra-ionic contributions ($a''$ and $P''$) are environment-dependent but the intra-ionic parts also reflect the surroundings. The lack of symmetry, for example, means that second-order terms appearing in the electric field expansion are dominant. These terms may bring about a situation where $H_{cf}$ is comparable to $H_{ex}$ and thus lead to quenching of $\langle J \rangle$. (The magnitude of $\langle J \rangle$ is only affected by $H_{cf}$ in second and higher order.) If $\langle J \rangle$ is quenched then it is evident that intra-ionic parameters will be affected.

Associated with a multiplicity of environments is a multiplicity of hyperfine parameters. In amorphous materials there is a quasi continuum of different environments resulting in "smeared out" spectral lines and

therefore a loss of information. Of particular interest is the smearing caused by a distribution of $V_{zz}$ with which a distribution of $P_t$ is associated. Equation (2.48) shows that the quadrupole splittings, from the centre, are $2P_t$, $4P_t$, and $6P_t$. The distribution in $P_t$ ensures that the outer lines are smeared more than the inner lines; the central line being unaffected by $P_t$. This mechanism causes a smearing of the wings of the spectrum but leaves the structure in the centre unaffected, and is invoked in the interpretation of nmr spectra in amorphous materials (chapters 5 and 6).

# CHAPTER 3: Models of Amorphous Magnetism

## 3.1 INTRODUCTION

Periodicity in the arrangement of atoms in a solid is not a necessary condition for the occurrence of magnetism. However, before the current interest in amorphous materials, most theories of magnetic phenomena have assumed the applicability of Bloch's theorem, either implicitly or explicitly. For a material to be ferromagnetic, only two conditions need to be satisfied; namely that a magnetic moment (and therefore uncompensated spin) exists on the atom and that when the atoms are assembled in a solid, they interact via exchange forces. The distinction between moments and exchange interactions is valid for the vast majority of metallic and insulating magnetic materials. It does not, however, apply to a few types of materials, weak itinerant ferromagnets, for example. The possibility of ferromagnetism in the amorphous state was first indicated by Gubanov (1960) but went largely unnoticed for a decade or so until possible technological applications of certain amorphous ferromagnets renewed interest in the subject.

In the interpretation of the magnetic properties of solids, effective field theories are usually the first resort. An approximate description of the general aspects of the phenomena being studied can be constructed by the application of such theories. Effective field theories act as guideposts indicating the description of more elaborate theoretical constructions and of more detailed experiments.

In this chapter, some relevant models of magnetism in amorphous systems, together with the various concepts entailed therein, are discussed. Particular emphasis is placed upon the mean-field model as a starting point for the interpretation of the magnetic properties of amorphous systems containing rare-earth elements.

## 3.2 EXCHANGE INTERACTIONS

The exchange interactions between two electronic spins usually tend to align them parallel or antiparallel. This can be represented phenomenologically by the isotropic Heisenberg interaction for a pair of localized moments $g\mu_B\underline{J}$ (see, for example, Smart 1966) as

$$H_{ij} = - J_{ij}\, \underline{S}_i \cdot \underline{S}_j \qquad (3.1)$$

where $J_{ij}$ is the exchange constant between spin $\underline{S}_i$ and $\underline{S}_j$ at sites i and j respectively. Despite the fact that most alloys are metallic, a description involving localized spins (equation 3.1) is a valid starting point since amorphous ferromagnets display large residual resistivities, indicating a strong localization tendency for electrons in amorphous materials. In fact, residual resistivities are larger than in corresponding crystalline alloys. The exchange constant is positive for ferromagnetic coupling and negative for antiferromagnetic coupling. Other interactions exist which favour a perpendicular configuration (I Dzyloshinkii 1958, T Moriya 1960); these can be represented by the antisymmetric Dzyloshinskii-Moriya (DM) term

$$H_{dm} = D_{ij}\, \underline{S}_i \times \underline{S}_j \qquad (3.2)$$

It should be noted, however, that the DM interaction is usually much weaker than the Heisenberg interaction.

Exchange coupling originates in the electrostatic interaction between electrons of different spins on different sites either directly, or via some intermediate electrons (see, for example, Mattis 1965). Exchange coupling mechanisms all tend to depend sensitively on the distance separating the electrons in question. A conseqence of this

distance dependence is that a distribution of interatomic separations, $r_{ij}$, can result in both ferromagnetic and antiferromagnetic coupling. A clear illustration of this is provided by the RKKY interaction which oscillates in sign as a function of r (figure 3.1) and is considered below in detail.

The RKKY interaction is the principal source of exchange coupling between 4f shells; it is also important in dilute 3d alloys where direct exchange cannot operate. The interaction of a localized spin with the polarization of the conduction band induced by other localized spins constitutes the RKKY interaction. As a first approximation, a free-electron model for the conduction electrons is assumed and calculations give

$$J(r) \propto -\frac{18Z^2 J_{sf}}{E_F}\left[\frac{\xi\cos\xi - \sin\xi}{\xi^4}\right] \qquad (3.3)$$

where $\xi = 2k_F r$, Z is the charge of the ion core, $J_{sf}$ is the interaction between the localized spins and the conduction electrons, $E_F$ and $k_F$ are the Fermi energy and the wave vector respectively. In an ideal crystalline material r is discrete-valued, and therefore so is J(r). In the amorphous state, however, static fluctuations in r will result in a distribution of J(r). The probability of finding an exchange interaction of a given sign and magnitude may be represented by P(J) (figure 3.2). In a perfect crystal J(r) will have one or more discrete values which can be represented by delta functions. Disorder in a solid will broaden the peaks even to the extent that interactions of both signs may be included in the distribution.

The standard expression for the RKKY interaction is derived on the assumption that translational invariance exists and therefore a plane-wave expansion is justified. There is a lack of long range order in amorphous materials which requires a modification of equation (3.3). In general, increasing the disorder of a system leads to the broadening

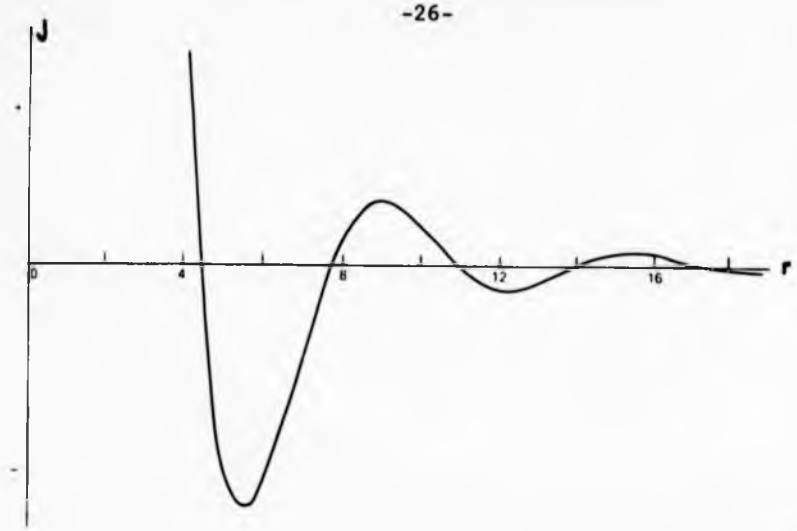


Figure (3.1) Schematic representation of the RKKY interaction.

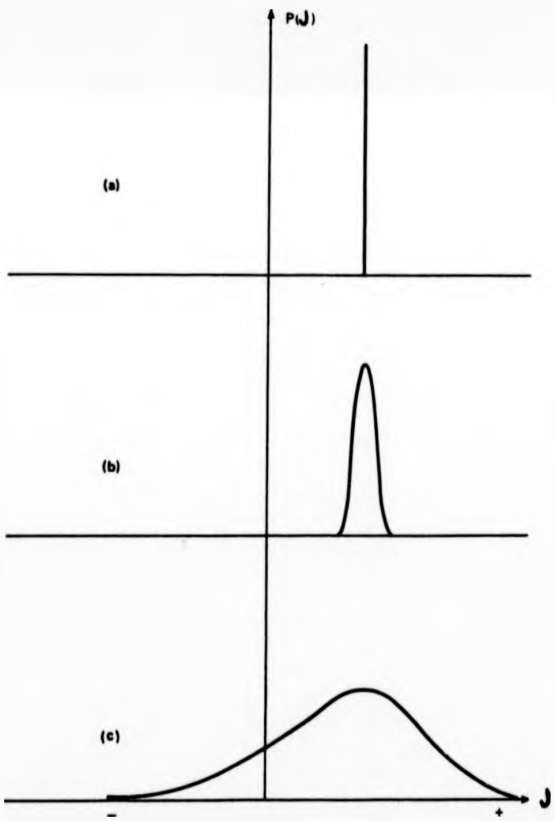


Figure (3.2) Probability of finding a given value of exchange (a) in a crystal and (b) and (c) in amorphous solids with different amounts of disorder.

of energy bands and changes the electronic wave functions. For a system with a finite mean free path, $\lambda$, it has been conjectured (de Gennes 1962) that equation (3.3) should be replaced by

$$J_{eff}(r) \propto F_{rk} \exp-(r_{ij}/\lambda) \qquad (3.4)$$

where $F_{rk}$ is the oscillatory RKKY function. Evidence for the attenuation factor $e^{-r/\lambda}$ has been found in crystalline (Au,Ag,Mn) spin glasses (Smith 1978), but no weakening of the interaction seems to occur for dilute amorphous $Gd_xLa_{80-x}Au_{20}$ alloys where the mean free path, deduced from conductivity measurements, is 1 to 2Å (Poon & Durand, 1977).

3.2.1 RANDOM ANISOTROPY

Magnetic properties are sensitive to atomic structure and are significantly influenced by single-ion anisotropy. An electrostatic field created by surrounding charges exerts an influence on a given ion or atom in a solid. Conduction electrons may also contribute to this field. A consequence of this field is a lifting of the degeneracy of the electronic states of ions with partly filled d or f shells. A local random magnetic anisotropy (RMA) arises from the Coulomb interaction of the non-spherical charge distribution with the electrostatic potential. The magnetic moment of the atom therefore prefers certain local "easy directions". The environment is topologically disordered in an amorphous structure and this disorder is reflected in the electrostatic potential. Classically, the single-ion anisotropy may be represented by a surface. This surface in a crystal reflects the symmetry of the point group of the atomic site. Generally in an amorphous solid, it only has an inversion centre; reversing the sign of an atomic moment does not change its energy. Since the point symmetry varies from site to site then so does the direction of the

moment with minimum energy, leading to random anisotropy. The consequences of RMA for amorphous magnetism are discussed in terms of various models in the following sections.

## 3.3 MAGNETIC STRUCTURES IN AMORPHOUS SYSTEMS

Disorder in amorphous magnetic systems leads to a variety of collinear and non-collinear magnetic structures, some of which have no counterparts in crystalline systems. Some of the phenomena responsible for producing these structures have been discussed in chapter 1; the intention here is to show how ideas such as frustration can lead to a particular type of magnetic ordering.

The discussion may, for the sake of convenience, be divided into collinear and non-collinear systems of one and two subnetwork systems (see figures 3.3 and 3.4). A subnetwork is defined as a group of atoms with similar magnetic interactions. Usually it is just a chemical sublattice, but on occasion it includes two or more elements whose interactions are not different in essence. Four possible one-subnetwork structures are shown in figure (3.3). If the exchange interaction is positive and significantly greater than the random anisotropy, then a ferromagnetic structure (figure 3.3a) results. If exchange coupling is such that interactions of equal magnitude and of both signs are present simultaneously, i.e. the distribution P(J) is symmetric about J=0, the result is that moments freeze in random orientations with no average correlations. The resulting structure is termed speromagnetic (figure 3.3c). A symmetric P(J) is not the only cause of speromagnetism; dominant local anisotropy results in speromagnetism if randomly oriented on a local scale (see, for example, Moorjani and Coey 1984).

In a system where random anisotropy is dominant, a local easy axis is defined at each site if the anisotropy parameter, D, is positive (negative D results in easy planes) and either direction is possible for

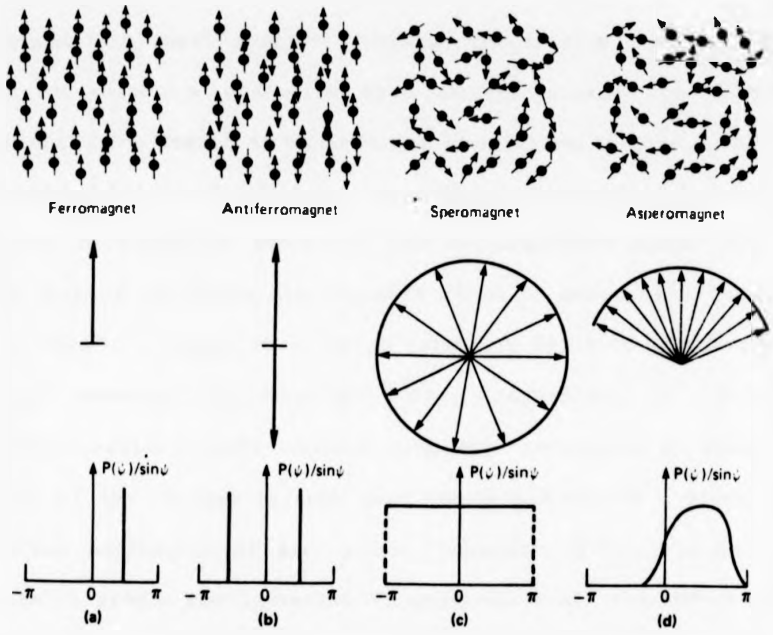


**Figure (3.3)** Possible one-subnetwork magnetic structures in amorphous solids showing schematically the spatial distribution of moment directions and the corresponding normalized angular probability distribution $P(\psi)/\sin\psi$.

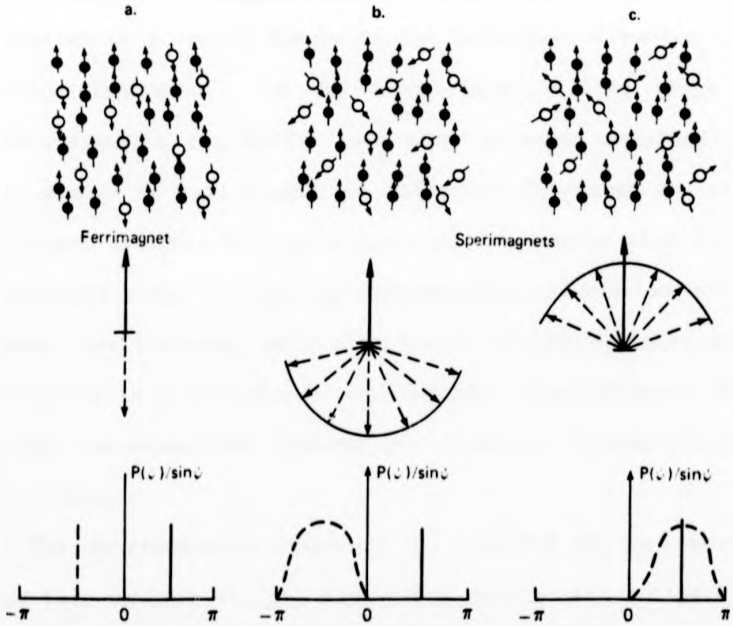


**Figure (3.4)** Possible two-subnetwork magnetic structures in amorphous solids showing the spatial distribution of moment directions and the corresponding normalized angular probability distributions $P(\psi)/\sin\psi$. Solid and dashed lines represent moments for two chemical species.

the moment. A small positive exchange interaction, however, causes a moment to select a direction most nearly parallel to that of its neighbours. The result is asperomagnetic ordering (figure 3.3d).

Despite the variety of magnetic ordering in amorphous systems, it is difficult to visualise amorphous antiferromagnetism since there is no obvious way of assigning the magnetic atoms to one or the other of the "sublattices". A negative exchange parameter leads to antiferromagnetic coupling between neighbouring spins, regardless of periodicity. Frustration arises with antiferromagnetic interactions whenever the geometry of the lattice is such that the neighbours of a given atom are themselves neighbours of each other (Toulouse 1977). It is then not possible to find a configuration of spins where all the interactions are simultaneously satisfied. Frustration will therefore ensure that a true antiferromagnetically ordered state cannot exist in amorphous magnetism (Simpson 1974). There is experimental evidence for all the structures shown in figure (3.3) except the antiferromagnetic structure. In fact, frustration is a major factor in the formation of random non-collinear magnetic structures. If the interaction is long range and partly antiferromagnetic (eg RKKY), then bond disorder introduces frustration if the change in bond lengths is sufficient to change the sign of $J(r)$. Topological disorder is always prone to frustration when it involves an odd-numbered ring. Competing interactions, single-ion anisotropy and exchange, for instance, will also result in non-collinear structures if their preferred directions do not coincide. Non-collinear structures of one- and two-subnetwork systems are shown in figures (3.3) and 3.4), respectively.

The ferrimagnetic structure is typified by the amorphous Tb-Fe alloys (see chapter 6). The rare-earth moments are antiparallel to the iron moments and form a two-subnetwork system. In amorphous $TbFe_2$, for example, there is a strong, positive Fe-Fe exchange coupling resulting

in a ferromagnetically aligned iron "sublattice". The Tb-Fe exchange is negative and weaker so that the Tb "sublattice" is coupled antiparallel to the iron. The anisotropy of the Tb subnetwork, however, is much greater than that of iron and therefore dictates the direction of the iron "sublattice". The resulting ferrimagnetic order is illustrated in figure (3.4a) and is analogous to that found in crystalline Tb-Fe alloys.

Since the total moments on the two subnetworks are unequal, there is a spontaneous magnetization. Below $T_c$ the temperature dependence of the magnetization of the different subnetworks is, in general, not the same. As a consequence, the resultant magnetisation may vanish at a temperature much lower than $T_c$. This intermediate temperature is called the compensation temperature, $T_{comp}$. Similarly, at a given temperature the magnetization, as a function of rare-earth concentration, also displays a compensation composition at which the resultant magnetization is zero (see chapter 6).

## 3.4 NON-UNIFORM LOCAL FIELD DISTRIBUTIONS

A characteristic feature of amorphous magnetism is that no two sites are identical. Site inequivalency leads to a distribution of magnetic moments, hyperfine fields and electrostatic fields. The inhomogeneous distributions of local fields are reflected in physical properties such as magnetic structure.

As an illustration of the dramatic consequences of a distribution of the local magnetic field, Chappert *et al* (1981) have shown that in amorphous $Y_{1-x}Fe_x$ ferromagnetic interactions in competition with antiferromagnetic interactions result in an asperomagnetic structure (see figure 3.5).

Random second order electrostatic interactions, and therefore distributions of $V_{zz}$, have been studied extensively by Czjzek *et al*

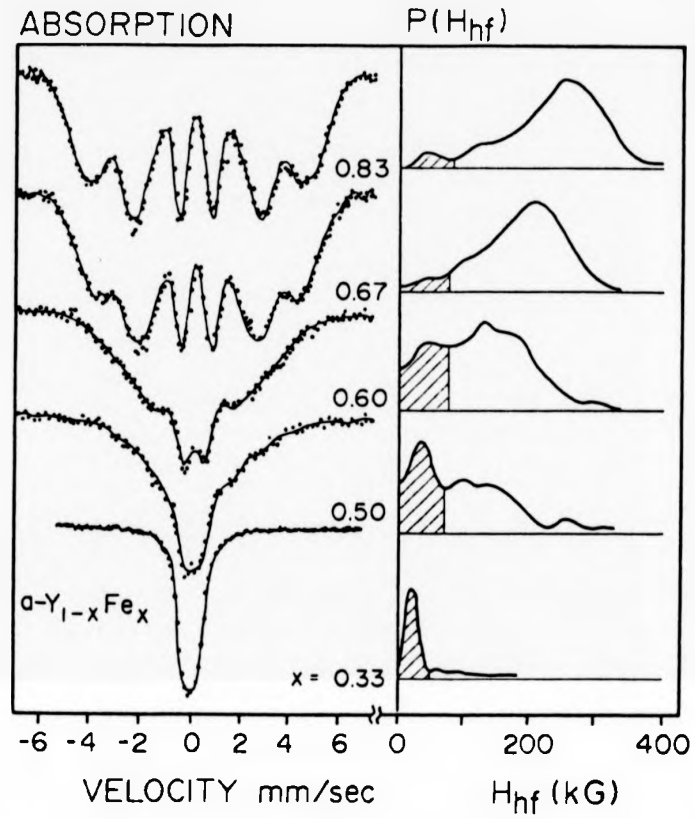


**Figure (3.5)** Mössbauer spectra of sputtered amorphous $Y_{1-x}Fe_x$ at 1.6 K. Corresponding hyperfine field distributions are shown on the right, where the shaded portions correspond to non-magnetic iron which shows some quadrupole splitting (Chappert *et al* 1981).

(1981). By employing $^{155}$Gd Mössbauer spectroscopy, the complication of intra-ionic contributions to $V_{zz}$ has been avoided since Gd is an S-state ion. Distribution functions have been calculated for $V_{zz}$ and $\eta$ assuming point charge calculations of the EFG to be valid and a dense random packing of hard spheres model (DRPHS). Only nearest neighbour coordination shells have been taken into account. The joint probability function is given by

$$P(V_{zz},\eta) = \frac{1}{\sqrt{2\pi\sigma^5}} V_{zz}^4 \eta(1-\eta^2/9) \exp\left[\frac{-V_{zz}(1-\eta^2/3)}{2\sigma^2}\right] \qquad (3.5)$$

The individual probability distributions for $V_{zz}$, $Q(V_{zz})$, and $\eta$, $R(\eta)$, are shown in figure (3.6). It can be seen that there is a broad hole around $V_{zz} = 0$, indicating that zero second order electrostatic fields have a vanishingly small probability of occurring in random structures. Fields with $\eta \approx 0$ also have a small probability of occurring. It should be noted that $P(V_{zz},\eta)$ is strongly dominated by the first coordination shell contribution, which may deviate considerably from equation (3.5). If successive coordination shells are taken into account then $Q(V_{zz})$ is generally skew; the field gradient has a preferred sign and therefore in an amorphous solid the quadrupole splitting of the nuclear levels should be well defined and the interaction should have a preferred sign.

## 3.5 MODELS OF AMORPHOUS MAGNETISM

A wide variety of models for amorphous magnetism exist, ranging from the purely phenomenological to the highly theoretical. It is not the intention here to review the literature but only to describe the relevant models and to mention the others in passing.

Broadly speaking, models of amorphous magnetism assume a random space distribution of exchange (Edwards and Anderson 1975) or a random

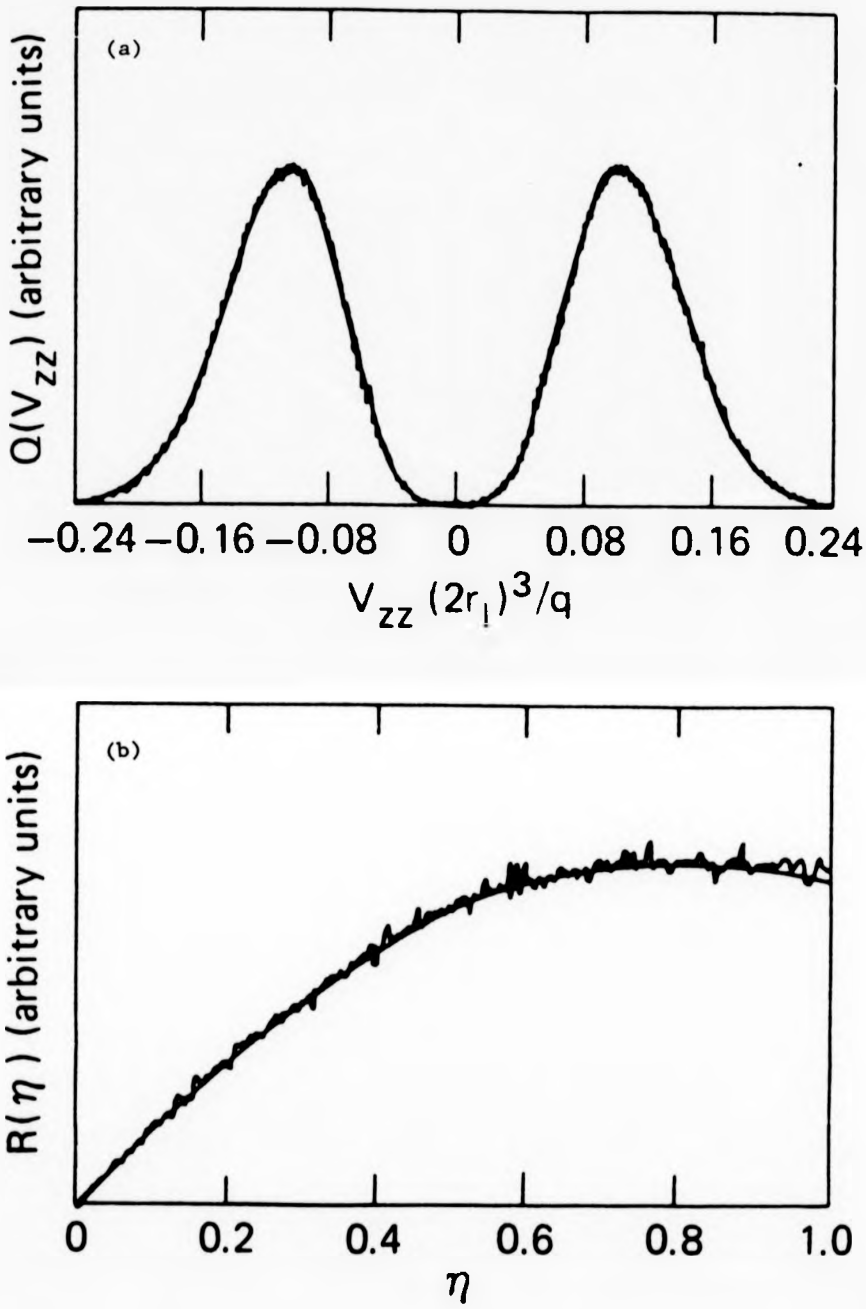


**Figure (3.6)** Probability distributions for (a) $V_{zz}$ and (b) $\eta$ for the random electric field gradient created by a single shell of ions of charge q. The radius of the shell, $r_1$, was chosen to be six times the ionic radius (Czjzek *et al* 1981).

distribution of anisotropy axes (Harris *et al* 1973). In recent years the random anisotropy model, due to Harris, Plischke and Zuckermann (1973) and hereafter referred to as the HPZ model, has received considerable attention. Other more sophisticated, models have also been developed, the Chudnovsky and Serota model (1983), for instance. A number of theoretical studies (Pelcovits *et al* 1978, Alben *et al* 1978, Imry and Ma 1975) have demonstrated, by using the renormalization group technique, that long range ferromagnetic order is destroyed by local random anisotropy in less than four dimensions. Chudnovsky and Serota have developed a model on the basis of these results which indicates that local random anisotropy, however small, results in a correlated spin glass (characterized by a smooth rotation of the magnetization over the volume so that the directions of magnetization are correlated on the length $R_D >> R_c$, where $R_D$ is the disordering length and $R_c$ is the scale of the spatial correlation length of the easy axis). The model is applicable to systems with ferromagnetic exchange and small random anisotropy in two classes of materials; amorphous alloys with a concentration of magnetic ions above the threshold for ferromagnetism and polycrystalline ferromagnets, consisting of very small single-domain crystallites. Within the model, the two classes of materials differ mainly in the extent of the spatial correlation of the easy axes.

Under the right conditions data obtained from nmr and Mössbauer spectroscopy can yield very accurate values for parameters such as crystal field parameters and hyperfine field values. In amorphous systems, however, due to the multiplicity of environments, much of this information is obscured by broadened linewidths etc. The experimental data presented in later chapters, therefore, is not sufficiently informative to comment on the more sophisticated models such as the Edwards-Anderson model for random exchange and the Chudnovsky-Serota model. From an nmr point of view, a highly correlated cluster system

does not appear to differ greatly from a polycrystalline structure. Information concerning correlation lengths is not readily available from nmr. Consequently it is inappropriate to comment on the more involved models given that the present work has not yielded the required information. Models such as the Chudnovsky-Serota type differentiate between long range ferromagnetic order and correlated clusters. On the basis of the data presented in this thesis it is not possible to make such differentiations and so analysis has been carried out almost exclusively within the framework of the HPZ model.

### 3.5.1 THE HPZ MODEL

The magnetic properties of amorphous R alloys containing a non-S state R ion can be described remarkably successfully by a simple model (Harris *et al* 1973). In crystalline materials, R ions with $L \neq 0$ show a strong coupling to the local environment. This observation led Harris, Plischke and Zuckermann (1973) to propose that the magnetic properties of amorphous materials with non-S-state R ions should be dominated by the random electrostatic fields that exist in such compounds. The HPZ model assumes that each R ion is strongly influenced by the random electric fields from the immediate environment but without any overriding symmetry due to lattice periodicity. The model is summarized below.

Following the notation and theory developed in chapter 2, the energy of an electron in an unfilled shell in the electric field of atomic point charges can be written as

$$W(\underline{r}_k) = -e \sum \frac{q_j}{|\underline{R}_j - \underline{r}_k|} \qquad (3.6)$$

For 4f electrons in the rare earths

$$E = \sum_{l=0}^{6} \sum_{l=0}^{6} A_{l,m} \langle r_k Y_{l,m}(\theta_k, \phi_k) \rangle \qquad (3.7)$$

where

$$A_{l,m} = \Sigma \frac{q_j}{R_j^{l+1}} (-1)^m Y_{l,m}(\Theta_j,\Phi_j) \qquad (3.8)$$

Semiclassical calculations by Cochrane *et al* (1974) have shown that the effective lowering of symmetry in amorphous materials makes the second order crystal field terms dominant. To a first approximation then, terms of order greater than l = 2 may be neglected. In terms of the theory given in chapter 2, the crystal field Hamiltonian can be written as

$$\begin{aligned} H = \sum_i & A^i_{zz}\left[3[J_z(i)]^2 - J(J+1)\right] + A^i_{yy}\left[[J_y(i)]^2\right] + A^i_{xx}\left[[J_x(i)]^2\right] \\ & + A^i_{xy}\left[J_x(i)J_y(i) + J_y(i)J_x(i)\right] + A^i_{xz}\left[J_x(i)J_z(i) + J_z(i)J_x(i)\right] \\ & + A^i_{yz}\left[J_y(i)J_z(i) + J_z(i)J_{y(i)}\right] \qquad (3.9) \end{aligned}$$

If the principal axes are chosen to coincide with the coordinate system then equation (3.9) simplifies considerably and becomes

$$H = \Sigma A^i_x\left[J_{x_i}(i)\right]^2 + B^i_y\left[J_{y_i}(i)\right]^2 + C^i_z\left[J_{z_i}(i)\right]^2 \qquad (3.10)$$

where $x_i$, $y_i$, and $z_i$ are the principal axes of the local second order crystal field. This is called the RMA approximation.

A further approximation is made by choosing $z_i$ locally such that $C^i_z$ is numerically larger than $A^i_x$ and $B^i_y$. In this sense $z_i$ becomes the local easy axis and the simplest approximation to RMA is to keep the $C^i_z[J_{z_i}(i)]^2$ terms only, replacing each $C^i_z$ by an average value, -D. The

crystal field Hamiltonian is then written as

$$H = -D \Sigma\left[J_{zi}(i)\right]^2 \qquad (3.11)$$

where i labels a particular ion and $z_i$ the local easy axis. The amorphous nature of the system is described by assuming that the local easy axes are ramdomly directed.

The model, though attractively simple, does pose some obvious problems; it allows negative values of D, which suggest the possibility of local easy planes. Easy planes cannot exist because the symmetry of the uniaxial Hamiltonian is destroyed if we include the neglected terms from equation (3.10). Also, for a purely axial crystal field, a change of sign of D would be expected when, for a fixed field, one replaces an R ion that is oblate in the moment direction ($Tb^{3+}$, $Ho^{3+}$) by one that is prolate ($Er^{3+}$, $Tm^{3+}$). If D is negative such that $|J_{zi} = \pm 1/2\rangle$ or $|J_{zi} = 0\rangle$ states are lowest in energy, then the paramagnetic susceptibility should be reduced considerably; for Kramers ions ($Dy^{3+}$, $Er^{3+}$) the susceptibility should be reduced by a factor of approximately two from that predicted by the HPZ model (Fert and Campbell 1978). More dramatically, for non-Kramers ions with D negative, the ground state is $|J_{zi} = 0\rangle$ and the susceptibility should become of Van Vleck type at low temperatures. Measured susceptibilities agree closely with those expected from the HPZ model; experimental results do not suggest a negative value for D.

The question of negative D values has been considered in detail by Fert and Campbell (1978) who analysed the general quadrupole electric field Hamiltonian of equation (3.10) and have shown that the assumption of a non axial electrostatic field, with a random distribution of $A_x^i$, $B_y^i$, and $C_z^i$, is nearly equivalent to the assumption of an axial crystal field with D positive, for large J in particular.

In the classical limit of an electric quadrupole plus magnetic dipole "ion" in the field of equation (3.10), there will be an energy minimum for one orientation of the quadrupole, except in the case $A_x^i > B_y^i - C_z^i$, for which the energy minimum is any orientation in the plane perpendicular to the x-axis. Except in such a particular case, the ground state is a doublet $|J, J_z = \pm J\rangle$, as it is for an axial field model with D positive.

In reality, however, R ions are quantum objects and the lifting of their (2J+1)-fold degeneracy by equation (3.10) must be considered. It may be assumed that A+B+C = 0 (because $J_x^2 + J_y^2 + J_z^2 = J(J+1)$ can be added to the Hamiltonian of equation (3.10) without changing the energy level scheme). $A_x^i$ may be defined as the most positive coefficient and $C_z^i$ as the most negative. Equation (3.10) can now be analysed in terms of a parameter $\eta'$, defined as

$$\eta' = \frac{3B}{A-C} \tag{3.12}$$

$\eta'$ can vary between -1 (corresponding to a site with B = C i.e axial field gradient along the x-axis with D negative) and +1 (uniaxial field along the z-axis with D positive). In addition (C-A) is assumed to be constant which gives an approximately constant overall crystal field splitting, in agreement with the results of Cochrane *et al* (1975). Thus, the coefficients A, B and C can be written as

$$A = \frac{3 - \eta'}{A - C} K \tag{3.13a}$$

$$B = \frac{\eta'}{3} K \tag{3.13b}$$

$$C = -\frac{3 + \eta'}{6} K \tag{3.13c}$$

Fert and Campbell (1978) investigated the evolution of the crystal field splitting of the ground state and the first excited state between the uniaxial field limits, $\eta' = +1$ and $\eta' = -1$.

For a non-Kramers ion, the ground state for $\eta' = 1$ is the doublet $|J_z = \pm J\rangle$. For large values of J the doublet persists for most of the range of $\eta'$ and splits into a pair of singlets only when $\eta'$ is close to -1. At $\eta' = -1$ the lower singlet is the state $|J_x = 0\rangle$ while the other singlet joins a higher state and forms with it the doublet $|J_x = \pm 1\rangle$.

For a Kramers ion the situation is somewhat different; the ground state is always a doublet, in accordance with Kramers' theorem. As $\eta'$ is varied from +1 to -1 there is an evolution from the doublet $|J_z = \pm J\rangle$ to the doublet $|J_z = \pm 1/2\rangle$. Deviations from the predictions of the HPZ model are, however, much less apparent.

For non-Kramers ions the energy difference between the two singlets, as a function of $\eta'$, for several values of J is shown in figure (3.7). When J = 8, $\Delta E$ is vanishingly small for most of the range of $\eta'$. Where the splitting is negligible the quasidoublet, $|J_z = \pm 8\rangle$, is formed. It has been shown that there is a negligible admixture of states with $J_z \neq 8$

For large J, the classical limit is approached where the ground state is split only when $\eta' = -1$. For $Ho^{3+}$ (J=8) we expect the vast majority of ions to be in the fully polarized ground state and thus be described fairly well by the uniaxial model, but with D always positive. When J is smaller (i.e in $Pr^{3+}$, J = 4) there will be a significant number of sites where the ground state is a well separated singlet and thus one would expect deviations from the predictions of the HPZ model.

The complete Hamiltonian for the amorphous ferromagnet requires two additional terms. The exchange interactions between the R moments are mediated by the conduction electrons (an RKKY-like mechanism) and can be represented as follows:

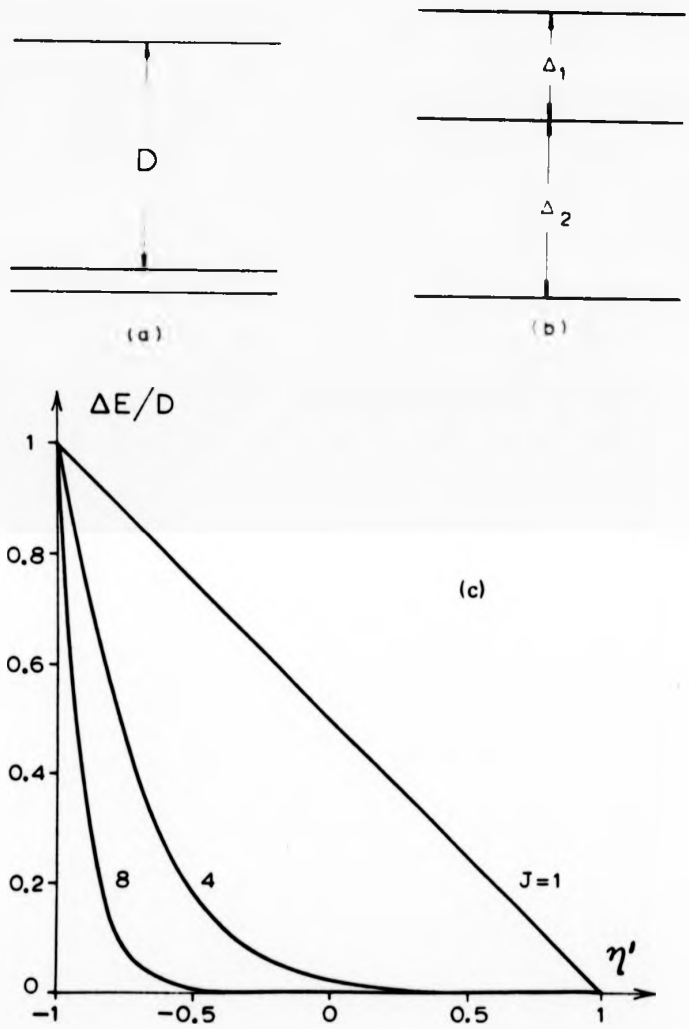


**Figure (3.7)** Typical crystal-field level structure for J = 1: (a) HPZ model, (b) the cluster model (Cochrane *et al* 1975) and (c) the energy difference between the two lowest crystal-field eigenstates as a function of $\eta'$ for various values of J.

$$H_{ex} = -\frac{1}{2} \sum_{i,j} J_{ij}\, \underline{J}_i . \underline{J}_j \qquad (3.14)$$

It should be noted that structural disorder leads to a distribution in $J_{ij}$. The effect of an applied field, B, in the unique z-direction is represented by the usual Zeeman term:

$$H_{mag} = -g\mu_B B \sum J_{iz} \qquad (3.15)$$

We approximate further and sum over nearest neighbours in equation (3.14). Putting together equation (3.11), (3.14) and (3.15), the resulting Hamiltonian is

$$H = -D \sum_i J_{izi} - \frac{1}{2} J \left[ \sum_{i,j} \right] \underline{J}_i . \underline{J}_j - g\mu_B B \sum_i J_{iz} \qquad (3.16)$$

where J is an average value of $J_{ij}$ and the square brackets indicate a sum over nearest neighbours only.

# CHAPTER 4: Experimental Techniques

## 4.1 INTRODUCTION

In this chapter a rudimentary description of nmr and Mössbauer spectroscopy is given. The two techniques are well established and therefore only a brief discussion is presented; where appropriate, the reader is referred to more authoritative texts. More specifically, then, $^{155}$Gd Mössbauer spectroscopy and rare-earth nmr spectroscopy where the rare-earth is $^{165}$Ho, $^{159}$Tb and $^{141}$Pr, are outlined in the following sections.

## 4.2 $^{155}$Gd MÖSSBAUER SPECTROSCOPY

The phenomenon of $\gamma$-ray emission or absorption, without loss of energy due to recoil of the nucleus and without thermal broadening is the Mössbauer effect. Its unique feature is the production of monochromatic electromagnetic radiation with a narrowly defined energy spectrum allowing the resolution of correspondingly small energy differences. Of the numerous isotopes that display the Mössbauer effect, $^{155}$Gd has been used for the experiments reported in this thesis; in particular the 86.54 keV $\gamma$-rays have been utilized. (For the detailed decay scheme and nuclear data of $^{155}$Gd see, for example, Stevens and Stevens 1978.) The energy levels involved in the 86.54 keV transition ($I_g = 3/2$ and $I_e = 5/2$ where $I_g$ and $I_e$ are nuclear spins of the ground and excited states, repectively) are shown in figure (4.1) for (a) magnetic interaction only and (b) quadrupole interaction only, with $\eta = 0$. For Mössbauer spectra obtained above the Curie temperature, for which only the quadrupole interaction needs to be taken into account, the resolution of the five transitions is determined by the ratio of the nuclear quadrupole moments of the excited state to ground state, $R_Q$. The value of $R_Q$ for $^{155}$Gd is 0.2 ± 0.05 (Stevens and Stevens, 1978). The quadrupole-split excited state is practically a

# CHAPTER 4: Experimental Techniques

## 4.1 INTRODUCTION

In this chapter a rudimentary description of nmr and Mössbauer spectroscopy is given. The two techniques are well established and therefore only a brief discussion is presented; where appropriate, the reader is referred to more authoritative texts. More specifically, then, $^{155}$Gd Mössbauer spectroscopy and rare-earth nmr spectroscopy where the rare-earth is $^{165}$Ho, $^{159}$Tb and $^{141}$Pr, are outlined in the following sections.

## 4.2 $^{155}$Gd MÖSSBAUER SPECTROSCOPY

The phenomenon of $\gamma$-ray emission or absorption, without loss of energy due to recoil of the nucleus and without thermal broadening is the Mössbauer effect. Its unique feature is the production of monochromatic electromagnetic radiation with a narrowly defined energy spectrum allowing the resolution of correspondingly small energy differences. Of the numerous isotopes that display the Mössbauer effect, $^{155}$Gd has been used for the experiments reported in this thesis; in particular the 86.54 keV $\gamma$-rays have been utilized. (For the detailed decay scheme and nuclear data of $^{155}$Gd see, for example, Stevens and Stevens 1978.) The energy levels involved in the 86.54 keV transition ($I_g = 3/2$ and $I_e = 5/2$ where $I_g$ and $I_e$ are nuclear spins of the ground and excited states, repectively) are shown in figure (4.1) for (a) magnetic interaction only and (b) quadrupole interaction only, with $\eta = 0$. For Mössbauer spectra obtained above the Curie temperature, for which only the quadrupole interaction needs to be taken into account, the resolution of the five transitions is determined by the ratio of the nuclear quadrupole moments of the excited state to ground state, $R_Q$. The value of $R_Q$ for $^{155}$Gd is 0.2 ± 0.05 (Stevens and Stevens, 1978). The quadrupole-split excited state is practically a

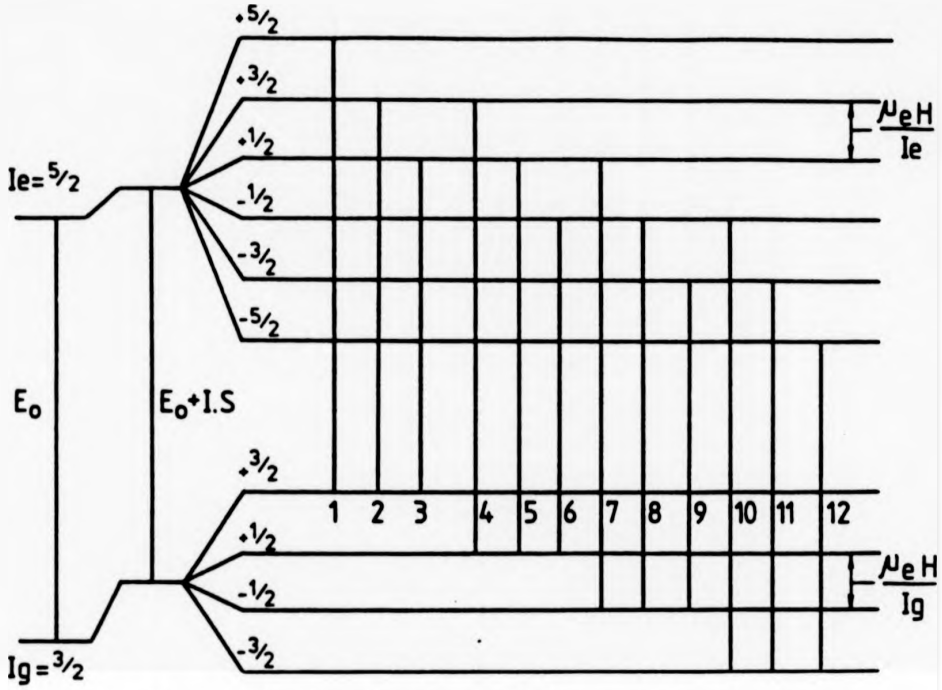


(a) magnetic dipole splitting.

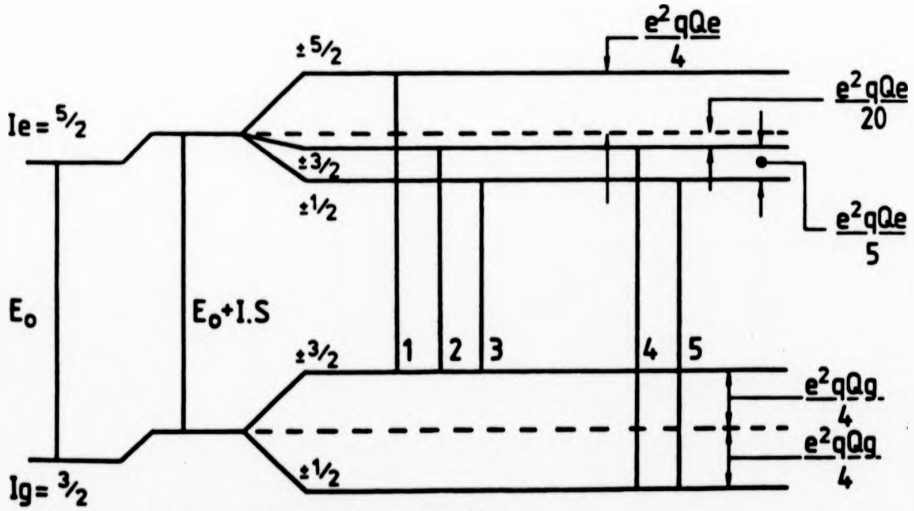


(b) quadrupole splitting.

Figure (4.1) Nuclear states involved in the 86.54 keV Mössbauer transition in $^{155}Gd$ (a) for magnetic dipole splitting and (b) for quadrupole splitting.

singlet; as a consequence only two effective transitions are seen; it is not possible to determine the sign of $V_{zz}$ from such spectra.

If zero-phonon states are available to take the recoil energy, $E_R$, then the whole lattice will move in order to conserve the initial zero momentum of the system. The recoil energy is thus negligible since the recoiling mass is now the mass of the whole system. Therefore the energy of the $\gamma$-ray is just the difference between the energy of the nuclear states involved in the emission. The precision with which this energy is defined is determined by the lifetime of the excited state. The probability of zero-phonon events or the recoil-free fraction, f, depends on the free-atom recoil energy (which is proportional to the square of the $\gamma$-ray energy), the properties of the lattice and the ambient temperature. A small $\gamma$-ray energy, firm binding of the atom in the lattice and low temperature result in a favourable value for the recoil-free fraction. Expressions have been derived using various models for the vibrational modes of the solid (Einstein and Debye models, for instance) but are of limited value since amorphous solids are the subjects of experiment here. It is nevertheless prudent to use such expressions as indicators; Chaudhry (1983) has found that $f_a$, the recoil-free fraction relating to the absorber, for $^{155}$Gd is $\approx$10 % at 4.2 K.

Mössbauer spectra and their interpretation are strongly dependent on the effective absorber thickness, $T_a$, which is given by (Margulies and Erhman 1961)

$$T_a = f_a n_a \sigma_0 t_a \qquad (4.1)$$

where $f_a$ is the recoil-free fraction, $n_a$ is the natural abundance of the Mössbauer isotope, $\sigma_0$ is the effective cross-section and $t_a$ is the physical thickness of the absorber. It has been shown (Margulies and

Erhman 1961) that by taking $T_a = 1$, non-linear absorption effects can be avoided with the consequent preservation of Clebsch-Gordon (C-G) intensities (see below).

The intensity of a hyperfine transition (see Greenwood and Gibb 1971, for example) can be expressed as a product of two terms, one of which is angle dependent and the other is angle independent (C-G coefficients squared). For a randomly oriented sample the angular dependence may be neglected since integration over all directions gives unity. For a thin absorber ($T_a \lesssim 1$), the intensities are determined by the C-G coefficients entirely.

Adhering to the requirement that $T_a \lesssim 1$ has the unfortunate consequence that a substantial number of recoil-free $\gamma$-rays pass through the absorber without being absorbed. This coupled with the intrinsically low recoil-free fraction in $^{155}Gd$ means that the data acquisition time is necessarily long (approximately 15 days) if a reasonable signal to noise ratio (50:1) is to be achieved.

In summary, application of the Mössbauer effect to the study of hyperfine interactions depends on the smallness of the $\gamma$-ray linewidth compared to the characteristic energies associated with the hyperfine interaction. A hyperfine spectrum is obtained in the following way: the source material is placed in a host where the nuclear levels remain unsplit and the host is mounted on a velocity modulator. A stationary absorber is placed between the source and detector. Nuclear levels in the absorber are split by the hyperfine interaction resulting in a number of different energies at which absorption takes place. The counting rate at the detector will drop whenever the Doppler velocity applied to the source brings the emitted $\gamma$-ray into coincidence with an absorption energy in the absorber. The Mössbauer spectrum is just the count rate plotted against velocity of the source.

A detailed account of the experimental set-up of the Manchester

$^{155}$Gd Mössbauer absorption spectrometer has been given by Chaudhry (1983). The Mössbauer experiments reported in chapter 5 were mainly carried out at 4.2 K, in zero and applied fields. The resultant spectra were fitted using a computer programme based on the method of least-squares.

## 4.3 SPIN-ECHO NMR SPECTROSCOPY

The resonance phenomenon is of particular advantage in that it can enable the selection and measurement of a specific component of a given physical quantity. This is dramatically illustrated by the observation of weak nuclear paramagnetism of iron against a dominating background of electronic ferromagnetism. The fumdamental nature of nmr experiments is an investigation of the response of the nuclear magnetization, $\underline{m}$, to an applied oscillating magnetic field, $\underline{B}_1(t)$. The response of $\underline{m}$ is only significant when $\nu$, the frequency of oscillation, is close to one of the transition frequencies $\nu_{nm}$ defined in equation (2.48). The spin-echo technique has a number of advantages over the simpler free precession method which will be mentioned in due course. Before embarking on a discussion of spin-echos, it is necessary to outline the motion of isolated spins.

### 4.3.1 MOTION OF ISOLATED SPINS

The equation of motion of a magnetic moment, $\underline{\mu}$ in a field $\underline{B}$ is given by

$$\frac{d\underline{\mu}}{dt} = \underline{\mu} \times \gamma \underline{B} \qquad (4.2)$$

Equation (4.2) can be solved by use of the rotating frame method (see Slichter 1978, for example). If the frame is rotating with an angular velocity $\Omega$ and $\delta\underline{\mu}/\delta t$ represents the time rate of change of $\underline{\mu}$ with respect to the rotating frame, then

$$\frac{\delta \underline{\mu}}{\delta t} = \underline{\mu} \times (\gamma \underline{B} + \underline{\Omega}) \qquad (4.3)$$

It is clear that motion of $\underline{\mu}$ in the rotating frame obeys the same equation as in the laboratory coordinate system, provided that the actual field is replaced by an effective field $\underline{B}_{eff}$:

$$\underline{B}_{eff} = \underline{B} - \frac{\underline{\Omega}}{\gamma} \qquad (4.4)$$

The motion of $\underline{\mu}$ in a static field $\underline{B} = B_0\underline{k}$ can now easily be solved for by choosing $\underline{\Omega} = -\gamma B_0\underline{k}$ such that $\delta\underline{\mu}/\delta t = 0$; $\underline{\mu}$ remains fixed in the rotating frame and therefore rotates at an angular velocity of $\underline{\Omega} = -\gamma B_0\underline{k}$ in the laboratory frame. The angular frequency $\gamma B_0$ is called the Larmor frequency and is identical to that required for magnetic resonance absorption.

If an alternating field $\underline{B}_1$, of angular frequency $\omega$, is applied to the system then the equation of motion for $\underline{\mu}$ becomes

$$\frac{\delta \underline{\mu}}{\delta t} = \underline{\mu} \times \gamma[(B_0 - \frac{\omega}{\gamma})\underline{k} + B_1\underline{i}] = \underline{\mu} \times \underline{B}_{eff} \qquad (4.5)$$

where

$$\underline{B}_{eff} = \underline{k}(B_0 - \frac{\omega}{\gamma}) + \underline{i}B_1 \qquad (4.6)$$

If the resonance condition is fulfilled ($\omega = \gamma B_0$) then the effective field is simply $B_1\underline{i}$. A magnetic moment that is parallel to the static field initially will then precess in the y-z plane, but always remaining perpendicular to $B_1$. If $B_1$ is applied for a short length of time, $\tau_p$,

$$\frac{\delta \underline{\mu}}{\delta t} = \underline{\mu} \times (\gamma \underline{B} + \underline{\Omega}) \qquad (4.3)$$

It is clear that motion of $\underline{\mu}$ in the rotating frame obeys the same equation as in the laboratory coordinate system, provided that the actual field is replaced by an effective field $\underline{B}_{eff}$:

$$\underline{B}_{eff} = \underline{B} - \frac{\underline{\Omega}}{\gamma} \qquad (4.4)$$

The motion of $\underline{\mu}$ in a static field $\underline{B} = B_0\underline{k}$ can now easily be solved for by choosing $\underline{\Omega} = -\gamma B_0\underline{k}$ such that $\delta\underline{\mu}/\delta t = 0$; $\underline{\mu}$ remains fixed in the rotating frame and therefore rotates at an angular velocity of $\underline{\Omega} = -\gamma B_0\underline{k}$ in the laboratory frame. The angular frequency $\gamma B_0$ is called the Larmor frequency and is identical to that required for magnetic resonance absorption.

If an alternating field $\underline{B}_1$, of angular frequency $\omega$, is applied to the system then the equation of motion for $\underline{\mu}$ becomes

$$\frac{\delta \underline{\mu}}{\delta t} = \underline{\mu} \times \gamma[(B_0 - \frac{\omega}{\gamma})\underline{k} + B_1\underline{i}] = \underline{\mu} \times \underline{B}_{eff} \qquad (4.5)$$

where

$$\underline{B}_{eff} = \underline{k}(B_0 - \frac{\omega}{\gamma}) + \underline{i}B_1 \qquad (4.6)$$

If the resonance condition is fulfilled ($\omega = \gamma B_0$) then the effective field is simply $B_1\underline{i}$. A magnetic moment that is parallel to the static field initially will then precess in the y-z plane, but always remaining perpendicular to $B_1$. If $B_1$ is applied for a short length of time, $\tau_p$,

i.e a pulse of radiation, then the moment will rotate through an angle $\theta_p = \gamma B_1 \tau_p$. It is clear that $B_1\tau_p$ can be chosen to give any desired tipping angle, assuming enough power is available.

4.3.2 SPIN-ECHOS

The formation of spin-echos can most easily be understood by considering a $\pi/2 - \tau - \pi$ pulse sequence. Initially a pulse is applied which tips the nuclear magnetization by $\pi/2$. After a short time $\tau$, a second pulse is applied which tips the spins by $\pi$. A spin-echo arises a time $\tau$ after the second pulse; the scheme is shown pictorially in figure (4.2).

A discussion of spin-echos is necessarily incomplete without mention of the associated characteristic relaxation times and line broadening mechanisms. There are three distinct contributions to line broadening in nmr. The most straightforward of these, instrumental broadening, arises from sources such as the inhomogeneity of the alternating magnetic field used to induce the nuclear transitions. In rare-earth nmr instrumental broadening can usually be made small in comparison to the total linewidth. Of more fundamental interest is the broadening caused by the spin-spin and spin-lattice interactions which limit the lifetime of the hyperfine energy levels and imparts to them a natural linewidth $(\Delta\nu)_h$, in accordance with the Heisenberg uncertainty principle. Finally, individual nuclei in a given sample can experience different environmental effects. A continuum of different environments, as in an amorphous solid for example, has a similar spread of hyperfine parameters associated with it. This results in "smeared" spectral lines and is known as microscopic inhomogeneous broadening, $(\Delta\nu)_{ih}$.

The time constant for the restoration of $m_z$, the component of $\mathbf{m}$ along $\mathbf{B}_t$, is known as the spin-lattice relaxation time, $T_1$. The excitation energy absorbed by the nuclear spins is dissipated into the lattice through this longitudinal relaxation process. The phases of

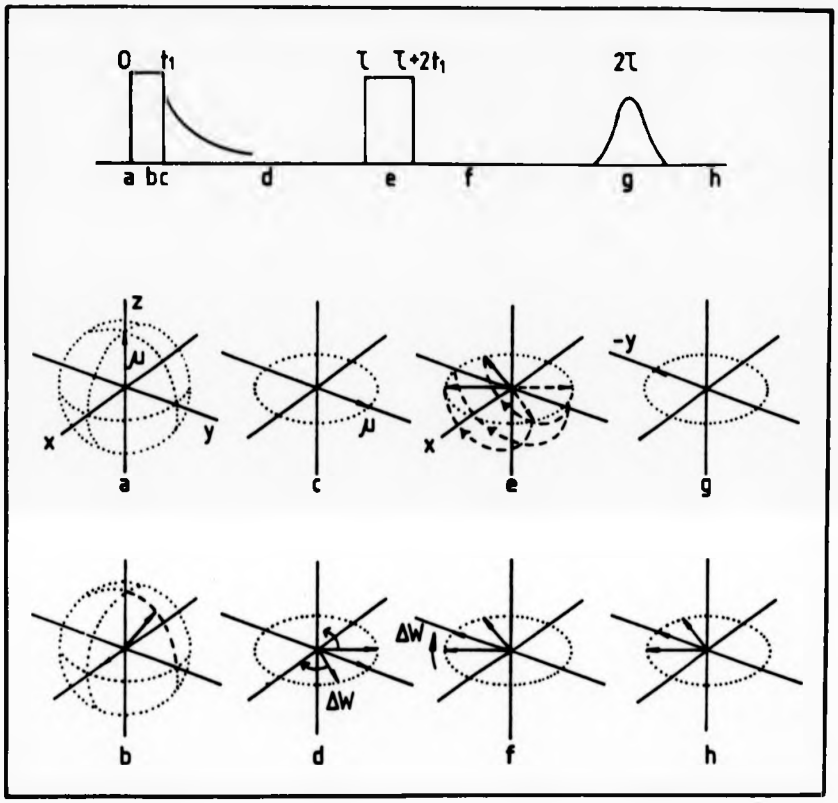


Figure (4.2) Schematic representation of the nmr pulse sequence and the formation of the spin echo. The steps in the echo formation can be summarized as

(1) a pulse of duration $t_1$ rotates $\mu$ by $\pi/2$; at $t = t_1$, $\mu$ is along y,

(2) after $B_1$ is removed, $\mu$ rotates with y at an angular velocity $\omega$ about z, for a time $\tau \gg t_1$; some dephasing of the spins occurs during this time.

(3) a second pulse of duration $t_2 = 2t_1$, rotates $\mu$ by an angle $\pi$ about x toward a position along -y.

(4) after the second pulse, the spins regroup and the echo is observed at a time $t = 2\tau$.

precessional motions of individual nuclei become randomized by spin-spin and spin-lattice interactions. This leads to a steady and irretrievable reduction of $\mathbf{m}_1$, the transverse component of the nuclear magnetization. The time scale of this process is called the transverse relaxation time or phase memory time, $T_2$. In the presence of inhomogeneous broadening, the total transverse relaxation time is denoted by $T_2^*$. A necessary condition for the observation of spin-echos is that

$$T_2^* < \tau < T_2 < T_1 \qquad (4.7)$$

The spin-echo technique hinges on the fact that the dephasing of the nuclear spins brought about by inhomogeneous broadening, unlike that caused by homogeneous broadening, is reversible. The spins can be brought back into phase by the appplication of a second pulse, if this is achieved in a time comparable with $T_2$.

It should be noted that the classical picture presented here relates to a system without quadrupole splitting. Where quadrupole splittings occur, the application of an alternating field close to a particular transition frequency $\nu_{nm}$ will directly affect only that portion of the nuclear magnetization which corresponds to the states $|\varepsilon_n\rangle$ and $|\varepsilon_m\rangle$. The detailed motion of the nuclear magnetization can be obtained in a rigorous manner by use of the density matrix technique (see Mackenzie 1969, for example).

Before concluding this section it is important to draw attention to three important advantages rendered by use of spin-echo nmr over the simpler free precession technique, whenever inhomogeneous broadening is dominant; amorphous alloys being a severe case in point. Two of the advantages conferred are of practical and the third of fundamental importance. Firstly, the signal is separated from the excitation pulses in the time domain, thereby mitigating receiver recovery time problems

and secondly, the shape of the echo signal prevents confusion with the "ringing" of the resonant cavity. Finally, the phase memory time $T_2$ can be studied by observing the reduction in the echo intensity as $\tau$ is increased, hence allowing information about homogeneous broadening to be extracted from systems dominated by inhomogeneous broadening.

4.3.3 THE NMR SPECTROMETER

In this section a brief description of the Manchester pulsed nmr spectrometer is given. For a complete description of the instrument the reader is referred to Waind (1983), Wagg (1974) and Mackenzie (1969). The spectrometer employs phase-coherent detection and is capable of being operated in the 3 – 8 GHz frequency range, at temperatures of 1.3 and 4.2 K. Cryogenic facilities include a superconducting magnet which can generate fields of up to 8 T at 4.2 K. The major components of the machine (excluding cryogenics) are shown in figure (4.3).

Referring to figure (4.3), the main oscillator provides continuous, frequency variable, microwaves. Pulses are produced by the action of a microwave switch, S1. The low power pulses thus produced are amplified by a travelling-wave-tube (TWT) amplifier before being admitted into the cavity via a circulator. The switch S2 suppresses the TWT amplifier noise after the passage of the pulses and S3 protects the receiver from transmitter "spikes" reflected from the specimen cavity. In this respect it is clear that the pulse timing control unit is of critical importance since it controls the operation of the microwave switches.

The echo signal of frequency $\nu$ emerges via the circulator and S3 and is amplified before being mixed with a reference signal of frequency $\nu+\Delta\nu$, where $\Delta\nu$ is the intermediate frequency (I.F) and is a constant. It is this resulting I.F signal that is subsequently processed and phase-coherently detected.

A detailed description of the resonant cavities will not be given

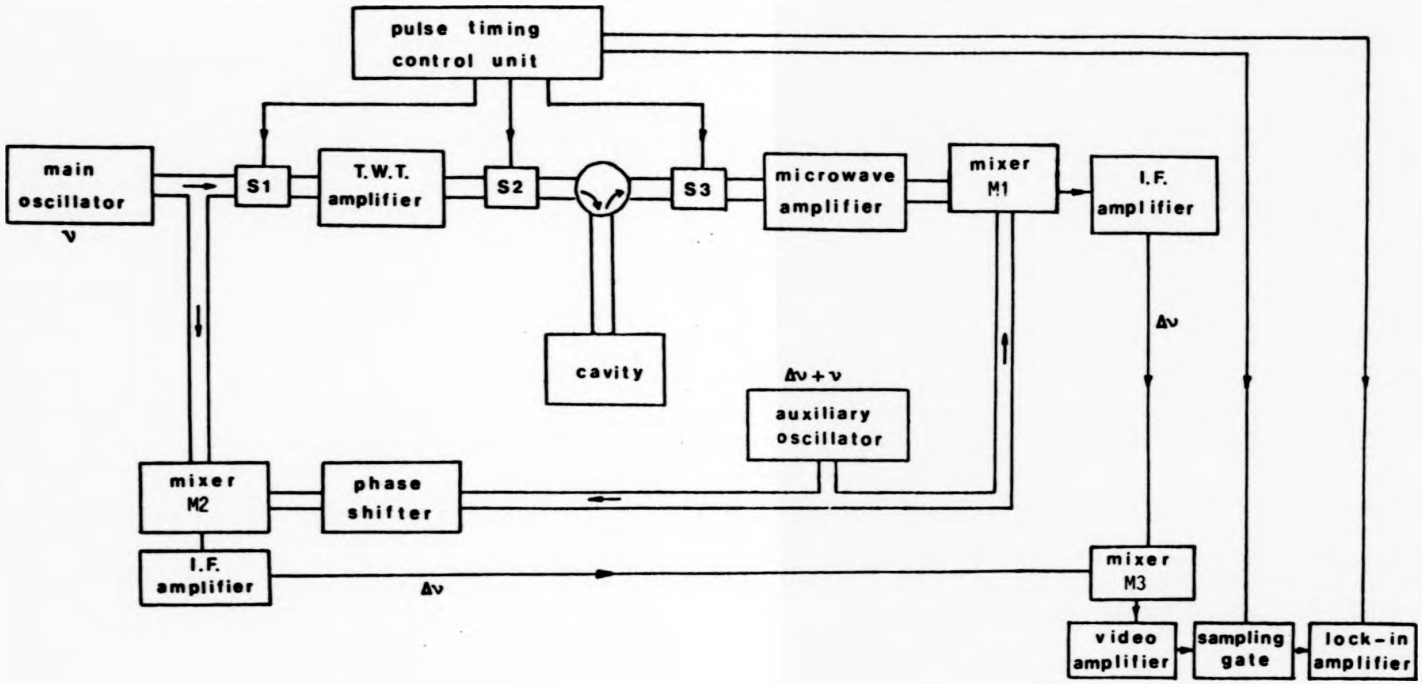


**Figure (4.3)** Schematic diagram of the phase-coherent spin-echo nmr spectrometer; for clarity the cryogenics have been omitted.

here; it is sufficient to note that only one cavity has been used throughout the experimental work described in this thesis. The 1/4 wavelength coaxial cavity is tunable by adjustment of the length of the central conductor. The sample is embedded in epoxy resin and mounted on the central conductor at the point of maximum r.f field. For a more detailed description of cavity design and application, the reader is referred to McMorrow (1987) and Waind (1983).

# Chapter 5: Amorphous R:(Gd,Y,Cu) and R:(Gd,Ag) Alloys

## 5.1 INTRODUCTION

In this chapter the results of nmr and Mössbauer experiments on the series R:(Gd,Y,Cu) and R:(Gd,Ag), where R = Ho, Tb or Pr, are presented. Specific compositions are given later (sections 5.1.1 and 5.1.2).

A number of factors, some of practical importance and others of a more fundamental nature, have played a part in the choice of these series. First and foremost, excluding the probe ions there is only one magnetic species, Gd, and the systems are therefore relatively simple, magnetically speaking. Gd is an S-state ion and crystal field effects are consequently very small. These effects are much smaller than the broadened linewidths etc that are encountered in the amorphous state. Crystal field effects on the Gd ion are therefore neglected. The R:(Gd,Ag) series displays an additional feature of fundamental interest, namely that in the crystalline state GdAg is antiferromagnetic (see Köbler *et al* 1981, for example) whereas its amorphous counterpart is ferromagnetic (Boucher 1976).

Turning to practical considerations, the samples were initially prepared by the Southampton group in the form (Gd,Y,Cu) and (Gd,Ag) for magnetization and susceptibility measurements (Lee *et al* 1987), for which bulk samples are required. Although this restriction does not apply to high frequency nmr and Mössbauer spectroscopies, it is nevertheless useful to be able to consult complementary studies. Bulk samples are difficult and expensive to prepare by the sputtering technique; the compositions studied here were chosen because, for them the melt-spinning method was feasible.

It is recognized that metallic glass formation is favoured for compositions near deep eutectics in the equilibrium phase diagram (see

Luborsky 1983, for example). For this reason the compositions were chosen to be $R'_{63}Cu_{37}$, where R' is the total rare-earth plus yttrium content for the R:(Gd,Y,Cu) series, and for the R:(Gd,Ag) series the samples centred around $R'_{40}Ag_{60}$. It has been established (Rainford *et al* 1982) that $Y_{63}Cu_{37}$ is an ideal amorphous matrix. The material can be readily melt-spun to produce amorphous ribbons and when doped with rare earths, electron microprobe studies show no evidence of segregation up to a resolution of approximately 1 $\mu$m.

5.1.1 R:(Gd,Y,Cu) ALLOYS

The precise composition of the alloys studied here is of the form $R_1Gd_xY_{62-x}Cu_{37}$, where R = Ho, Tb, or Pr serve as probe nuclei for nmr experiments, and $Gd_{50}Y_{13}Cu_{37}$ for Mössbauer studies. For the nmr samples, x takes the values 45, 50, and 60. From the low field ac susceptibility meaurement of Mohammed and Lanchester (1986), compositions with x $<$35 appear to behave as spin glasses whereas for x $>$35 the samples behave increasingly like ferromagnets. Additional evidence from magnetization measurements (Lee *et al*, 1987) shows that even samples with the highest concentrations of Gd are not simple ferromagnets. The origin and nature of spin glass-like behaviour in magnetically concentrated samples has been shown (Mohammed and Lanchester 1986) to be well described by the cluster mean-field theory (Soukoulis 1978). It has already been noted in chapter 3 that on the basis of the experimental measurements presented here it is not possible to differentiate between long-range ferromagnetic order and correlated clusters; therefore no further attempt will be made to comment on the validity of the correlated cluster model.

5.1.2 R:(Gd,Ag) ALLOYS

Existing information relating to (Gd,Ag) alloys is based on samples produced by sputtering (Charles *et al* 1973). The advantages and disadvantages of experimentation on sputtered films are

well-illustrated by the work of Hauser (1975). Hauser was able to measure transition temperatures, but failed to determine the nature of the magnetically ordered state. A plot of the transition temperatures as a function of composition is shown in figure (5.1). Unfortunately sample preparation proved to be a problem because of the limited range of compositions that can be accessed by melt-spinning. Only alloys in the intermediate composition range (see figure (5.1)) have been studied; repeated attempts to produce amorphous alloys in the spin-glass and ferromagnetic regions failed.

An extensive study of amorphous and crystalline $Gd_xY_{50-x}Ag_{50}$ alloys, where x = 20, 30, and 50 has been made by means of $^{155}Gd$ Mössbauer spectroscopy and magnetization measurements (Jeandey *et al* 1986). They found that in amorphous alloys $Gd_{50}Ag_{50}$ the total hyperfine field, $B_{hf}$, is substantially larger than in the crystalline compound GdAg, although for the samples with smaller concentrations of Gd there is closer agreement. From a linear extrapolation of the concentration dependence of the hyperfine fields $B_{hf}(x)$ measured in crystalline alloys Jeandey *et al* (1986) have obtained $|B_{hf}(x = 0)| = 22 \pm 1$ T. From this figure they derive a value for the transferred hyperfine field, $B_n$, of 11 T, the magnitude of which agrees well with the result derived by Goebel and Dormann (1979) from nmr measurements of $^{139}La$ in crystalline $Gd_{50-x}La_xAg_{50}$; the sign however is just the opposite. The value of the transferred hyperfine field is of considerable importance in the interpretation of the work presented in this chapter; it is as well to note the disagreement.

## 5.2 SAMPLE PREPARATION

The production of amorphous ribbons was a two stage process; firstly, polycrystalline alloys were fabricated by melting together appropriate quantities of the constituent elements in an argon arc-furnace. Each button was turned over and remelted three

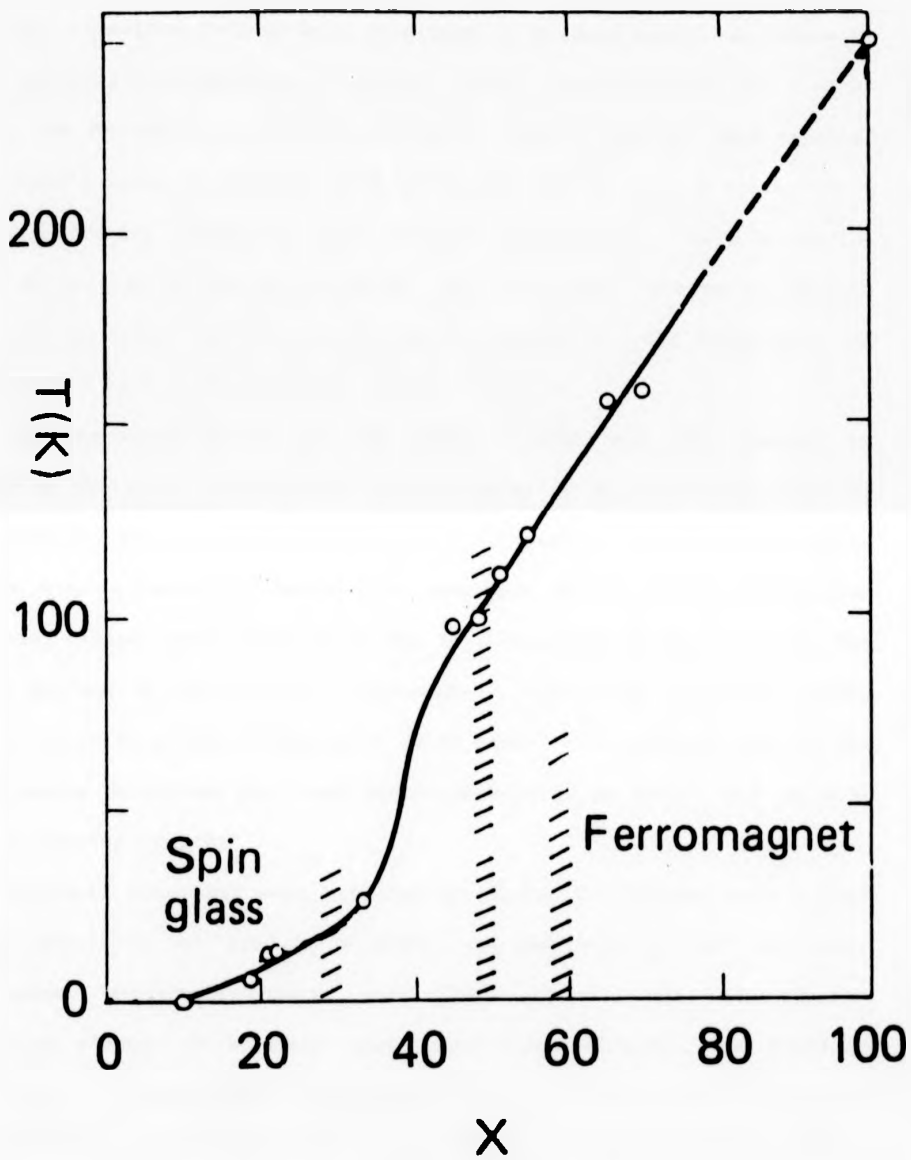


Figure (5.1) Magnetic ordering temperatures determined for amorphous $Gd_xAg_{1-x}$ (Hauser 1975, Boucher 1976).

times in an effort to promote homogeneity. The loss in the total mass after alloying was less than 0.1 % and this has been taken as justification for assuming that the proportion of elements in the final amorphous samples was the same as that of the starting mixture.

The arc-melted buttons were then used to produce amorphous ribbon by melt spinning (Lierbermann and Graham 1976). Approximately 0.5 g of an alloy was melted by r.f induction in a quartz crucible and expelled immediately under a pressure of 5 to 10 psi of high purity argon onto a rapidly rotating (4000-6000 rpm), massive copper wheel. In this way the melt solidifies sufficiently rapidly for amorphous ribbons to result. The samples used in this study were prepared at the University of Southampton by K.A Mohammed and S.H Kilcoyne.

The amorphous nature of the ribbons used here was checked by studying the X-ray diffraction pattern using Cu $K_\alpha$ radiation; most of the patterns show a single broad peak. For some of the thicker ribbons a few weak crystalline peaks were observed in the X-ray diffraction pattern. These were found to be due to a thin crystalline crust on the upper surface of the ribbons. Fortunately, this crust could be removed simply by rubbing the surface with emery paper. The ribbons used in the experiments described here were approximately 25 $\mu$m thick, 2-5 mm wide and of varying lengths.

Mössbauer absorbers were prepared by gluing the ribbons onto a flat paper substrate to produce a sheet approximately 4 $cm^2$ in area. Subsequent "amorphous sheets" were glued on top; the axes of the amorphous ribbons in adjacent layers were perpendicular, thus avoiding any holes in the absorber that would allow $\gamma$-rays to pass straight through and cause problems in the statistics of the counting process. Finally, a circular disc was cut from the composite absorber and mounted in a holder using epoxy resin to reduce unwanted vibrations.

Samples for high frequency nmr measurements contain much less

material (less than 1 g) and are more readily fabricated than those required for Mössbauer experiments. A small amorphous ribbon, which had been checked by X-ray diffraction and found to be non-crystalline, was cut into small pieces (less than 1 $mm^2$) and glued randomly onto the stainless-steel central conductor of a resonant cavity.

## 5.3 EXPERIMENTAL PROCEDURE AND RESULTS

$^{155}$Gd Mössbauer spectra were taken for $Gd_{50}Y_{13}Cu_{37}$ and $Gd_{30}Ag_{70}$ in zero field and in an applied field of 6 T, at 4.2 K. A spectrum also was taken for $Gd_{30}Ag_{70}$, above its Curie temperature, at 46 K (Shah *et al* 1986). In addition to the usual constraints imposed by studying amorphous samples, the high-temperature Mössbauer experiment involved extra difficulties. At 46 K the recoil-free fraction is greatly reduced and therefore long counting times, approximately 3 weeks, are necessary to achieve an acceptable signal to noise ratio. The temperature of the cryostat had to be controlled for this period of time.

Nmr measurements on the fast-relaxing rare-earth nuclei were carried out in the frequency range 3 to 7.3 GHz in magnetic fields up to 8 T at 1.3 K. Fast spin-spin relaxation (approximately 300 ns) necessitated minimum pulse separation (of the order of 200 ns) and the lowest temperature (1.3 K) attainable on the Manchester spectrometer. It should be noted that the priority of the nmr experiments was to obtain spectroscopic information. Relaxation phenomena were investigated purely to provide diagnostic information and therefore will only be mentioned in passing.

### 5.3.1 AMORPHOUS R:(Gd,Y,Cu) ALLOYS

$^{155}$Gd Mössbauer spectra were taken for $Gd_{50}Y_{13}Cu_{37}$ at 4.2 K in zero field and an applied field of 6 T (see figure (5.2)). It is clear that the application of a 6 T applied field has very little effect on the spectrum, as evidenced by the super-

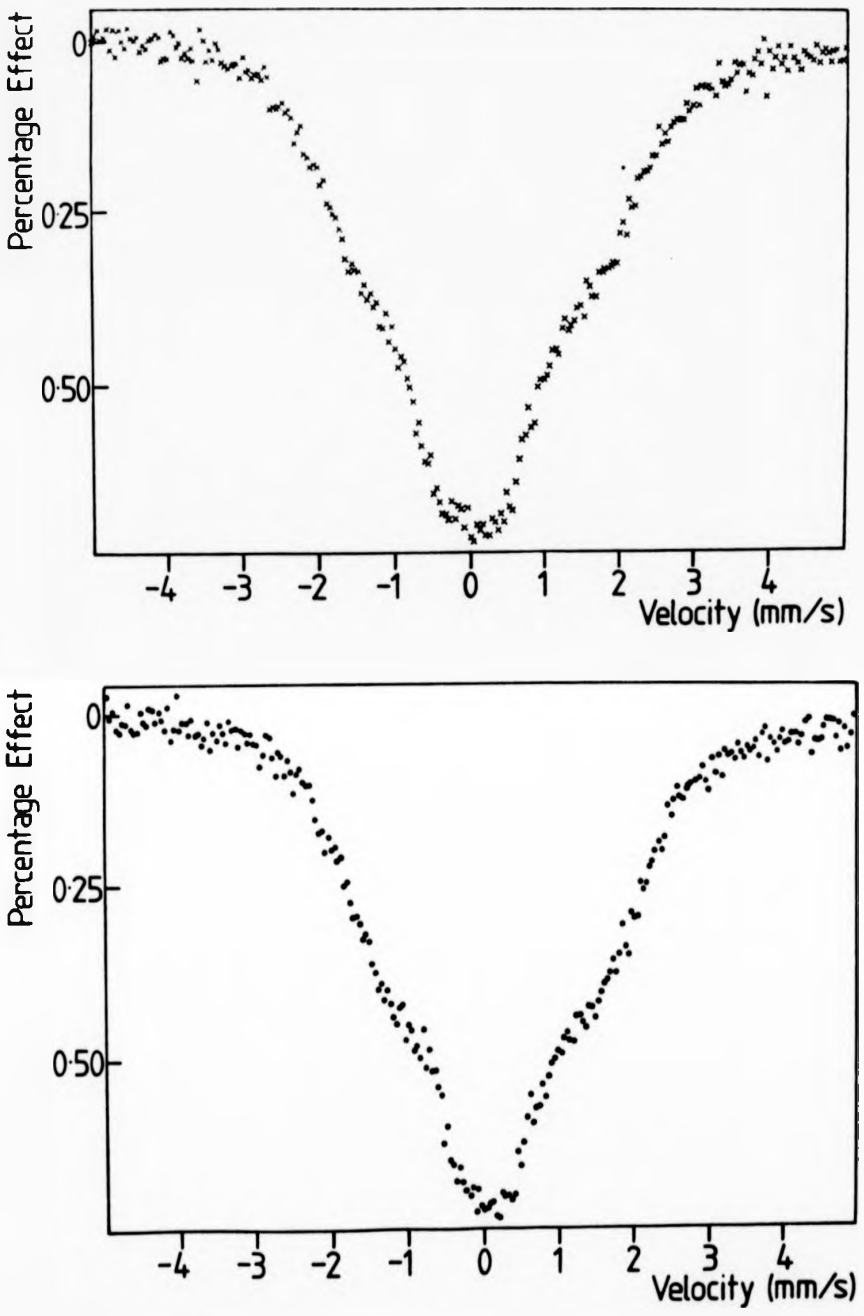


Figure (5.2) $^{155}$Gd Mössbauer spectra of $Gd_{50}Y_{13}Cu_{37}$ at 4.2 K. The crosses represent zero-field data and the dots 6 T applied-field data.

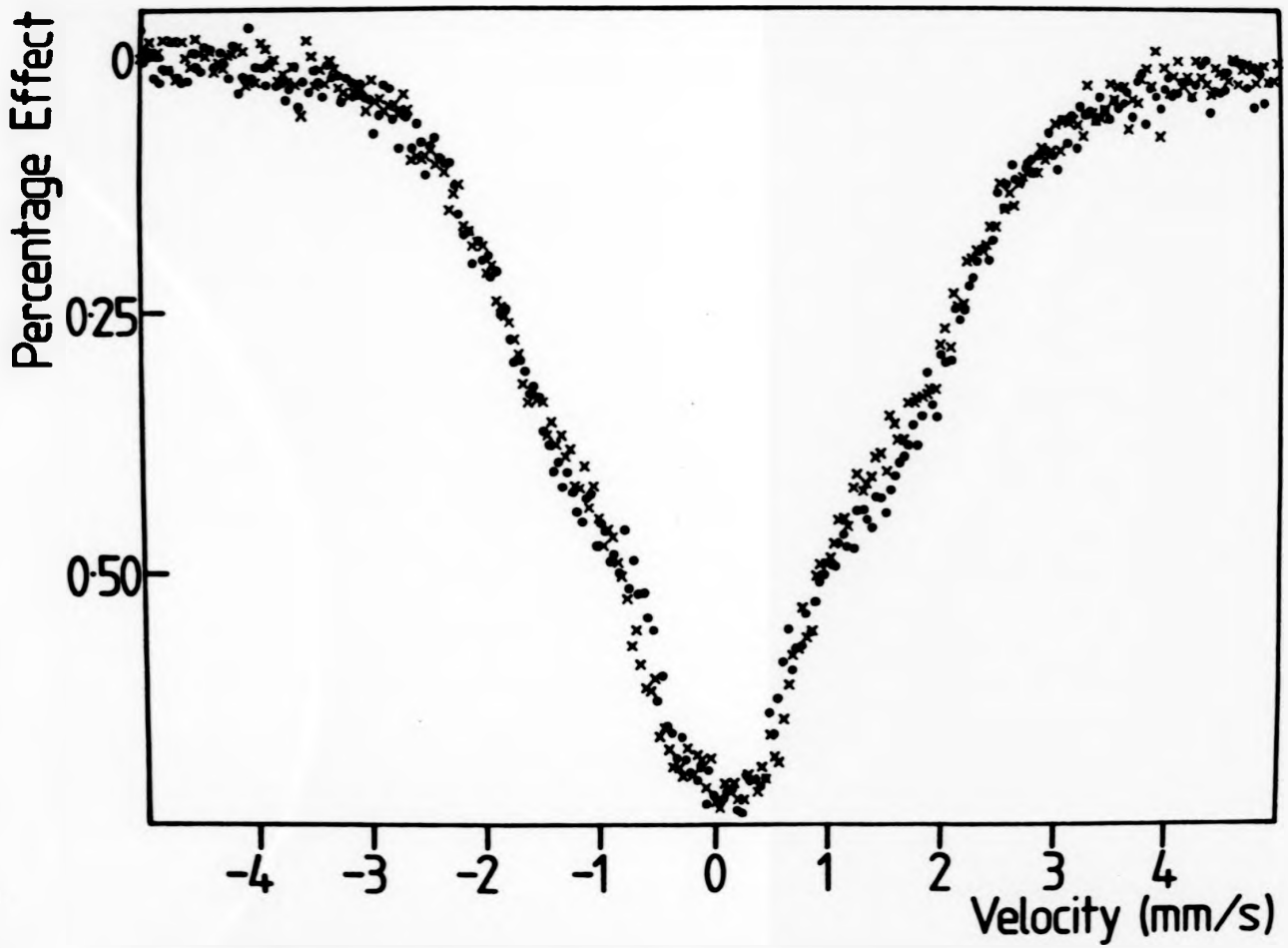


**Figure (5.3)** The superposition of the two spectra show in figure (5.2) indicating very weak field dependence.

position of zero and applied field data (see figure (5.3)).

It was not possible to fit accurately the Mössbauer spectra with a unique hyperfine field and fixed line intensity ratios. Fitting of $^{155}Gd$ Mössbauer spectra to obtain a hyperfine field distribution is a non-trivial task since the nuclear quadrupole and magnetic dipole interactions are of similar magnitude. Analysis of the data using a fitting procedure containing a number of discrete values of the hyperfine field is a rather fruitless exercise because of the large number of parameters involved, and was therefore not attempted.

The zero-field nmr spetra for the three alloys in the Ho:(Gd,Y,Cu) series (one is illustrated in figure (5.4)) are all broad and unresolved with a centroid at 6360 ±50 MHz and a width of 600 to 700 MHz. Field behaviour is composition independent; the results for $Ho_1Gd_{60}Y_2Cu_{37}$ are shown in figure (5.5). Application of a 4 T field has a very small effect on both the centroid and the width of the spectra, although an 8 T field causes the centroid to move up in frequency by approximately 50 MHz, leaving the width unchanged. If there is any compositional dependence, it is obscured by broadening effects (see figure (5.5)).

The $^{165}Ho$ nmr results can be interpreted in the scheme developed in chapter 2, where the resonant frequency is given by:

$$\nu_{m,m-1} = |a_t+(2m-1)P_t| \qquad (2.48)$$

As indicated in chapter 2, both $a_t$ and $P_t$ can be separated into intra-ionic (dependent on $\langle J_z \rangle$ and $\langle J_z^2 \rangle$, respectively) and extra-ionic terms. Single prime denotes the intra-ionic and double prime the extra-ionic contribution. In a crystalline compound with cubic symmetry and the Ho ions in a fully polarised state, $|J, J_z = \pm J\rangle$, $a_t \propto a' \propto a_0' = 6497$ MHz (extra-ionic contributions are two orders of magnitude smaller) and $P_t \propto P' \propto P_0' \propto 63$ MHz, (where $a_0'$ and $P_0'$ are the fully polarized free ion

position of zero and applied field data (see figure (5.3)).

It was not possible to fit accurately the Mössbauer spectra with a unique hyperfine field and fixed line intensity ratios. Fitting of $^{155}Gd$ Mössbauer spectra to obtain a hyperfine field distribution is a non-trivial task since the nuclear quadrupole and magnetic dipole interactions are of similar magnitude. Analysis of the data using a fitting procedure containing a number of discrete values of the hyperfine field is a rather fruitless exercise because of the large number of parameters involved, and was therefore not attempted.

The zero-field nmr spetra for the three alloys in the Ho:(Gd,Y,Cu) series (one is illustrated in figure (5.4)) are all broad and unresolved with a centroid at 6360 ±50 MHz and a width of 600 to 700 MHz. Field behaviour is composition independent; the results for $Ho_1Gd_{60}Y_2Cu_{37}$ are shown in figure (5.5). Application of a 4 T field has a very small effect on both the centroid and the width of the spectra, although an 8 T field causes the centroid to move up in frequency by approximately 50 MHz, leaving the width unchanged. If there is any compositional dependence, it is obscured by broadening effects (see figure (5.5)).

The $^{165}Ho$ nmr results can be interpreted in the scheme developed in chapter 2, where the resonant frequency is given by:

$$\nu_{m,m-1} = |a_t+(2m-1)P_t| \qquad (2.48)$$

As indicated in chapter 2, both $a_t$ and $P_t$ can be separated into intra-ionic (dependent on $\langle J_z \rangle$ and $\langle J_z^2 \rangle$, respectively) and extra-ionic terms. Single prime denotes the intra-ionic and double prime the extra-ionic contribution. In a crystalline compound with cubic symmetry and the Ho ions in a fully polarised state, $|J, J_z = \pm J\rangle$, $a_t \approx a' \approx a_0' = 6497$ MHz (extra-ionic contributions are two orders of magnitude smaller) and $P_t \approx P' \approx P_0' \approx 63$ MHz, (where $a_0'$ and $P_0'$ are the fully polarized free ion

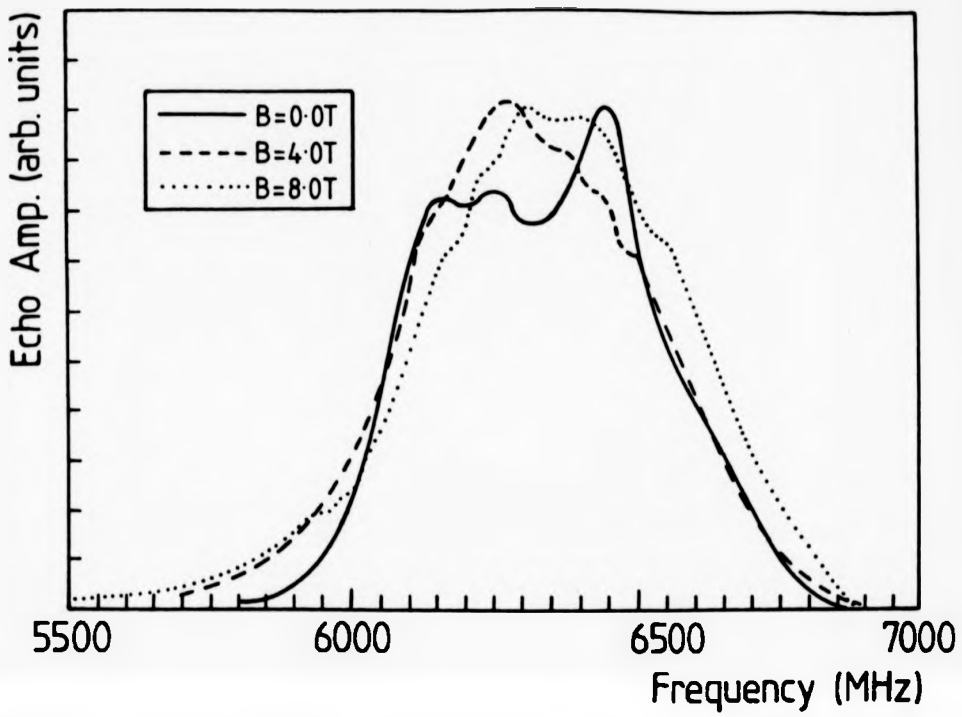


Figure (5.4) Ho nmr spectra of $Ho_1Gd_{60}Y_2Cu_{37}$ at 1.3 K, showing field dependence.

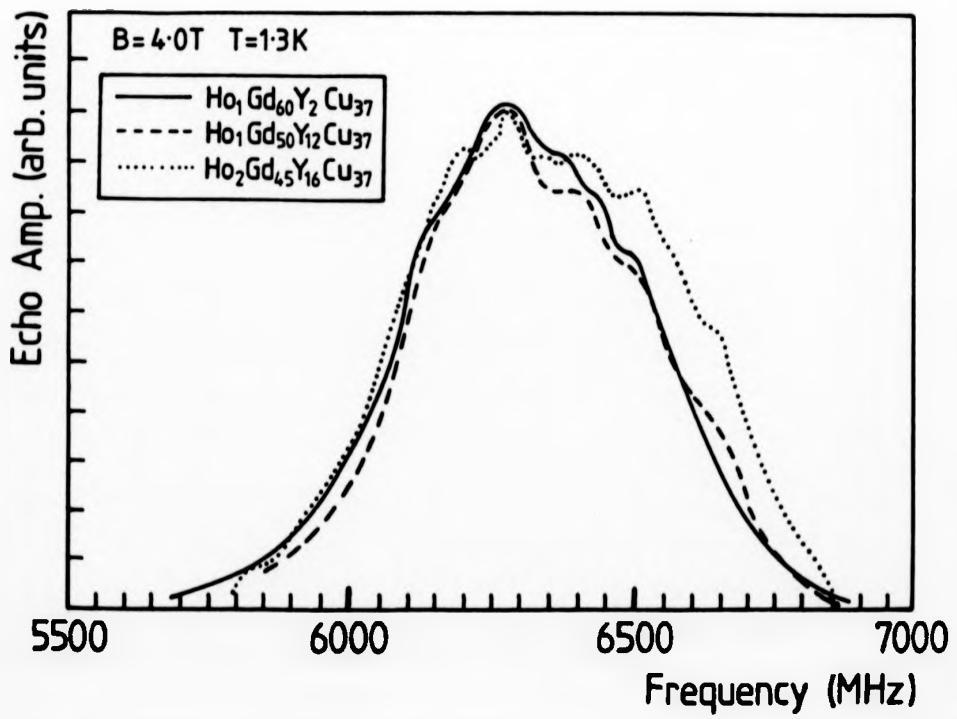


Figure (5.5) Composition dependence of the Ho nmr spectra for Ho:(Gd,Y,Cu) at 1.3 K in a field of 4 T.

parameters (Bleaney 1972)). For such a material, the nmr spectrum is a seven line pattern with a central frequency of $a_t$, each line being approximately 20 MHz wide and separated by 126 MHz. Comparing this with the observed spectra we see that the multiplicity of Ho environments in the amorphous samples has led to a "smearing out" of the individual lines. However, the centroid at 6360 MHz is within 2 % of the value expected if all the Ho ions are in the fully polarised electronic state. This difference could be accounted for by the extra-ionic contribution to $a_t$ due to the transferred hyperfine field ($B_n''$) from neighbouring Gd ions together with the hyperfine field due to the polarization of the conduction electrons by the parent holmium moment ($B_p''$). The values of $B_n''$ and $B_p''$ are not known in amorphous R:(Gd,Y,Cu) alloys but in crystalline antiferromagnetic GdAg, $B_n''$ = -9.73 ±0.03 T (Goebel and Dormann 1979). The difference between $a_t$ as measured and that as calculated suggests that $B''$ at the Ho nucleus in amorphous Ho:(Gd,Y,Cu) is approximately -15 ±5 T, if the Ho ions are assumed to be in a fully polarized state.

The quadrupole interaction does not affect the centroid of the nmr spectrum but a distribution of electronic field gradients would broaden the lines to give unresolved spectra as observed. If this is the result of only the extra-ionic quadrupole contribution changing from site to site then we can estimate the magnitude of line shifts from the high temperature $^{155}$Gd Mössbauer result (see section 5.3.2). The value of $V_{zz}$ at the $^{155}$Gd nucleus obtained from the Mössbauer fit is due to the extra-ionic contribution only (since $^{155}$Gd is an S-state ion). The Sternheimer antishielding factor is approximately constant for the lanthanides and it is therefore assumed that the extra-ionic contribution to $V_{zz}''$ at the $^{165}$Ho nucleus in $Ho_1Gd_{39}Ag_{60}$ is similar to that at the $^{155}$Gd nucleus. $V_{zz}$ of magnitude 4.5 x $10^{21}$ $Vm^{-2}$ leads to a $|P''|$ of 10 MHz for the $^{165}$Ho nucleus. The reduced width of the spectra

indicates that $V''_{zz}$ is negative. The central line (m = 1/2) of the nmr spectrum is unaffected by $P_t$. Since there is a distribution of $V_{zz}$ a corresponding distribution in $P_t$ is expected. Equation (2.48) shows that the quadrupole splittings, from the centre, are $2P_t$, $4P_t$, and $6P_t$. The distribution in $P_t$ ensures that the outer lines will be more smeared than the inner lines. This mechanism is sufficient to cause a total smearing of the wings of the spectrum but it leaves structure in the centre. Thus, it may be concluded that the extra-ionic contribution to $P_t$ alone is not sufficient to cause the required broadening of the seven line spectrum.

The absence of a resolved central resonance line indicates that a distribution of transferred hyperfine fields ($B''_n$) together with a distribution of $P_t$ is probably responsible for the unresolved nature of the spectra.

Due to a lack of knowledge of the extra-ionic magnetic hyperfine fields in amorphous R - noble metal alloys, the possibility that slight quenching of $J_z$ (approximately 2 %) might occur cannot be neglected. If the width of the distribution of $\langle J_z \rangle$ is also roughly 2 % the spectra would be as observed. (Computer calculations show that quenching will significantly affect the off-diagonal terms in the quadrupole interaction (Prakash 1985).)

Both interpretations, however, show that the nmr data qualitatively support the HPZ model for non-Kramers ions with large total angular momentum, such as Ho (J=8), in amorphous alloys.

The nuclear spin of $^{159}$Tb, I = 3/2, ensures that for a given set of hyperfine parameters the nmr spectrum consists of three lines. Unfortunately, due to the restricted range of the spectrometer, it was possible to obtain the resonant frequencies of the upper two lines only. The limitations imposed by this condition are not too severe in that it is still possible to obtain the total magnetic hyperfine parameter $a_t$

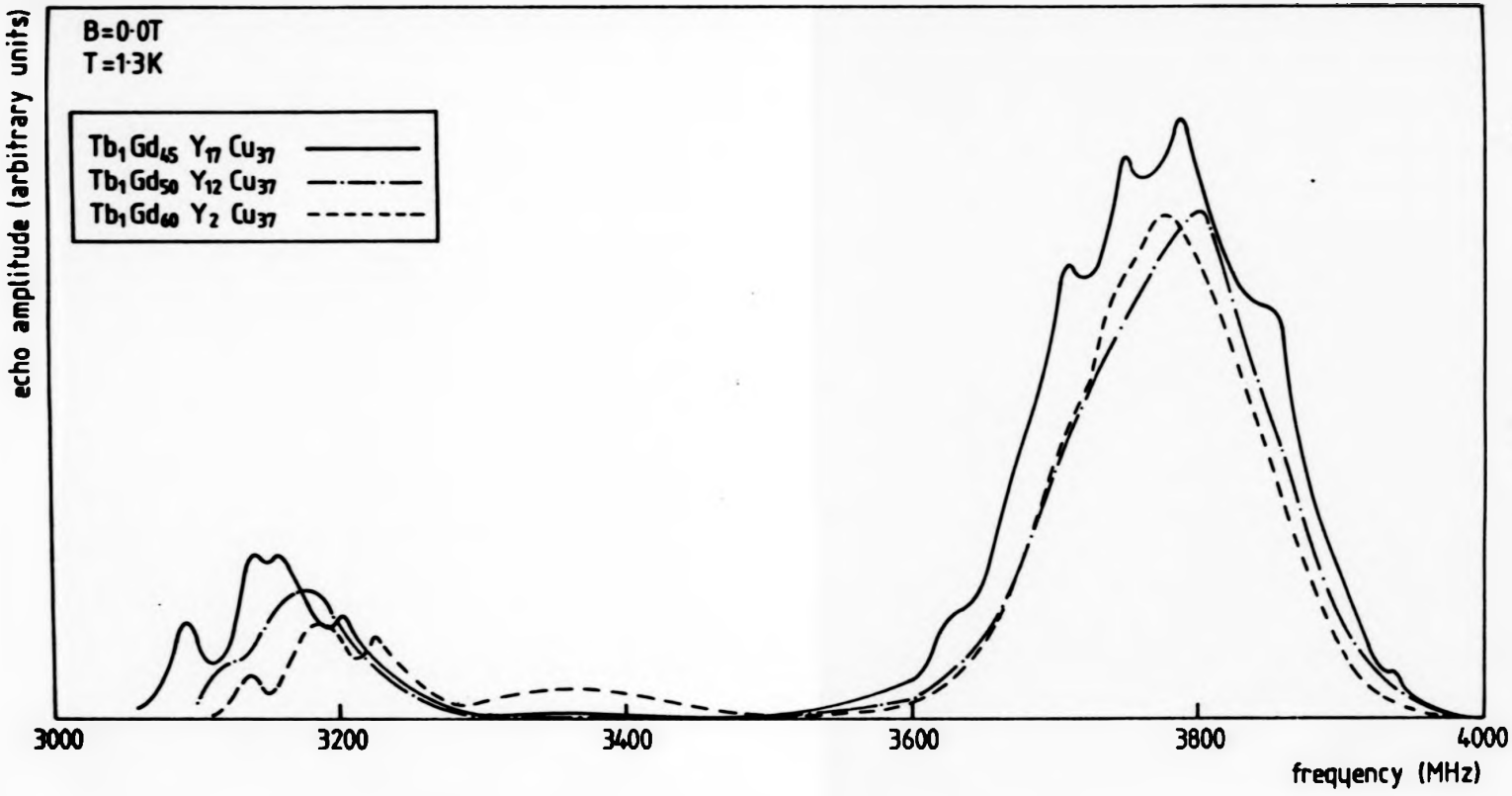


**Figure (5.6)** Composition dependence of the Tb nmr spectra for Tb:(Gd,Y,Cu) at 1.3 K in zero applied field.

and the total nuclear quadrupole parameter $P_t$. The zero-field spectra for the Tb:(Gd,Y,Cu) series are shown in figure (5.6).

The results show the central and upper lines which are well resolved but are nevertheless significantly broadened. The degree of resolution is a direct consequence of the large nuclear quadrupole moment interacting with the e.f.g. There is an increase in the value of $a_t$ as the concentration of Gd increases, although the systematic increase in $a_t$ is not accompanied by a similar change in $P_t$.

Field-dependent behaviour is shown in figure (5.7) for the $Tb_1Gd_{45}Y_{17}Cu_{37}$ composition. The spin-echo signal decreased rapidly with applied field and it was therefore not possible to make measurements in a field of greater than 2 T. The applied field leads to an increase in the frequency of the upper line of about 20 MHz; this is in good agreement with the expected gyromagnetic shift, 10.1 MHz/T, for Tb.

The results quantitatively support the HPZ model in that the Tb ions appear to be nearly fully polarized (see table 5.1). Although the measured value of $P_t$ is significantly reduced from that calculated, it should be noted that $P''$ has been calculated using $V_{zz}''$ obtained for amorphous $Gd_{30}Ag_{70}$ and should therefore be regarded as only a very rough indication of the true value.

| Composition | $a_t$(meas.) | $2P_t$(meas.) | $P_0'$ | $P''$ | $2P_t$(calc.) |
|---|---|---|---|---|---|
| $Tb_1Gd_{45}Y_{17}Cu_{37}$ | 3170 (15) | 630 (30) | 386 (20) | -40 (4) | 692 (24) |
| $Tb_1Gd_{50}Y_{12}Cu_{37}$ | 3180 (15) | 575 (30) | " | " | " |
| $Tb_1Gd_{60}Y_2Cu_{37}$ | 3200 (15) | 605 (30) | " | " | " |

TABLE 5.1 Calculated and measured spectral parameters, in MHz, for the series Tb(Gd, Y, Cu). Errors are given in brackets.

As indicated in chapter 2, the nmr spectrum of $^{141}Pr$ is a single broadened peak for a given set of hyperfine parameters; the nuclear spin of Pr is 5/2 but the very small quadrupole moment ensures that the five

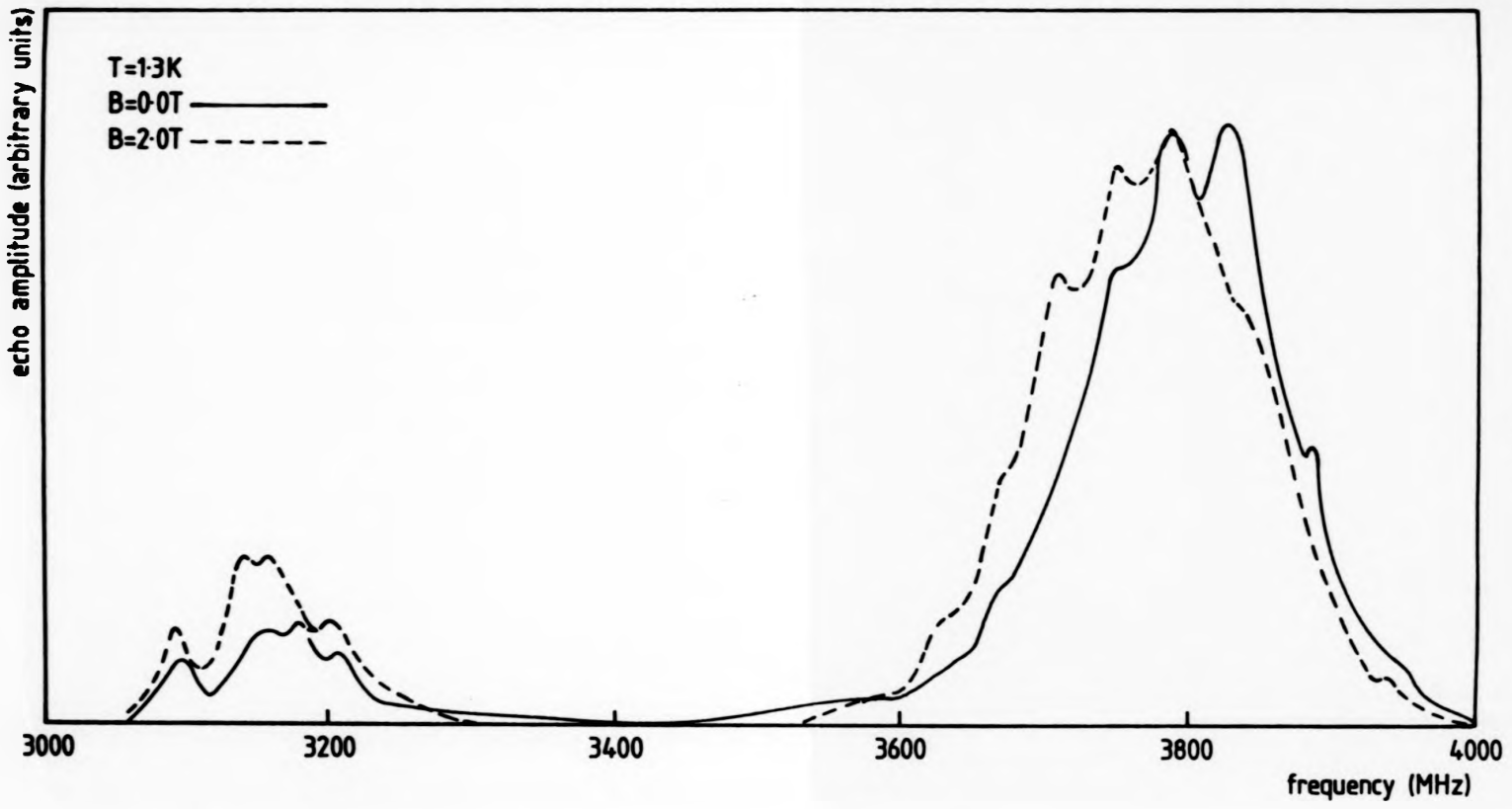


**Figure (5.7)** Tb nmr spectra of $Tb_1Gd_{45}Y_{1,}Cu_{3,}$ at 1.3 K, showing field dependence.

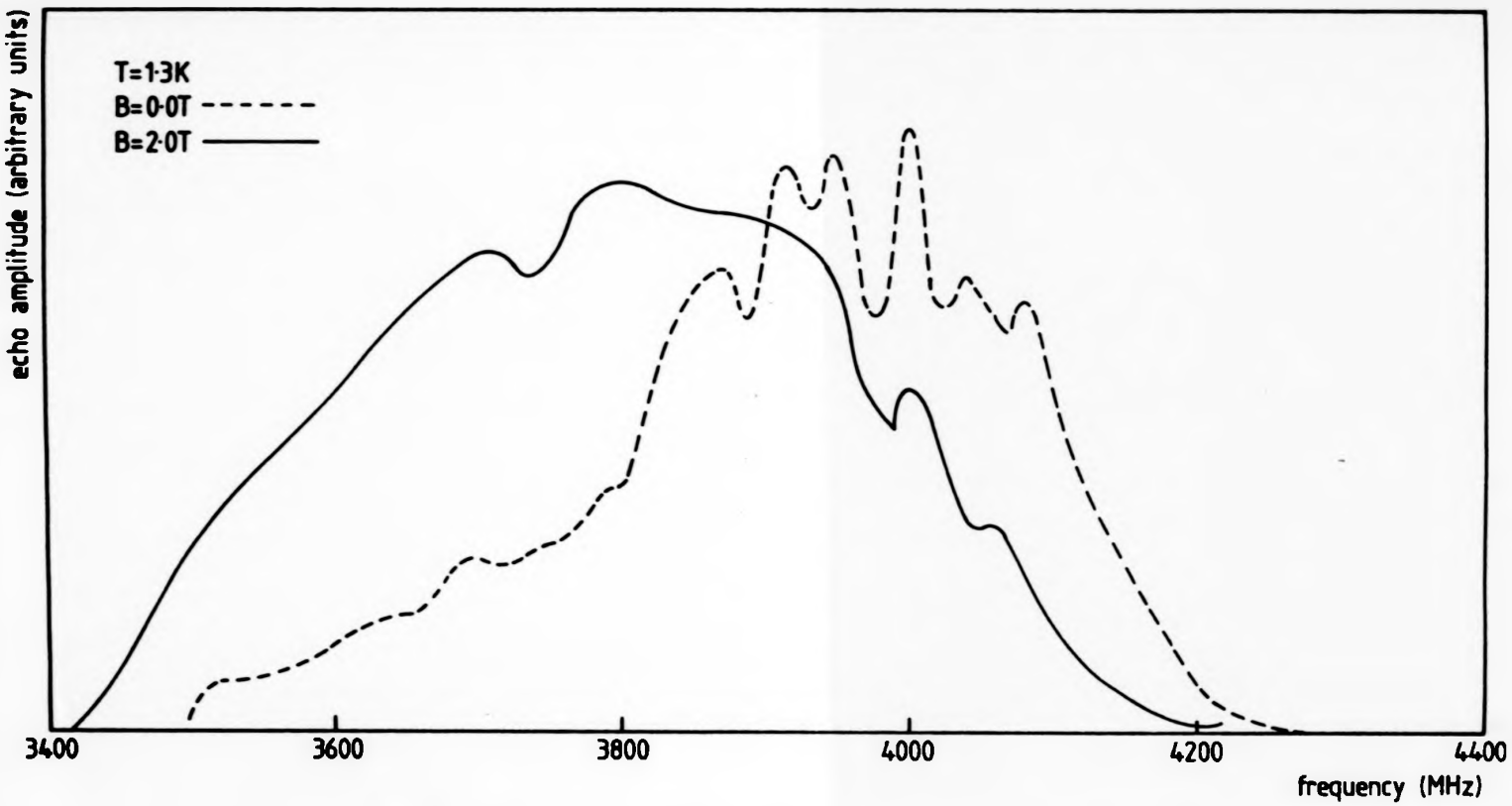


**Figure (5.8)** Pr nmr spectra of $Pr_1Gd_{45}Y_{1,7}Cu_{3,7}$ at 1.3 K, showing field dependence.

transitions are smeared to form one broadened line, of approximately 20 MHz width.

The nmr data for $Pr_1Gd_{45}Y_{17}Cu_{37}$ obtained at 1.3 K in zero field and an applied field of 2 T are shown in figure (5.8). It is evident, from the spread of resonant frequencies, that there is a large distribution of $a_t$ values which implies that there is a corresponding distribution of $J_z$.

Once again field behaviour could not be studied for a wide range of field values due to the rapid reduction of the nmr signal in an applied field. Nevertheless, a spectrum was taken in an applied field of 2 T; the scatter of the echo-amplitude values at low frequency is due to a combination of small signals and a less than optimum spectrometer frequency range. Disappearance of the signal in high fields is probably a result of "domain walls" being swept out. The field behaviour indicates that the probe Pr ions and the host Gd ions are oppositely aligned, as expected with a light rare-earth in a mainly Gd matrix.

5.3.2 AMORPHOUS R:(Gd,Ag) ALLOYS

$^{155}$Gd Mössbauer spectra were taken for $Gd_{30}Ag_{70}$ in zero field and in an applied field of 6 T at 4.2 K. A spectrum was also taken above the Curie temperature, at 46 K, for the same material. The 4.2 K results (see figures (5.9) and (5.10)) are very similar to those obtained for $Gd_{50}Y_{13}Cu_{37}$; the application of a field has no observable effect on the spectra and it was not possible to obtain an adequate fit of the data with a single hyperfine field and fixed line intensity ratios. The Mössbauer results for the two series do differ with regard to their respective halfwidths. The larger halfwidth of the $Gd_{50}Y_{13}Cu_{37}$ indicates larger hyperfine fields and probably a wider distribution thereof.

A fit to the 46 K spectrum (see figure (5.11) yielded a broadened linewidth of 1.17 mm/s, in agreement with Czjzek *et al* (1981) (natural

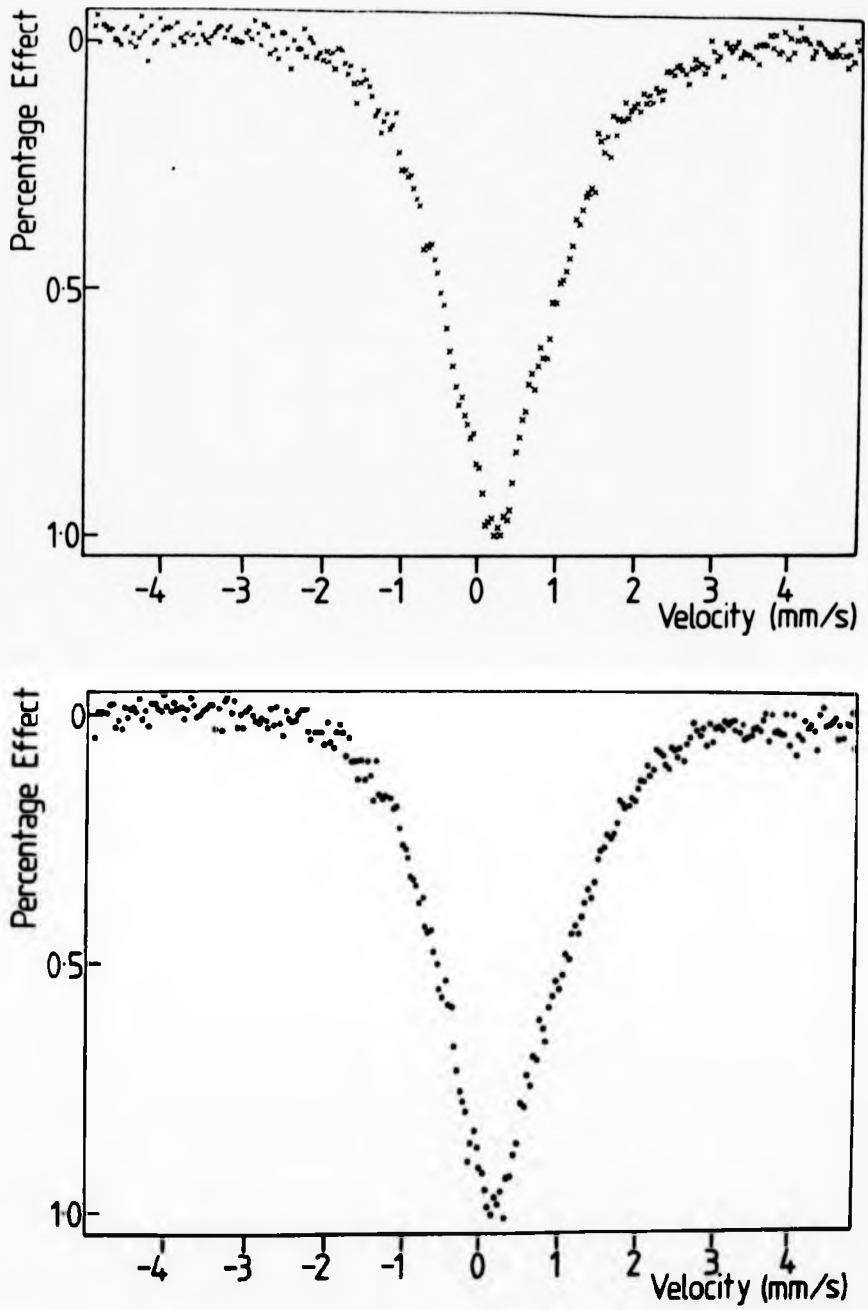


Figure (5.9) $^{155}Gd$ Mössbauer spectra of $Gd_{30}Ag_{70}$ at 4.2 K. The crosses represent zero-field data and the dots 6 T applied-field data.

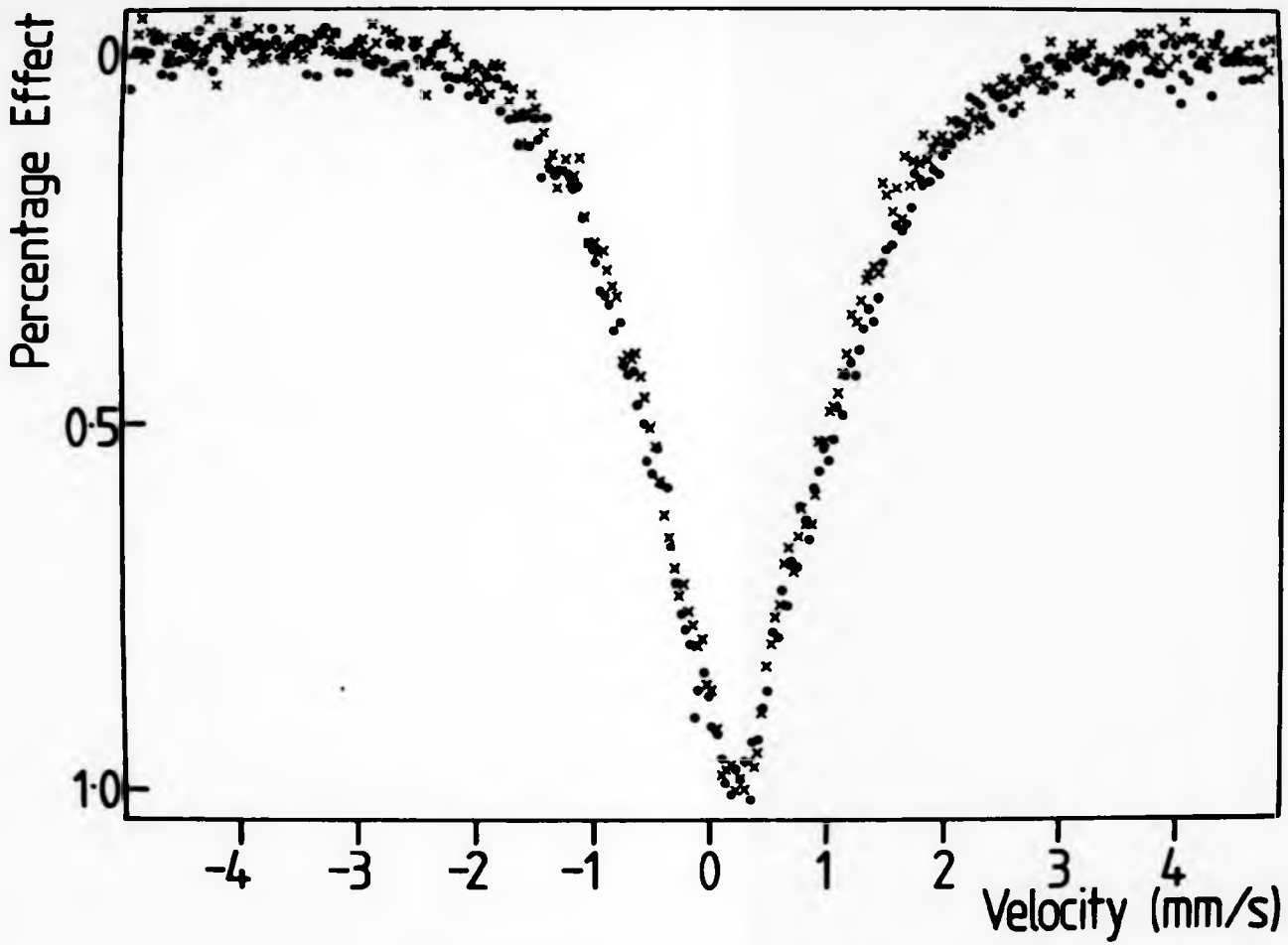


**Figure (5.10)** Superposition of the two spectra shown in figure (5.9) indicating very weak field dependence.

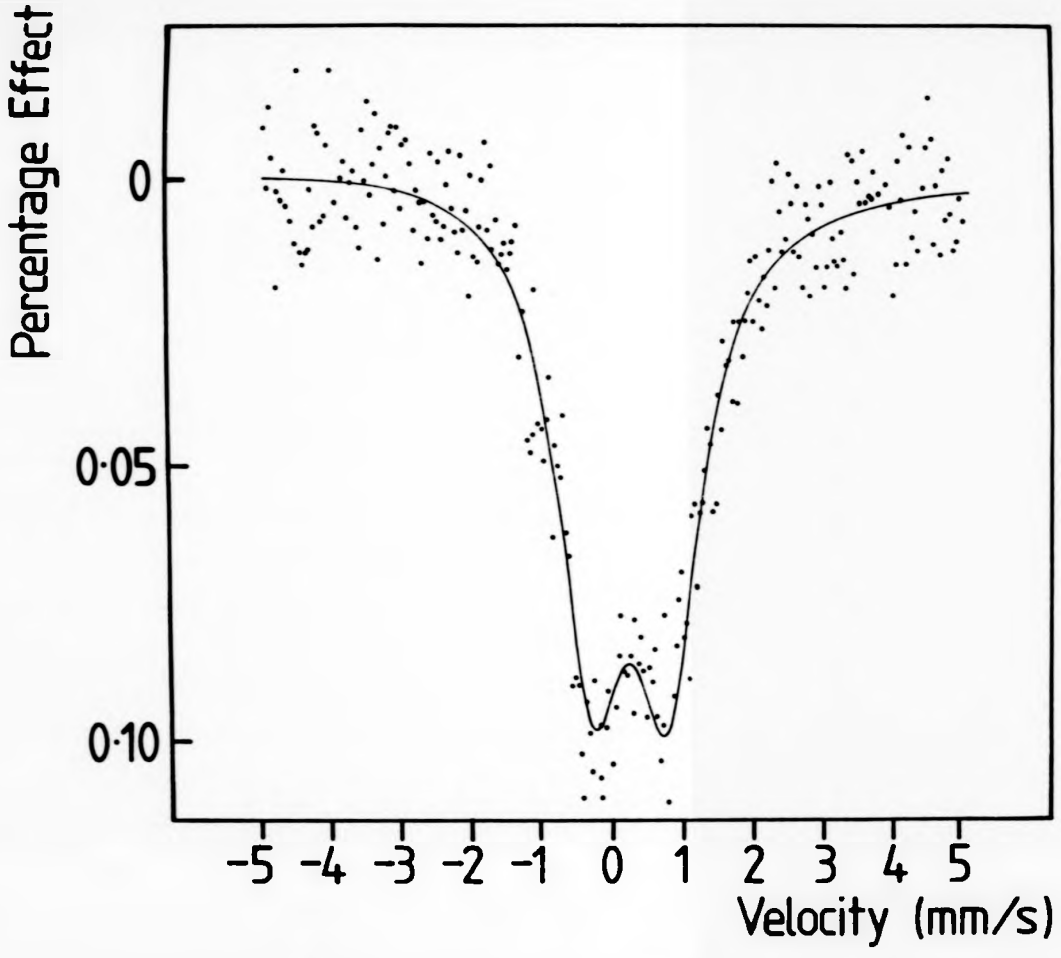


**Figure (5.11)** Mössbauer spectrum of $Gd_{30}Ag_{70}$ at 46 K. The full line represents a least-squares fit with $|V_{zz}| = 4.5 \times 10^{21}$ $Vm^{-2}$.

linewidth is approximately 0.5 mm/s and in a thin crystalline absorber this increases to around 0.65 mm/s) and a value for $|V_{zz}|$ of $4.5 \times 10^{21}$ $Vm^{-2}$. To a first approximation we may assume this is the dominant value of the e.f.g. in the distribution.

A thorough investigation of the R:(Gd, Ag) series has not been possible due to difficulties experienced during the melt-spinning stage. Nmr results are presented for $R_1Gd_{39}Ag_{60}$, where R = Ho and Tb, and $Pr_1Gd_{29}Ag_{70}$. The field behaviour of $Ho_1Gd_{39}Ag_{60}$ is shown in figure (5.12). The zero-field spectrum is broad and unresolved with a centroid at 6350 ±50 MHz; it differs significantly in that there is a "sharp peak" at around 6500 MHz after which the signal falls off rapidly with increasing frequency. The application of a field considerably broadens the spectra thereby obscuring any gyromagnetic shifts that may be present. It is nevertheless fairly clear that the Ho ions are almost fully polarized.

For the other two compositions investigated in the R:(Gd,Ag) series, $Tb_1Gd_{39}Ag_{60}$ and $Pr_1Gd_{29}Ag_{70}$, the nmr spectra are shown in figures (5.13) and (5.14), respectively. The $^{159}Tb$ resonances in $Tb_1Gd_{39}Ag_{60}$ are broad but well resolved. The central-line frequency is 3180 ±10 MHz, indicating that the Tb ions are nearly fully polarized, and the upper-quadrupole satellite has a frequency of 3815 ±10 MHz. The resultant $P_t$ value is slightly larger than that for the R:(Gd,Y,Cu) series . If a negative extra-ionic contribution, P", of magnitude ≈40 MHz is assumed (calculated from the high temperature Mössbauer spectrum obtained for $Gd_{30}Ag_{70}$) then P', the intra-ionic contribution to $P_t$, agrees well with the free-ion value $P_0'$. This lends further support to the proposition that the Tb ions are nearly fully polarized.

The $^{141}Pr$ nmr spectrum for $Pr_1Gd_{29}Ag_{70}$ is shown in figure (5.14). The width indicates a distribution of $a_t$ values, which corresponds to a similar distribution in $\langle J_z \rangle$. The reduction in the echo amplitude below

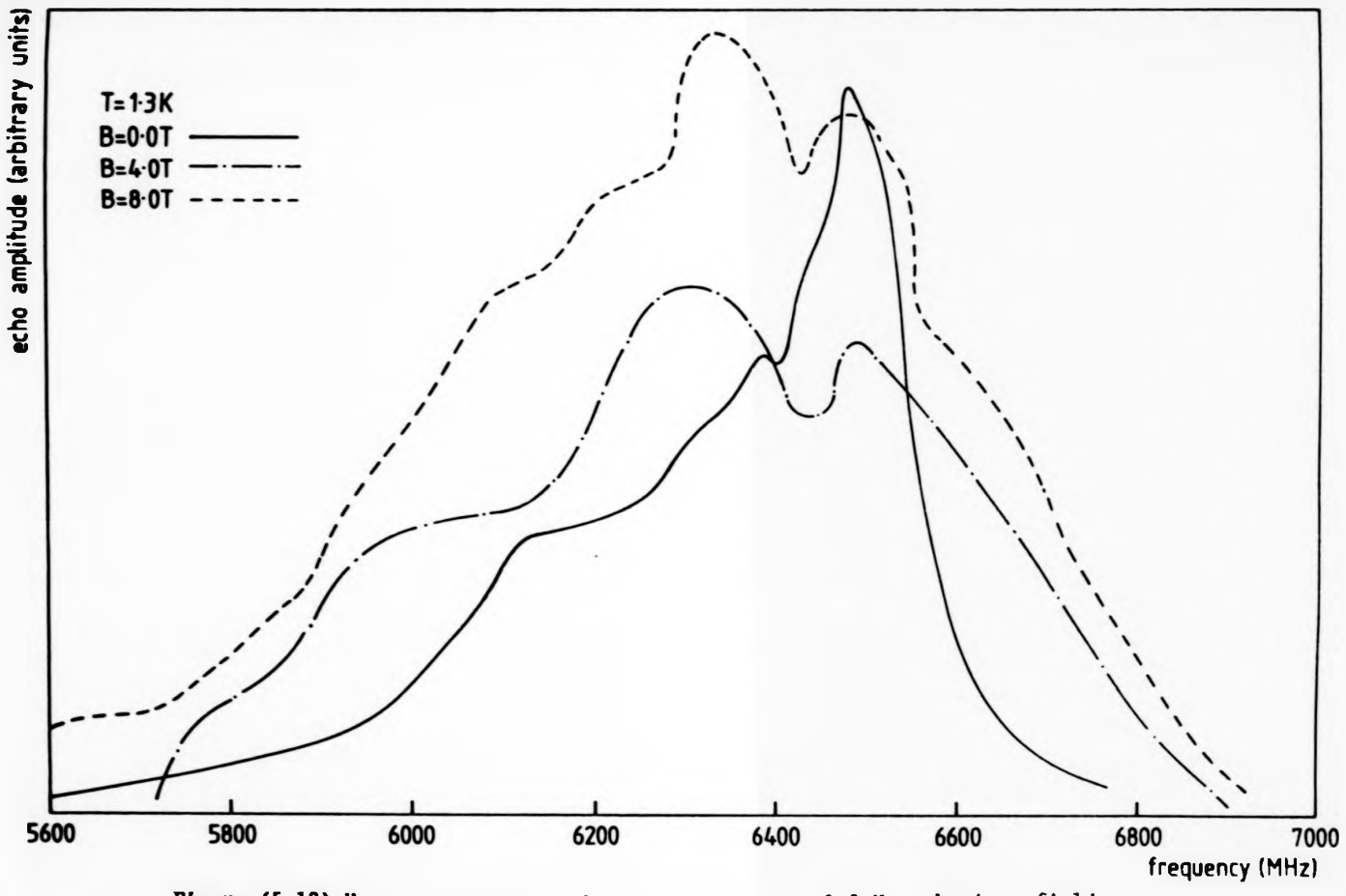


**Figure (5.12)** Ho nmr spectra of $Ho_1Gd_{39}Ag_{60}$ at 1.3 K, showing field dependence.

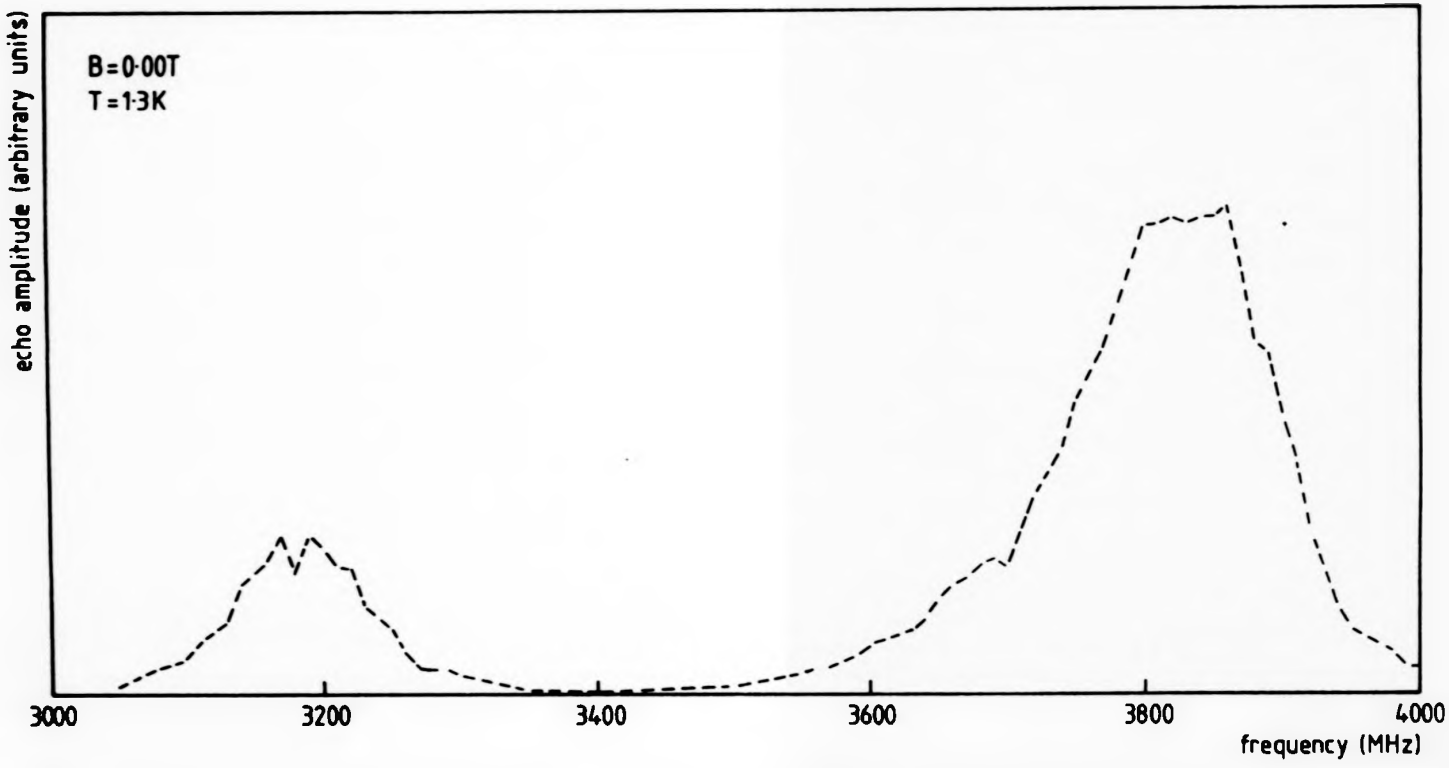


**Figure (5.13)** Zero-field Tb nmr spectrum of $Tb_1Gd_{39}Ag_{60}$ at 1.3 K.

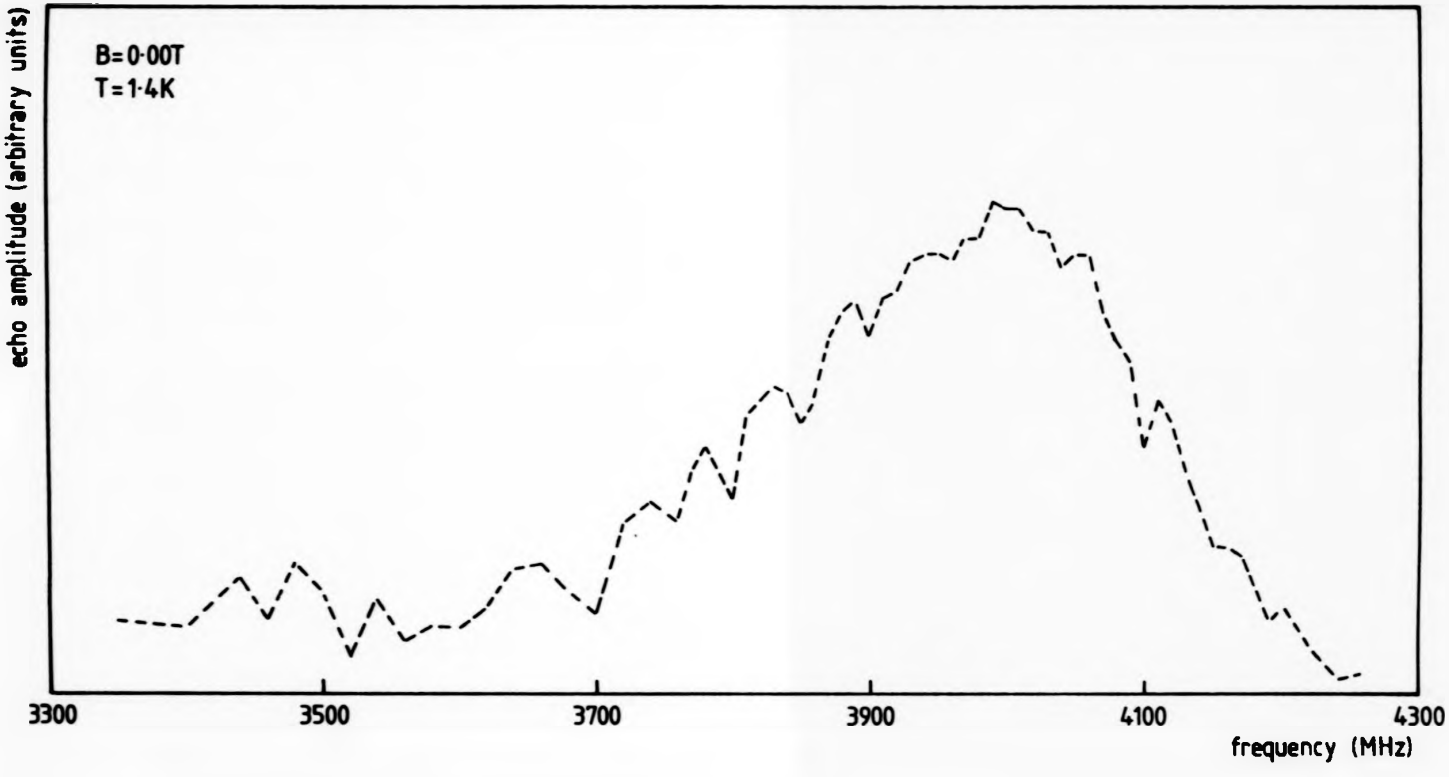


**Figure (5.14)** Zero-field Pr nmr spectrum of $Pr_1Gd_{29}Ag_{70}$ at 1.3 K.

4000 MHz is due to a fall-off in the sensitivity of the receiver and the power output of the TWT amplifier together with any genuine signal loss. The resonant frequency of a Pr ion in a fully polarized state is 4372 MHz. The fact that there is no signal above 4250 MHz indicates that virtually all sites are quenched to some degree; any extra-ionic contributions to $a_t$, $B_n''$ for instance, are expected to increase the frequency of resonance and so cannot be responsible for the reduced resonant frequencies observed.

## 5.4 DISCUSSION AND CONCLUSIONS

As discussed in chapter 3, for non-Kramers' ions with large values of J, the HPZ model predicts that the ground state is the doublet $|J,J_z = \pm J\rangle$. The doublet persists for most of the range of $\eta'$ ($\eta'$ varies between uniaxial limits (see chapter 3 for a detailed account)). For large values of J, as in Ho (J = 8), for example, the majority of the rare-earth ions are expected to be in a fully polarized state. For smaller values of J, a significant number of sites are expected to be in a less than fully polarized ground state.

The nmr results presented in this chapter have been obtained using three probe nuclei, Ho (J = 8), Tb (J = 6) and Pr (J = 4), which have resonant frequencies accessible using the Manchester spectrometer. $^{165}$Ho and $^{159}$Tb nmr results clearly indicate that the rare-earth ions are in a nearly fully polarized ground state. A lack of detailed knowledge of extra-ionic contributions precludes an exact determination of $\langle J_z \rangle$ but nevertheless an upper limit of 2 % can be placed in the amount of quenching of $\langle J_z \rangle$ in all cases where the rare earth is Ho or Tb. If, in a given composition, the rare-earth probe is Pr then it is evident that there is a distribution of $\langle J_z \rangle$ values, as expected from the predictions of the HPZ model.

The applied field behaviour of the Ho:(Gd,Y,Cu) compositions is rather unusual in that no gyromagnetic shift of the resonant frequencies

is observed. Mössbauer measurements as a function of applied field in $Gd_{50}Y_{1,}Cu_{3,}$ confirm this behaviour. When the Ho probe is replaced by Tb or Pr then the compositions display the usual gyromagnetic shift.

$^{155}Gd$ Mössbauer spectra for $Gd_{30}Ag_{70}$ also appear to be field independent. It has not been possible to confirm this behaviour using nmr for two reasons: firstly, sample preparation has proved to be a major obstacle; only some of the compositions in the R:(Gd,Ag) series have been investigated, and secondly, a broadening of the nmr spectrum of $Ho_1Gd_{39}Ag_{60}$ in applied field has masked any gyromagnetic shift that may be present. Finally, it should be mentioned that the application of a field greater than 2 T in amorphous compositions containing Tb of Pr as probe nuclei has resulted in the reduction of the echo signal by an order of magnitude or more.

The field-dependence of the nmr and Mössbauer measurements reported here cannot be explained in an obvious and straightforward manner. It may perhaps be possible to understand this behaviour by studying a series of heat-treated alloys ranging from totally amorphous to completely crystalline.

Examination of the form of equation (2.48) reveals that for the central line of an nmr spectrum $P_t$ (and hence $V_{zz}$) is not involved in its frequency. It is clear, therefore, that the width of the central line is determined entirely by the distribution of $a_t$ and therefore of $\langle J_z \rangle$. The broadness of any other line is determined by a combination of both the distribution of $a_t$ and that of $P_t$. Examination of the nmr data (see figure (5.13), for example) show that there is an approximate distribution of 3 % in $a_t$ and 13 % in $P_t$.

It is not possible to measure the extra-ionic e.f.g., $V''_{zz}$, at the rare-earth site in the R:(Gd,Y,Cu) series by means of $^{155}Gd$ Mössbauer spectroscopy because the high Curie temperatures (approximately 100 K); The recoil-free fraction above the Curie temperature would be

prohibitively small. However, attempts were made to measure $V''_{zz}$ by means of low frequency nmr using the spectrometer at the University of St Andrews. The probe nuclei were both Gd and Y and, in principle, information relating to the transferred hyperfine field, as well as $V''_{zz}$, could be obtained. Unfortunately, an nmr signal was not found, either at 4.2 K or at 1.3 K.

The problem of producing amorphous samples of R:(Gd,Ag) can be overcome in one of two ways: the addition of small amounts of "glass formers" such as boron, is known to promote the formation of the amorphous state; secondly, use of the sputtering technique is always an option when a broad composition span is required.

# CHAPTER 6: Amorphous $Tb_xLa_5(Fe_{82}B_{18})_{95-x}$ Alloys

## INTRODUCTION

Over a decade ago there was a great deal of interest in the magnetoelastic properties of crystalline R-Fe alloys which stemmed from the discovery of their huge room-temperature magnetostrictions, $\lambda$ (Koon *et al* 1971, Clarke and Belson 1972). Binary R-Fe alloys have large magnetocrystalline anisotropies and therefore require large magnetic fields to achieve their high magnetostrictions. R-Fe alloys have been fabricated, over a wide concentration range, in an amorphous state which is stable at room temperature (Rhyne *et al* 1974). The considerable interest in the potential applications of such amorphous materials centres around the fact that large single-ion anisotropy, which is usually associated with non-S-state rare-earth elements, averages out on a macroscopic scale because of the isotropic nature of the amorphous structure; amorphous materials are macroscopically isotropic and therefore cannot display conventional magnetic anisotropy. Generally in amorphous structures, magnetostrictive strains do not average to zero. Amorphous alloys containing non-S-state rare-earth elements therefore offer the possibilility of producing materials which combine small magnetic anisotropy and large isotropic magnetostriction.

If a material is to have widespread applications then fabrication in bulk is a necessary precondition. All the amorphous, binary R-Fe compositions investigated thus far have been manufactured by techniques which produce small quantities and are often expensive. In an effort to overcome this drawback, Koon and Das (1981) attempted to melt-spin Fe-B alloys with moderate amounts of rare-earth elements. X-ray diffraction patterns of these materials (Koon and Das 1981) revealed that the samples displayed a crystalline peak which was approximately seven times as intense as the amorphous peak (see figure (6.1a). Transmission

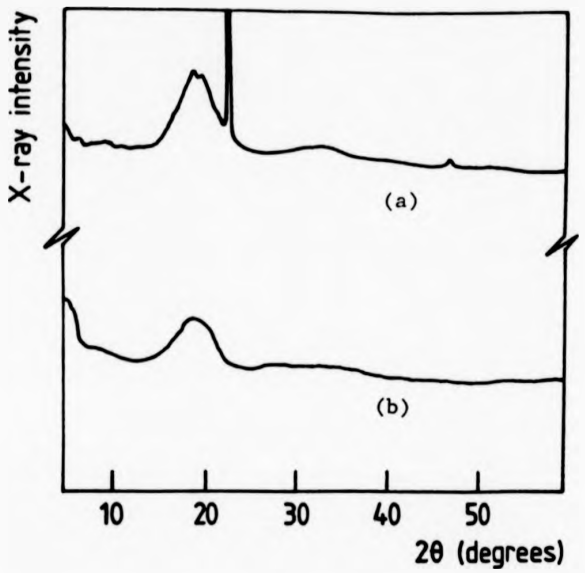


Figure (6.1) X-ray diffraction spectrum from the top surface of (a) as quenched $Tb_5(Fe_{82}B_{18})_{95}$ and (b) as quenched $Tb_5La_5(Fe_{82}B_{18})_{90}$ (Koon and Das 1981).

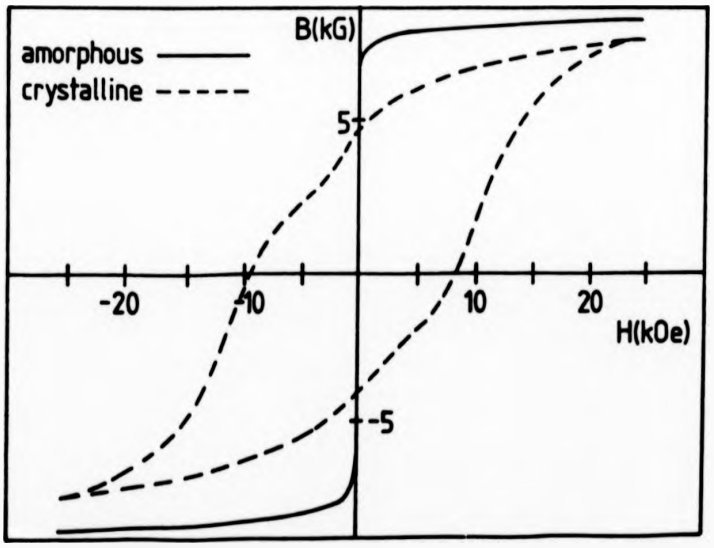


Figure (6.2) Intrinsic magnetization B - 4πM for amorphous and crystallized $Tb_5La_5(Fe_{82}B_{18})_{90}$. The crystallized alloy was annealed for 16 hours at 925 K (Koon and Das 1981).

electron microscope and X-ray studies have shown (Koon and Das 1981) that the crystalline component is due to an oriented phase which forms mainly near the free surface, suggesting surface-dominated nucleation. Spectra from the wheel-side of the ribbons showed no evidence of crystallinity.

Having noted that La does not form any stable compounds with Fe, Koon and Das (1981) added a small amount of La to the Fe-B-R alloys prior to melt-spinning. They found that La did indeed inhibit the formation of rare-earth intermetallic compounds during the quenching process. As little as 2 % La adequately suppressed the formation of crystalline phases. Subsequent studies were made on the composition $Tb_5La_5(Fe_{82}B_{18})_{90}$, the results of which are summarized below.

The magnetic properties of amorphous and crystalline $Tb_5La_5(Fe_{82}B_{18})_{90}$ have been studied by Koon and Das (1981). In the amorphous state the alloy is magnetically soft and has a low coercive force (<2 Oe) which is comparable to the corresponding alloy without rare-earths. The soft magnetic properties arise directly from the extremely homogeneous microstructure of the amorphous alloy. Upon annealing near the crystallization temperature of 900 K, the room-temperature intrinsic coercive force rises to 9 kOe, with a remanent magnetization of just under 5 kG (see figure (6.2)). The dramatic change from soft to hard magnetic properties which is brought about by recrystallizing the amorphous structure is of great practical significance; the hard magnetic properties render the heat-treated alloy $Tb_5La_5(Fe_{82}B_{18})_{90}$ suitable for use as permanent magnet material and, indeed, this composition initiated the development (Sagawa *et al* 1984) of the high performance Nd-Fe-B magnet (see chapter 7).

Annealing at a temperature $T_a$ just below the crystallization temperature, $T_x$, relieves stress frozen in during the quench and can improve the homogeneity and soft magnetic properties of an amorphous

material, provided $T_c < T_a < T_x$ (Fujimori *et al* 1981). The other annealing zone is just below $T_c$ where a long anneal in an applied field improves the final hysteresis loop if $T_a < T_x$ (Fujimori *et al* 1975). This process is known as magnetic annealing and induces anisotropy in the direction of the applied field.

The Curie temperature of $Tb_5La_5(Fe_{82}B_{18})_{90}$ is around 500 K, whereas the crystallization temperature is approximately 900 K. The effects of stress-relief annealing and magnetic annealing have been investigated by Geohagen *et al* (1982). Their results show a reduction in the coercive force following a brief stress-relief anneal (600 K for 10 minutes); the alloy magnetizes more readily at low fields. Magnetic annealing was found to increase the low field susceptibililty if the field was applied parallel to the principal axes of the ribbon; a transverse field had the opposite effect.

From magnetization measurements in bulk samples of amorphous $Tb_xFe_{1-x}$, Alperin *et al* (1977) deduced that the coupling of the moments is antiferromagnetic. However, more recent work on amorphous $RFe_2$ (Rhyne 1986) using neutron small-angle scattering contradicts this view and indicates that the structure is better classed as a spin glass, albeit a highly correlated one. It is further suggested, from the field-dependence of the neutron scattering data, that the ferromagnetic response of the bulk magnetization arises from an infinite cluster formed at relatively low field co-existing with increasingly smaller and uncorrelated residual clusters. It should be noted that due to the experimental conditions, correlation lengths of greater than 200 Å cannot be distinguished from infinity. Compositions of the form $Tb_xLa_5(Fe_{82}B_{18})_{1-x}$ should show similar coupling since the magnetic species are the same and can therefore be thought of as highly correlated spin glasses.

The work of Koon and Das (1981) has been extended by Butler and

Greenough (1986). They successfully melt-spun compositions of the form $Tb_xLa_5(Fe_{82}B_{18})_{1-x}$ where x ‹30 which have been used in this study. The rare-earth content considerably modifies the magnetic properties of the series, as evidenced by the variation of the saturation magnetization with Tb content (see figure (6.3)). The saturation magnetization exhibits a compensation composition and the purpose of the investigation presented here is to study this fundamental phenomenon by means of $^{159}Tb$ nmr and begin a characterization of the series; this is the first such study using nmr in these amorphous materials.

## 6.2 SAMPLE PREPARATION

Sample preparation was carried out as described in chapter 5. As an additional precaution to prevent oxidation, the copper wheel was placed in an inert atmosphere and the molten charge was forced onto it in the usual way. The sample compositions were of the form $Tb_xLa(Fe_{82}B_{18})_{95-x}$, where x = 5, 10, 15, 20, 25, and 30, ie six samples were prepared which spanned the compensation composition. It is of interest to note that the ribbons produced could not sustain a 180° bend; this being a crude test for amorphousness. Nevertheless, X-ray diffraction patterns showed no evidence of crystallinity.

Samples for nmr experiments were fabricated in the usual way (see chapter 5). In addition to this method, a small length of ribbon was glued, using conducting epoxy resin, onto the central conductor such that its principal axis was parallel to that of the conductor. Samples prepared in this manner were used to investigate growth-induced anisotropy effects.

## 6.3 EXPERIMENTAL PROCEDURE AND RESULTS

High frequency nmr measurements on the Tb nuclei in the series of samples $Tb_xLa_5(Fe_{82}B_{18})_{1-x}$ were carried out in the frequency range 3 to 4.8 GHz, in magnetic fields of up to 8 T, at 4.2 and 1.3 K. Prior to the investigation, the spectro-

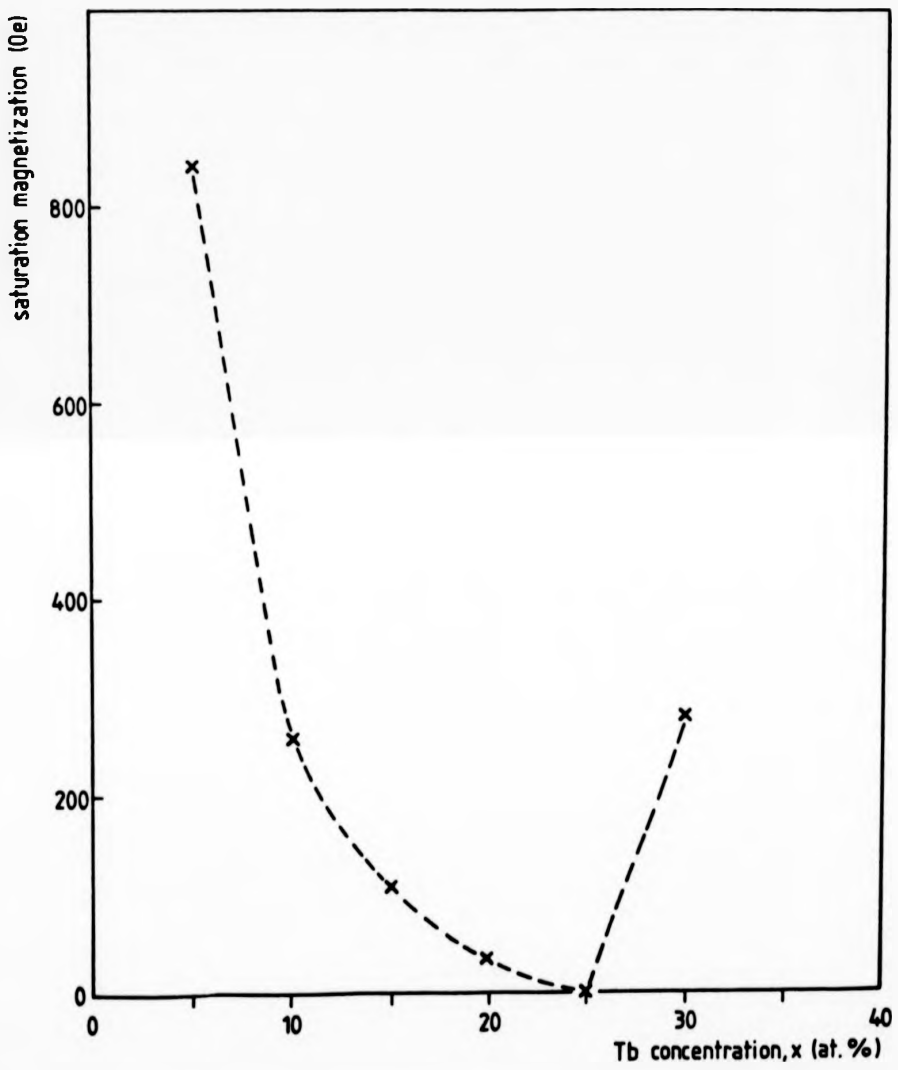


Figure (6.3) Saturation magnetization against Tb content for the series $Tb_xLa_5(Fe_{87})_{95-x}$ (Butler and Greenough 1986).

meter was optimised for maximum signal strength on a polycrystalline sample of $TbFe_2$ (Azevedo *et al* 1985). As mentioned earlier, growth-induced anisotropy effects were examined in $Tb_{20}La_5(Fe_{82}B_{18})_{95}$ (hereafter, for the sake of brevity, compositions of the form $Tb_xLa_5(Fe_{82}B_{18})_{1-x}$ will be referred to as the "$Tb_x$" samples etc). Once again relaxation phenomena were studied purely for comparative and diagnostic purposes.

Given that the Fe subnetwork is expected to be a prominent feature of the series, low frequency nmr measurements were made at the University of St Andrews, on the La, Fe and B nuclei. The results are detailed where appropriate.

The most striking features of the results are, without doubt, the variation of the signal strength and the spin-spin relaxation rates as a function of composition. It is highly unfortunate that in two of the compositions, $Tb_{20}$ and $Tb_{25}$, perhaps the most interesting ones since they are closest to the compensation point, no $^{159}Tb$ nmr resonance was detected. The appropriate frequency range was scanned thoroughly with all the experimental conditions optimized, i.e. minimum pulse separation (200 ns), lowest accessible temperature (1.3 K) and an applied field of 1 T. High and low power searches were conducted but despite such strenuous efforts, not even a hint of a signal was detected. In the $Tb_5$ composition a signal was detected without using the TWT amplifier, thereby eliminating a possible gain of approximately 37 dB. In conjuction with the TWT amplifier and a pulse separation of roughly 8 $\mu$s, the signal was still present. With the $Tb_{10}$ sample, the TWT amplifier was required and its use rendered the signal large enough to dispense with phase coherent detection. Once again, a pulse separation of about 8 $\mu$s was not enough to make the signal undetectable. Signal strength and relaxation behaviour were dramatically different in the $Tb_{15}$ composition. A small signal and fast spin-spin relaxation at 4.2 K

dictated the need to measure at 1.3 K with a pulse separation of 400 ns, in conjunction with the TWT amplifier and phase-coherent detection. As already noted, the $Tb_{20}$ and $Tb_{25}$ samples did not produce a signal in the accessible frequency range; the possible reasons will be examined in due course. In the $Tb_{30}$ composition , signal strength was once again large enough to enable detection without the TWT amplifier. Using the TWT amplifier, however, the signal could still be detected with a pulse separation of around 11 $\mu$s.

The zero-field $^{159}$Tb nmr spectra for the remaining four alloys are shown in figure (6.4). The spectra consist of two resolved but broadened lines; the resolution is once again a direct consequence of the large nuclear quadrupole moment of Tb. The higher-frequency resonances have a halfwidth which is considerably broader, at 400 MHz, than the lower-frequency resonances. There is a clear composition dependence which is detailed in table 6.1. The values of the magnetic dipole and electric quadrupole parameters, $a_t$ and $P_t$ respectively, show a general increase with decreasing rare-earth content.

In the description and discussion of the results that follow, the lower of the two resonances is referred to as the "central line" etc. The nomenclature is based on sound experimental evidence; a search for a third resonance at a frequency of 4700 MHz produced a null result, for all the samples. It is reasonable to assume, therefore, that the third line is at a frequency lower than that of the observed low-frequency resonance and outside the range of the spectrometer.

| Composition | $a_t$ (MHz) | $P_t$ (mHz) |
|---|---|---|
| $Tb_{30}La_5(Fe_{82}B_{18})_{65}$ | 3450 (15) | 650 (30) |
| $Tb_{15}La_5(Fe_{82}B_{18})_{80}$ | 3485 (15) | 655 (30) |
| $Tb_{10}La_5(Fe_{82}B_{18})_{85}$ | 3490 (15) | 670 (30) |
| $Tb_5La_5(Fe_{82}B_{18})_{90}$ | 3495 (15) | 715 (30) |

TABLE 6.1 Measured $^{159}$Tb nmr spectral parameters for the series $Tb_xLa_5(Fe_{82}B_{18})_{1-x}$. The errors are given in parentheses.

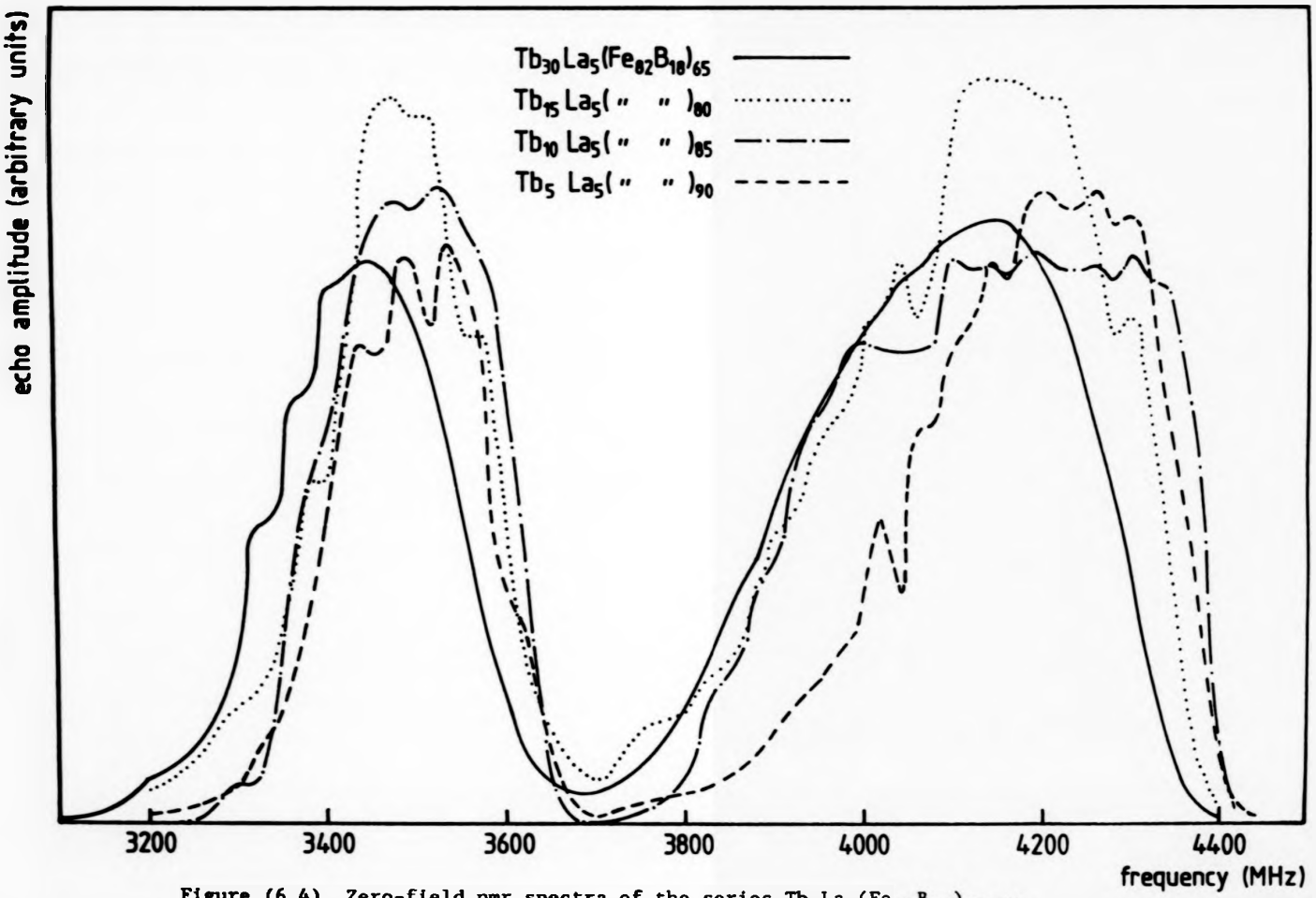


Figure (6.4) Zero-field nmr spectra of the series $Tb_xLa_5(Fe_{82}B_{18})_{95-x}$.

Field-dependent behaviour of the nmr spectra for the series is illustrated in figures (6.5) to (6.8). The $Tb_5$, $Tb_{10}$, and $Tb_{15}$ samples have a very similar field dependence (figures (6.5), (6.6) and (6.7), respectively). The application of a field causes a decrease in the resonant frequency. In a field of 8 T the gyromagnetic shift amounts to about 60-70 MHz, which is roughly 11 MHz less than the full value of 10.1 MHz/T. The reduction in the resonant frequency precipitated by an applied field is clear indication that the Fe and Tb subnetworks are oppositely aligned. Field dependence of the echo amplitude for the three alloys was very similar. A gradually applied field of 1 T caused a correspondingly gradual increase in the signal of approximately an order of magnitude. Thereafter, an increase in applied field produced a decrease in the echo amplitude.

Field behaviour of $Tb_{30}$ in 0, 4, and 8 T is very similar to that of the other three alloys; an applied field produces a negative gyromagnetic shift of the resonant frequencies (see figure (6.8)). This behaviour does not agree with predictions based on an antiparallel alignment of the Tb and Fe subnetworks. From the theory developed in chapter 2, it is straightforward to show that the direction of the hyperfine field, $B_{hf}$, at the Tb nucleus is the same as that of the Tb moment (see figure (6.9).

It can be seen from experiment that the contribution of $B_n$, the transferred hyperfine field, is positive i.e. in the same direction as $B_{hf}$. For the Fe-rich part of the series, the direction of the magnetization and the Fe moments will be collinear and oppositely directed to the Tb moments. An applied field will be in the negative direction, since it acts in the same direction as the magnetization, and therefore produces a negative gyromagnetic shift. This is indeed the case for the $Tb_5$, $Tb_{10}$, and $Tb_{15}$ compositions.

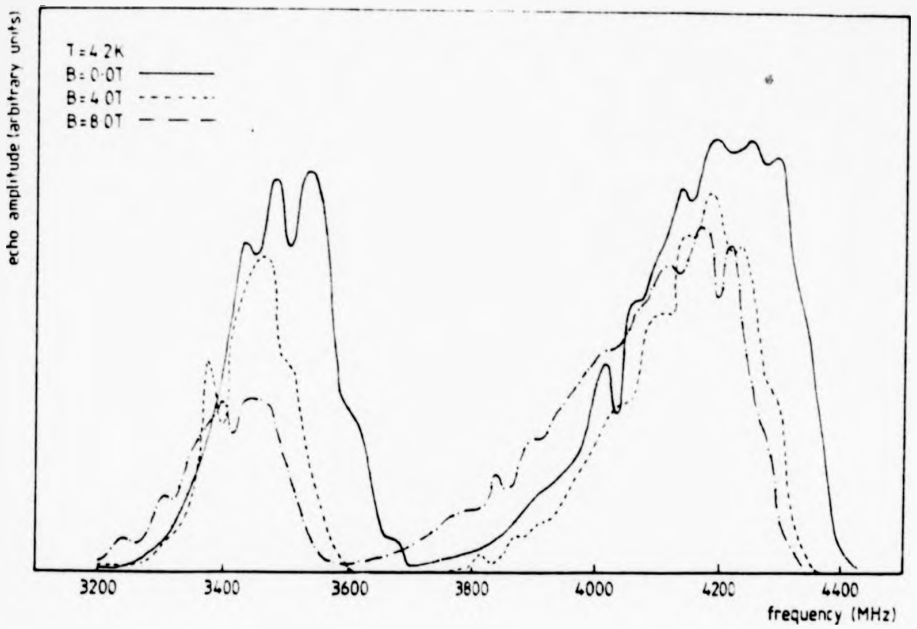


Figure (6.5) Tb nmr spectra of $Tb_5La_5(Fe_{82}B_{18})_{90}$ at 4.2 K, showing field dependence.

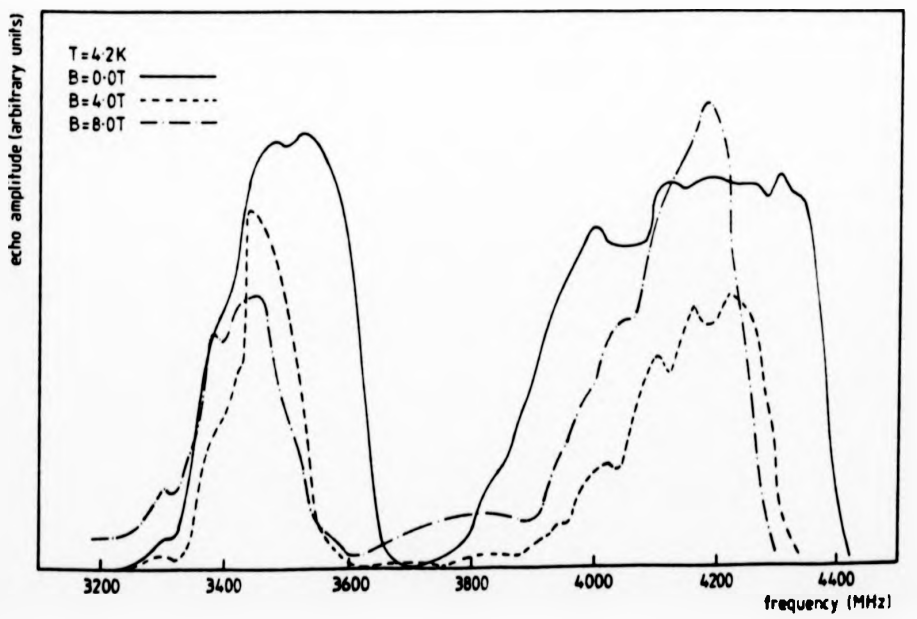


Figure (6.6) The nmr spectra of $Tb_{10}La_5(Fe_{82}B_{18})_{85}$ at 4.2 K, showing field dependence.

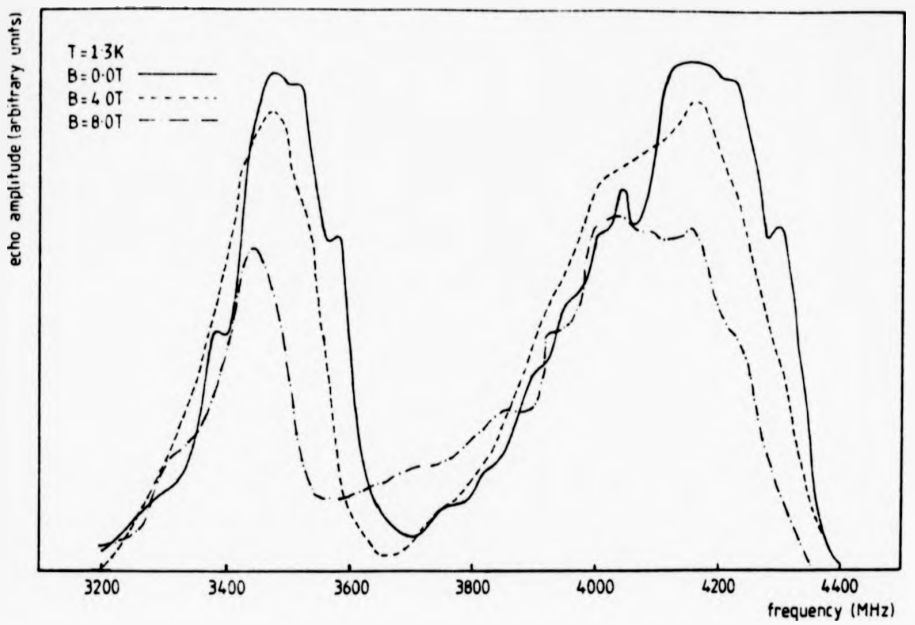


Figure (6.7) Tb nmr spectra of $Tb_{15}La_5(Fe_{82}B_{18})_{80}$ at 1.3 K, showing field depedence.

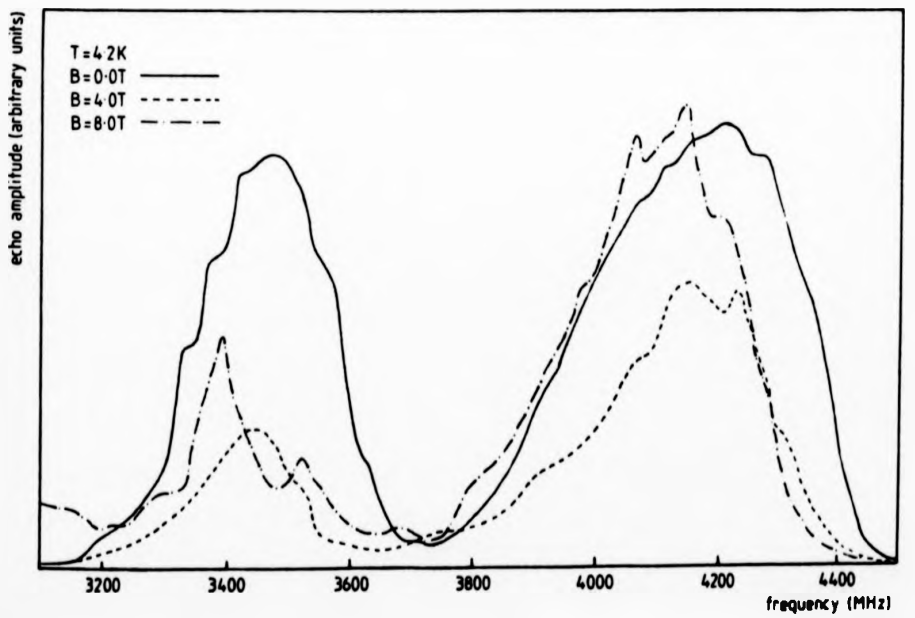


Figure (6.8) Tb nmr spectra of $Tb_{30}La_5(Fe_{82}B_{18})_{65}$ at 4.2 K, showing high-field behaviour.

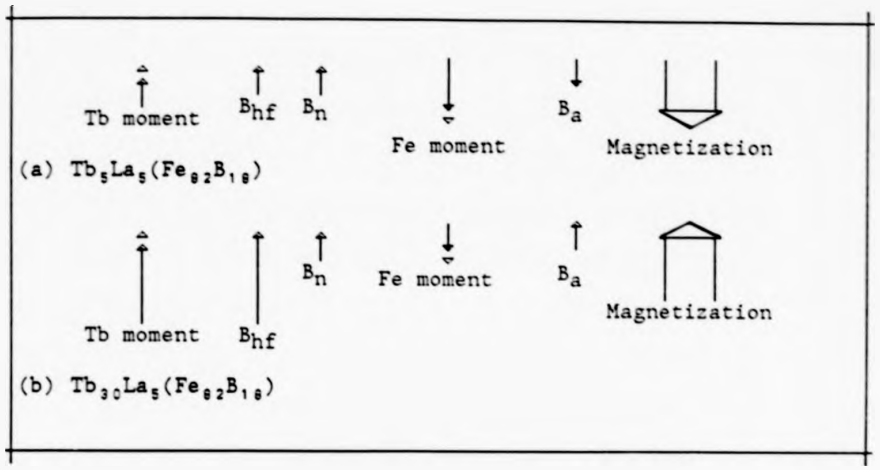


Figure (6.9) Schematic representation of the direction of the gyromagnetic contribution for the compositions (a) $Tb_5La_5(Fe_{82}B_{18})_{90}$ and (b) $Tb_{30}La_5(Fe_{82}B_{18})_{65}$.

With reference to figure (6.3), it can be seen that $Tb_{25}$ is the compensation composition. On the Fe-rich side of this point, i.e. $Tb_5$, $Tb_{10}$, $Tb_{15}$, and $Tb_{20}$, the magnetization is dominated by the Fe-subnetwork. The $Tb_{30}$ magnetization, however, is dominated by the Tb-subnetwork contribution and the total magnetization is in the direction of the Tb moments, and therefore in the direction of $B_{hf}$. As a consequence, an applied field will also be in the direction of $B_{hf}$ and would thus produce a positive gyromagnetic contribution. The experimental results indicate a negative gyromagnetic shift.

In view of the abovementioned inconsistency, further field-dependent measurements were made by taking $^{159}$Tb nmr spectra in applied fields of 1 and 2 T (see figure (6.10)). The application of a 1 T field produced two effects. Firstly, the echo amplitude increased by roughly an order of magnitude and secondly, there was a marked narrowing of the resonance lines. It is difficult to determine whether or not the applied field causes a gyromagnetic shift because of the errors associated with identifying the centroids of the lines; the errors are slightly greater

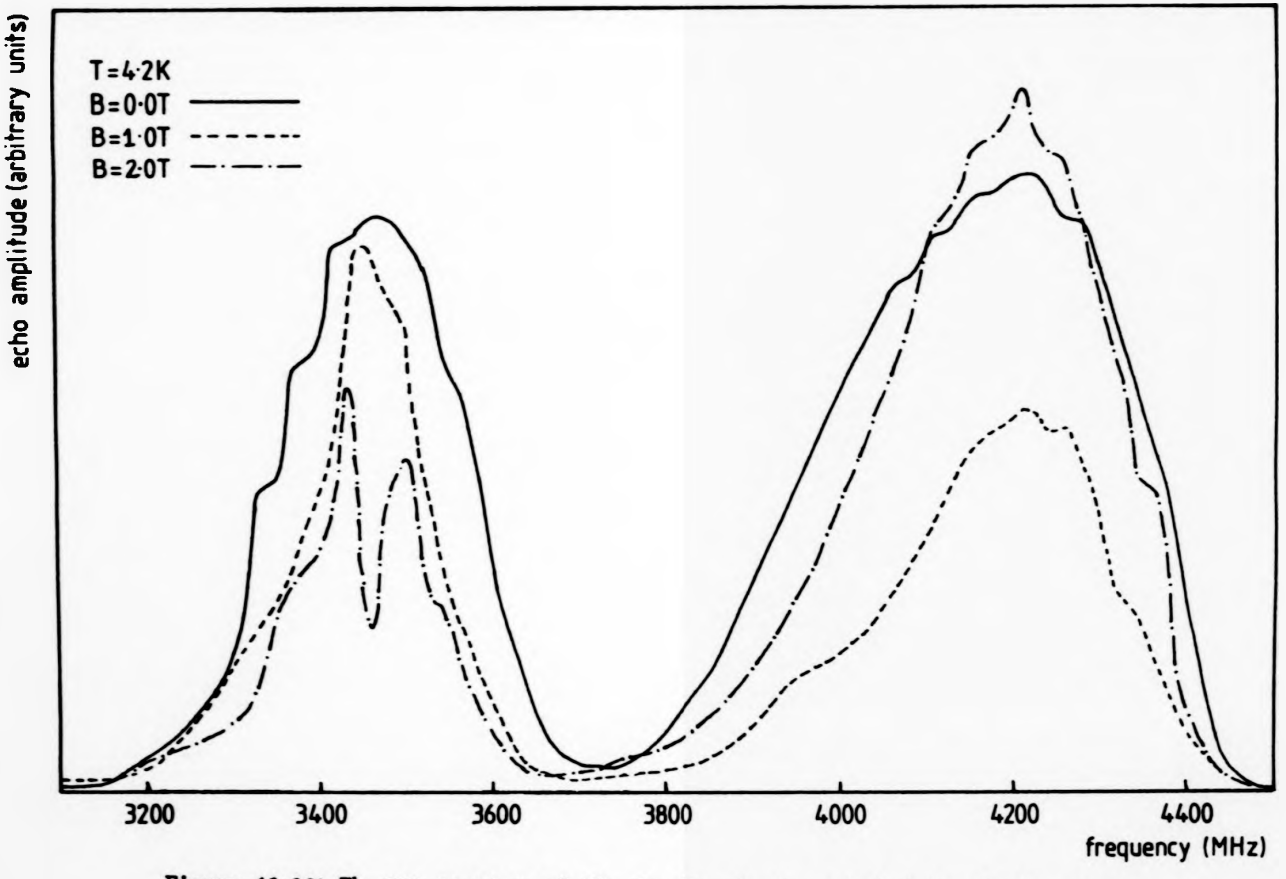


**Figure (6.10)** Tb nmr spectra of $Tb_{30}La_5(Fe_{82}B_{18})_{65}$ at 4.2 K, showing low field behaviour.

than the expected shift. (Attention is drawn to the fact that the 1 T applied-field behaviour of $Tb_{30}$ is very similar to that observed in the other three samples.)

The nmr spectrum obtained in an applied fied of 2 T displayed a broadening of the upper-quadrupole satellite. The central line, however, split into two resolved peaks; the latter feature made it difficult to estimate a gyromagnetic shift.

Growth-induced anisotropy effects were investigated in the $Tb_5$ composition. The zero-field nmr spectra for the two types of sample geometry were found to be virtually superimposable, after normalization of the echo amplitude. Field-dependent measurements were not made.

As mentioned earlier, low-frequency nmr experiments were carried out in an effort to obtain information relating to the transferred hyperfine field as well as the extra-ionic field gradient; this information can, in principle, be obtained from $^{139}La$ nmr. Thus far only the $Tb_{30}$ composition has produced echo signals at 4.2 K in zero field. The results are shown in figure (6.11). Of particular interest is the $^{139}La$ resonance shown in figure (6.11a). $^{139}La$ has a nuclear spin of 7/2 and its intra-ionic parameter $a_0'$ and $P_0'$ are zero since it is a non-magnetic S-state ion. The resonance frequency of $^{139}La$ is entirely due to extra-ionic effect; a knowledge of the gyromagnetic ratio, 6.0 MHz/T, and the resonant frequency allows a determination of the transferred hyperfine field at the La nucleus. A simple calculation, then, gives 25.7 ±2 T for the t.h.f.. In view of the seemingly contradictory $^{159}Tb$ nmr results for the $Tb_{30}$ sample, the low-frequency nmr work is of limited value but has been included for the sake of completeness.

For all four alloys the measured value of $a_t$ is greater than $a_0'$. The extra-ionic contribution to $a_t$, $a''$, must therefore be positive, although without a quantitative knowledge of $a''$ it is not possible to establish whether or not the rare-earth ions are quenched. The total

than the expected shift. (Attention is drawn to the fact that the 1 T applied-field behaviour of $Tb_{30}$ is very similar to that observed in the other three samples.)

The nmr spectrum obtained in an applied fied of 2 T displayed a broadening of the upper-quadrupole satellite. The central line, however, split into two resolved peaks; the latter feature made it difficult to estimate a gyromagnetic shift.

Growth-induced anisotropy effects were investigated in the $Tb_5$ composition. The zero-field nmr spectra for the two types of sample geometry were found to be virtually superimposable, after normalization of the echo amplitude. Field-dependent measurements were not made.

As mentioned earlier, low-frequency nmr experiments were carried out in an effort to obtain information relating to the transferred hyperfine field as well as the extra-ionic field gradient; this information can, in principle, be obtained from $^{139}La$ nmr. Thus far only the $Tb_{30}$ composition has produced echo signals at 4.2 K in zero field. The results are shown in figure (6.11). Of particular interest is the $^{139}La$ resonance shown in figure (6.11a). $^{139}La$ has a nuclear spin of 7/2 and its intra-ionic parameter $a_0'$ and $P_0'$ are zero since it is a non-magnetic S-state ion. The resonance frequency of $^{139}La$ is entirely due to extra-ionic effect; a knowledge of the gyromagnetic ratio, 6.0 MHz/T, and the resonant frequency allows a determination of the transferred hyperfine field at the La nucleus. A simple calculation, then, gives 25.7 ±2 T for the t.h.f.. In view of the seemingly contradictory $^{159}Tb$ nmr results for the $Tb_{30}$ sample, the low-frequency nmr work is of limited value but has been included for the sake of completeness.

For all four alloys the measured value of $a_t$ is greater than $a_0'$. The extra-ionic contribution to $a_t$, $a''$, must therefore be positive, although without a quantitative knowledge of $a''$ it is not possible to establish whether or not the rare-earth ions are quenched. The total

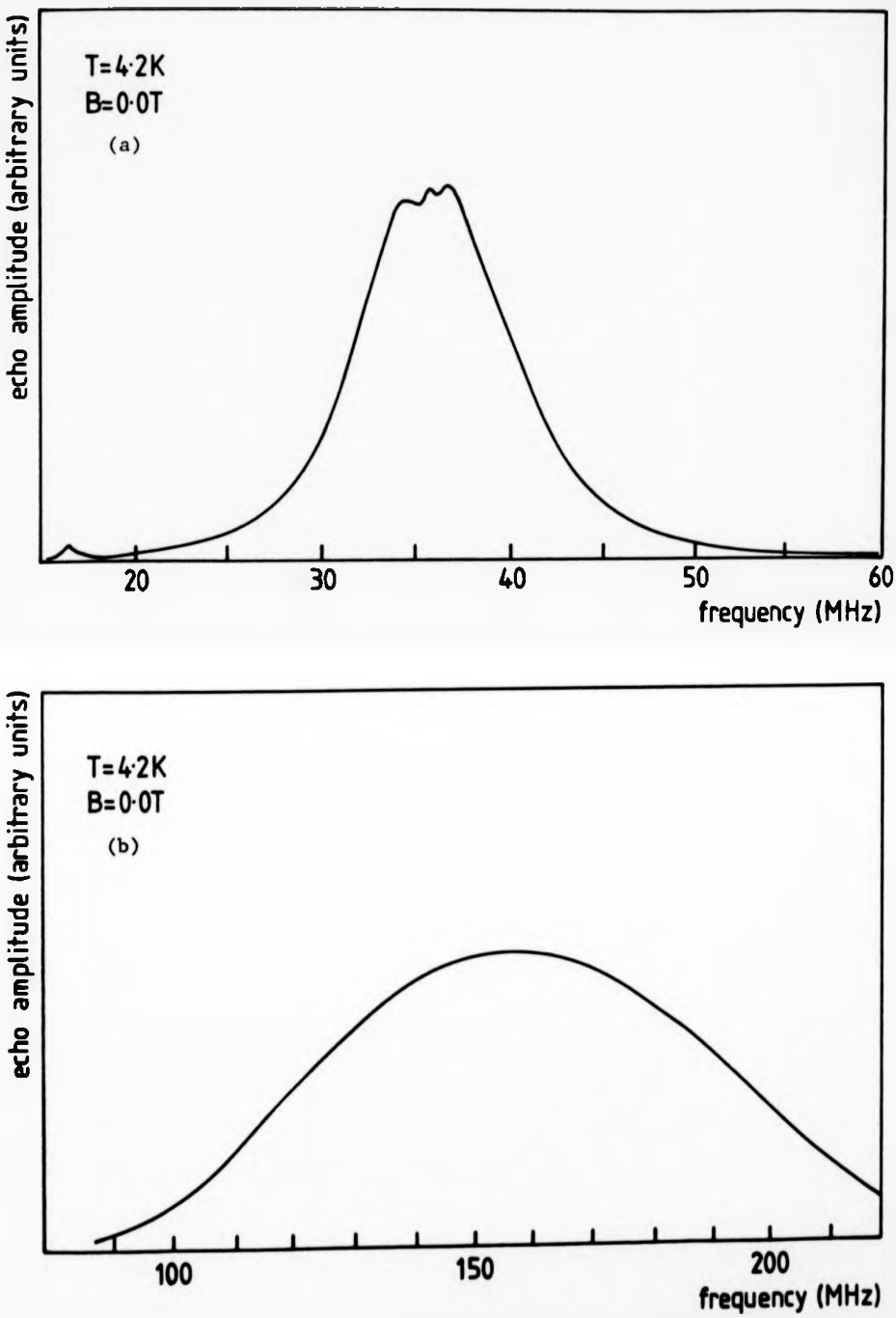


Figure (6.11) Low-frequency nmr spectra of $Tb_{30}La_5(Fe_{82}B_{18})_{65}$ where (a) the probe nucleus is B and (b) the probe nucleus is La.

nuclear quadrupole splitting, $P_t$, is smaller than the free-ion value $P_0'$ in each case. This could be due to quenching of the rare-earth moment, a negative extra-ionic contribution or a combination of both. (It has been pointed out that in exchange dominated systems, quenching of the rare-earth ions is unlikely (Koon and Rhyne 1980)).

It was shown in chapters 2 and 5 that a central resonance line is be unaffected by $P_t$ and any associated distribution. Quadrupole-split satellites, however, are affected by $P_t$ and are broadened by distributions in $P_t$. The results indicates a significant distribution of $P_t$ which arises from a distribution of $V_{zz}$. A smearing of the $^{139}La$ resonances shows that there is distribtion of $V_{zz}''$ (see figure (6.11a)). The distribution of $V_{zz}$ is much greater in the $Tb_xLa_5(Fe_{82}B_{18})_{95-x}$ series than in the R:(Gd,Y,Cu) series (see chapter 5), indicating more randomness in the local environment of the R ions in the former series than in the latter.

In some of the alloys, both high and low frequency spin-echo signals have been conspicuous by their absence. For those alloys which have a small saturation magnetization, a small enhancement factor would be expected and would explain the lack of a signal. It is puzzling, however, that the low-frequency nmr investigation only produced a result for the $Tb_{30}$composition.

## 6.4 DISCUSSION AND CONCLUSIONS

$^{159}Tb$ nmr experiments indicate that the coupling between the Fe-and Tb-subnetworks is antiferromagnetic. Assuming such a coupling, a simple determination of the direction of the gyromagnetic shift in the $Tb_{30}$ sample shows it to be positive, in direct contradiction of experimental evidence. Antiferromagnetic coupling of the R and Fe spins in crystalline (see chapter 7 and references therein) and amorphous (Alperin *et al* 1977) R-Fe compounds is well established . An unavoidable and probable conclusion, therefore, is that the $Tb_{30}$

composition is multiphase. Nevertheless, X-ray diffraction and nmr data indicate that the "phases" are amorphous.

In the absence of a more precise knowledge of the t.h.f. from the Fe-subnetwork, it is not possible to quantify $J_z$ for the rare-earth ions; examination of the data within the constraints of the HPZ model, or indeed any other model, is therefore inappropriate.

The general philosophy of the characterization study of the series $Tb_xLa_5(Fe_{82}B_{18})_{95-x}$ was to obtain a measure of $a_t$ and $P_t$ for the Tb ions form $^{159}$Tb nmr. By obtaining the extra-ionic contributions, a" and P", to these parameters from $^{139}$La nmr, a measure of the intra-ionic parameters can be obtained by a simple subtraction. By calculating the intra-ionic parameters, information relating to $\langle J_z \rangle$ and $\langle J_z^2 \rangle$ is readily available. The study has been thwarted by a lack of Tb resonances in the $Tb_{20}$ and $Tb_{25}$ samples, the two which are closest to the compensation composition. A more severe restriction is encountered by virtue of an absence of $^{139}$La spin-echo signals in all but the $Tb_{30}$ composition; the investigation reported here is therefore necessarily incomplete.

Further work is required to establish the exact nature of the $Tb_{30}$ composition. An electron microprobe study of the alloy could possibly reveal evidence of the segregation of the composite phases that are postulated. The Fe-subnetworks throughout the series can be examined by $^{57}$Fe Mössbauer experiments, valuable information concerning the magnitude and alignment, relative to an applied field, of the Fe moments can be obtained in this way; the main problem of a small recoil-free fraction that was encountered in using $^{155}$Gd as a Mössbauer probe would not hinder $^{57}$Fe Mössbauer measurements since the recoil-free fraction is relatively large.

The extra-ionic contributions to $a_t$ and $P_t$ can be most easily obtained by $^{139}$La nmr and therefore it is worthwhile to consider repeating the experiments at a lower temperature (1.3 K) and in a small

applied field (1 T). Furthermore, the enhancement factor could possibly be increased sufficiently by a stress-relief anneal followed by a magnetic anneal.

# CHAPTER 7: $R_2Fe_{14}B$ Compounds

## 7.1 INTRODUCTION

During the late 1970's, shortages of cobalt and samarium together with uncertainties in their prices led to a great deal of activity in developing permanent magnets which did not utilize either of these two elements. Much of the early effort centred on R-Fe binary alloys. As a result of the ferromagnetic coupling between the light rare-earths (LRE) and the Fe moments, binary LRE-Fe compounds have high saturation magnetizations. If the R ion has an orbital moment then large magnetocrystalline anisotropies are expected. However, the R-Fe binary alloys are not suitable for use as permanent magnets because the Curie temperatures of LRE-Fe alloys are low, LRE-Fe form few stable intermetallic phases and no R-Fe binary compound shows a uniaxial magnetic anisotropy. Two alternative approaches were adopted in order to overcome these problems. A wide range of metastable phases are accessible if melt-spinning is followed by heat treatment. The first step in this direction was taken as a result of the investigation of the properties of crystallized amorphous $Tb_5La_5(Fe_{82}B_{18})_{90}$ (Koon and Das 1984). Despite the ferrimagnetic alignment of the Tb and Fe moments, a remanent magnetization of 5 kG and a coercive force of 9 kOe were observed in this material. Further investigation of crystallized amorphous compositions of the form $R_{10}(Fe_{82}B_{18})_{90}$, where R = (Nd,La) and (Pr,La), led to a substantial increase in the magnetization since the exchange interaction between the Fe and LRE moments is ferromagnetic. A similar line of investigation led to the fabrication of several R-Fe-B materials (Hadjipanayis *et al* 1982 and Croat *et al* 1984). The phase responsible for the hard magnetic properties was identified as $R_2Fe_{14}B$. (Herbst *et al* 1984, Givord *et al* 1984).

A parallel, yet independent approach was adopted by Sagawa *et al*

(1984). The search was extended to ternary systems. Numerous compounds of LRE, Fe and small quantities of other elements were synthesized and various kinds of equilibrium phases were found to exist. Of these phases, a new ternary compound consisting of Nd-Fe-B was shown to possess magnetic properties eminently suitable for a permanent magnet material. Subsequently, the phase was identified as $Nd_2Fe_{14}B$. (Herbst *et al* 1984, Givord *et al* 1984)

## 7.2 MAGNETIC PROPERTIES OF $R_2Fe_{14}B$

The series of materials $R_2Fe_{14}B$, where R is a rare earth or yttrium, crystallize in a tetragonal structure (space group P4/mnm) with four formula units (68 atoms) per tetragonal unit cell. There are two distinct R sites of low symmetry (point group mm), six inequivalent Fe sites and one B site. The structure is shown in figure (7.1).

The magnetic coupling in $R_2Fe_{14}B$ is similar to that observed in binary R-Fe intermetallics, i.e. there is an antiferromagnetic coupling beween the Fe and R spins. For compounds in which R is a light rare-earth (J=L-S), the total R moment is coupled parallel to the Fe moment. However, when R is a heavy rare-earth (J=L+S), the total R moment is coupled antiparallel to the Fe moment.

The magnetic and structural properties of the $R_2Fe_{14}B$ compounds are given in table (7.1). A number of features, however, call for comment. The compositions with R = Sm, Er and Tm have magnetic easy axes along a [100] direction and the others along a [001] direction at 4.2 K, with the exception of $Nd_2Fe_{14}B$ and $Ho_2Fe_{14}B$ (these are discussed in more detail later (section 7.2.1)).

The unusually large values of $B_A$, the anisotropy field, particularly for those $R_2Fe_{14}B$ compounds in which R has a non-zero orbital moment, indicate that single-ion crystal-field induced anisotropy is the origin of the large values of $B_A$. A significant, though smaller magnetic

(1984). The search was extended to ternary systems. Numerous compounds of LRE, Fe and small quantities of other elements were synthesized and various kinds of equilibrium phases were found to exist. Of these phases, a new ternary compound consisting of Nd-Fe-B was shown to possess magnetic properties eminently suitable for a permanent magnet material. Subsequently, the phase was identified as $Nd_2Fe_{14}B$. (Herbst *et al* 1984, Givord *et al* 1984)

## 7.2 MAGNETIC PROPERTIES OF $R_2Fe_{14}B$

The series of materials $R_2Fe_{14}B$, where R is a rare earth or yttrium, crystallize in a tetragonal structure (space group P4/mnm) with four formula units (68 atoms) per tetragonal unit cell. There are two distinct R sites of low symmetry (point group mm), six inequivalent Fe sites and one B site. The structure is shown in figure (7.1).

The magnetic coupling in $R_2Fe_{14}B$ is similar to that observed in binary R-Fe intermetallics, i.e. there is an antiferromagnetic coupling beween the Fe and R spins. For compounds in which R is a light rare-earth (J=L-S), the total R moment is coupled parallel to the Fe moment. However, when R is a heavy rare-earth (J=L+S), the total R moment is coupled antiparallel to the Fe moment.

The magnetic and structural properties of the $R_2Fe_{14}B$ compounds are given in table (7.1). A number of features, however, call for comment. The compositions with R = Sm, Er and Tm have magnetic easy axes along a [100] direction and the others along a [001] direction at 4.2 K, with the exception of $Nd_2Fe_{14}B$ and $Ho_2Fe_{14}B$ (these are discussed in more detail later (section 7.2.1)).

The unusually large values of $B_A$, the anisotropy field, particularly for those $R_2Fe_{14}B$ compounds in which R has a non-zero orbital moment, indicate that single-ion crystal-field induced anisotropy is the origin of the large values of $B_A$. A significant, though smaller magnetic

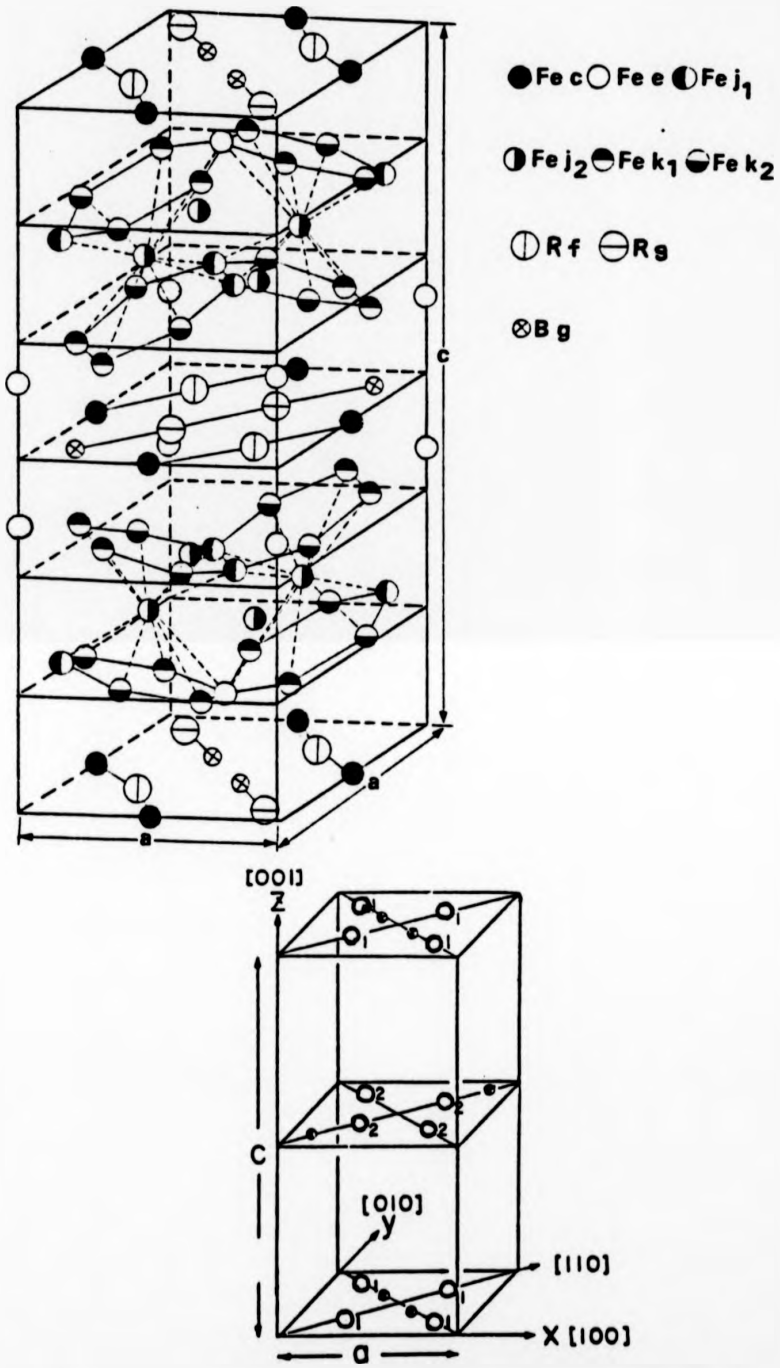


Figure (7.1) The tetragonal unit cell of the $R_2Fe_{14}B$ structure and (b) the same structure showing the position of the R and B atoms. (Herbst *et al* 1984)

| Lattice constants | | | $D_x$ | I(T) | | $M_S(\mu_B/f.u)$ | | $M_R(\mu_B)$ | $g_J J$ | $\alpha_J$ | $T_C$ | $B_A$(kOe) | |
|---|---|---|---|---|---|---|---|---|---|---|---|---|---|
| R | a(nm) | c(nm) | ($kg/m^3$) | 4.2K | 300K | 4.2K | 300K | | | | (K) | 4.2K | 300K |
| Y | 0.876 | 1.200 | 7.00 | 1.59 | 1.41 | 31.4 | 27.8 | 0 | 0 | 0 | 517 | 12 | 20 |
| Ce | 0.875 | 1.210 | 7.69 | 1.47 | 1.17 | 29.4 | 29.3 | - | 0 | 0 | 422 | 30 | 30 |
| Pr | 0.881 | 1.227 | 7.49 | 1.84 | 1.56 | 37.6 | 31.9 | 3.1 | 3.2 | | 569 | 320 | 87 |
| Nd | 0.881 | 1.221 | 7.58 | 1.85 | 1.60 | 37.7 | 32.5 | 3.2 | 3.3 | - | 586 | — | 67 |
| Sm | 0.882 | 1.194 | 7.82 | 1.67 | 1.52 | 33.3 | 30.2 | 1.0 | 0.7 | + | 620 | — | — |
| Gd | 0.874 | 1.194 | 8.06 | 0.915 | 0.893 | 17.9 | 17.5 | 6.7 | 7.0 | 0 | 659 | 16 | 25 |
| Tb | 0.877 | 1.205 | 7.96 | 0.664 | 0.703 | 13.2 | 14.0 | 9.1 | 9.0 | - | 620 | 306 | 220 |
| Dy | 0.876 | 1.199 | 8.07 | 0.573 | 0.712 | 11.3 | 14.0 | 10.1 | 10.0 | - | 598 | 167 | 150 |
| Ho | 0.875 | 1.199 | 8.12 | 0.569[a] | 0.807 | 11.2[a] | 15.9 | 10.1 | 10.0 | - | 573 | — | 75 |
| Er | 0.875 | 1.199 | 8.16 | 0.655 | 0.899 | 12.9 | 17.7 | 9.3 | 9.0 | + | 551 | — | — |
| Tm | 0.874 | 1.194 | 8.23 | 0.925 | 1.15 | 18.1 | 22.6 | 6.7 | 7.0 | + | 549 | — | — |

[a]The magnetization of $Ho_2Fe_{14}B$ at 4.2K was measured along the [001] direction.

**TABLE 7.1** Lattice constants and magnetic properties ot the $R_2Fe_{14}B$ series, measured on single crystals. $D_x$: density. I: saturation magnetization. $M_S$: saturation magnetization. $M_R$: rare-earth sublattice magnetization. $T_C$: Curie temperature. $B_n$: magnetocryustalline anisotropy field.

magnetic anisotropy is also found in compounds where R has zero orbital moment. This can be attributed to the Fe sublattice although such behaviour is rather unusual since the orbital angular momentum is completely quenched in most Fe-based metallic systems. The dipolar interaction between the magnetic moments could also be responsible for the magnetic anisotropy observed in $R_2Fe_{14}B$ where R is non-magnetic. It can be seen that $M_R$ is approximately equal to gJ for a given material. In view of the large contribution of the R ions to the magnetocrystalline anisotropy, the presence of a substantial crystal field is expected and it is by no means obvious that the crystal field ground state need correspond to the fully polarized state $|J,J_z = \pm J\rangle$. The observation of a maximum moment indicates that the exchange interaction, which is primarily associated with the 3d Fe electrons, is dominating the single-ion anisotropy of the R ions which is due to the crystal field acting on the 4f electrons; it should be noted, nonetheless, that the latter still determines the preferred direction of the 4f moments. There is an apparent inconsistency when the calculated Zeeman energy due to the exchange field acting on the R ions at zero kelvin is compared with crystal field splittings as derived from point charge calculations. The Zeeman energy ranges from 400 K in $Tm_2Fe_{14}B$ to 1300 K in $Gd_2Fe_{14}B$, whereas the crystal field splittings are in the range 360 K to 1100 K. A strong interplay between the exchange and crystal field can thus be expected if the calculations are assumed to be accurate. This is not a trivial assumption since the full crystal field Hamiltonian contains nine terms (Cadogon and Coey 1984); invariably only second order terms are used.

The temperature dependence of the R sublattice magnetization can be described by a two-sublattice molecular field model where only Fe-Fe and R-Fe interactions are taken into account. Magnetization of the Fe sublattice is assumed to be constant throughout the series and is

assigned the value of the magnetization in $Y_2Fe_{14}B$ (Sinnema *et al* 1984). The strength of the R-Fe interactions is much weaker than that of the Fe-Fe interactions and varies approximately as the projected spin of the R ion. The R sublattice magnetization would be expected to decrease rapidly as temperature increases, especially for the R ions with small projected spins.

Magnetization against temperature curves are shown in figure (7.2), and the variation of the anisotropy field with temperature for the series is shown in figure (7.3).

It is reasonably straightforward to calculate the Curie temperature in the mean-field approximation (Sinnema *et al* 1984). The relatively small R-R exchange energy is neglected and the calculated values can be compared with those obtained experimentally (see figure (7.4)). There is excellent agreement for the $R_2Fe_{14}B$ compounds containing HRE elements. For magnetic LRE compounds, the agreement is less satisfactory. The likely reason for the discrepancy is thought to be an enhanced polarization of the 5d electrons (Sinnema *et al* 1984).

In view of the analysis of nmr data that is presented here, it is appropriate to consider the contribution of the surrounding Fe atoms to the total hyperfine field, namely the transferred hyperfine field, $B_n$. Values of the total hyperfine field have been measured for R = Y, Nd, Gd, Dy and Lu in $R_2Fe_{14}B$ (Berthier *et al* 1986). In $Y_2Fe_{14}B$ and $Lu_2Fe_{14}B$ the measured hyperfine field is equal to that transferred from the surrounding Fe atoms, i.e $B_{hf} = B_n$, given that the 4f moment is equal to zero in Y and Lu. The ratio of $B_n$ at the R site in these two compounds is in excellent agreement with that predicted by the Campbell hyperfine coupling constants (Campbell 1969). In compounds with a magnetic R element, there is a large increase of $B_n$ at site II. Polarized neutron data on $Y_2Fe_{14}B$ and $Nd_2Fe_{14}B$ (Givord *et al* 1985) show that there is a large increase of the 3d moment at three of the inequivalent Fe sites,

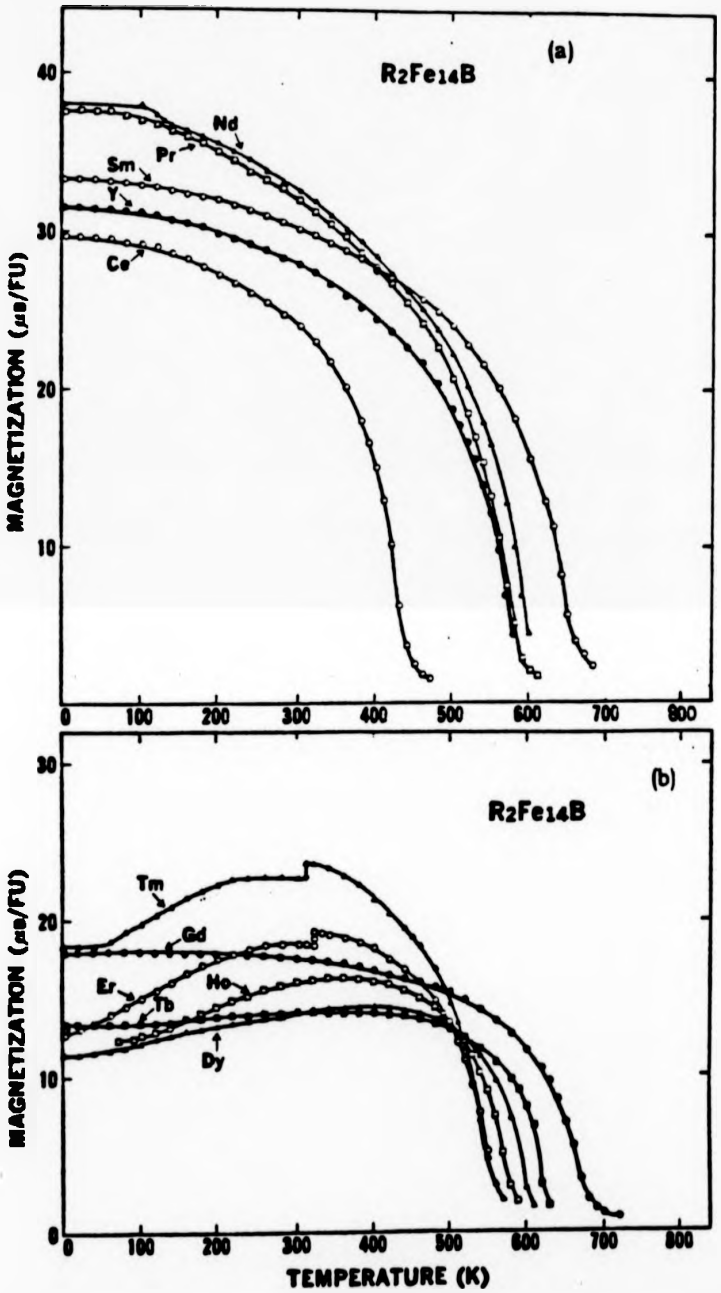


Figure (7.2) Temperature dependence of the magnetization of $R_2Fe_{14}B$ compounds where (a) R = Y, Ce, Pr, Nd, Sm, and (b) R = Gd, Tb, Dy, Ho, Er and Tm, measured on single crystals in an applied field of 800 kA/m (Hirosawa *et al* 1986).

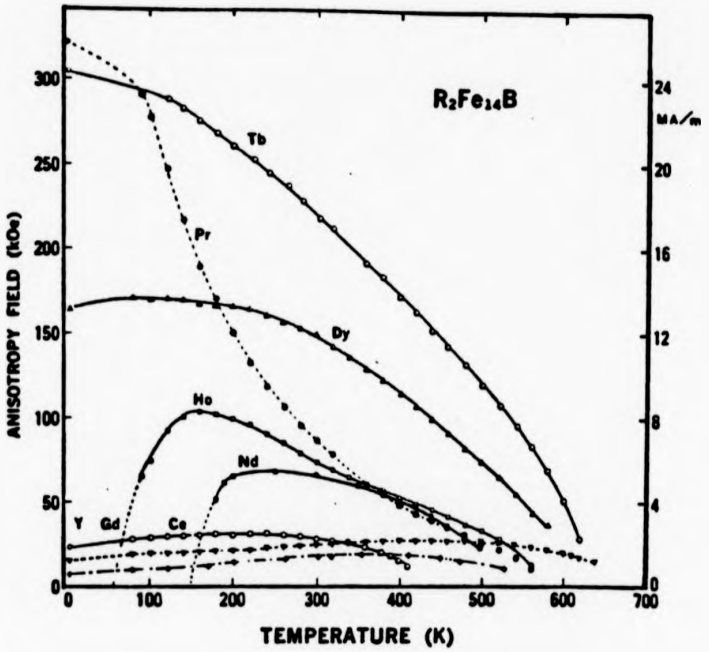


Figure (7.3) Temperature dependence of the magnetocrystalline anisotropy field, $B_A$, measured in a magnetic field of 1.5 T (after Hirosawa *et al* 1986).

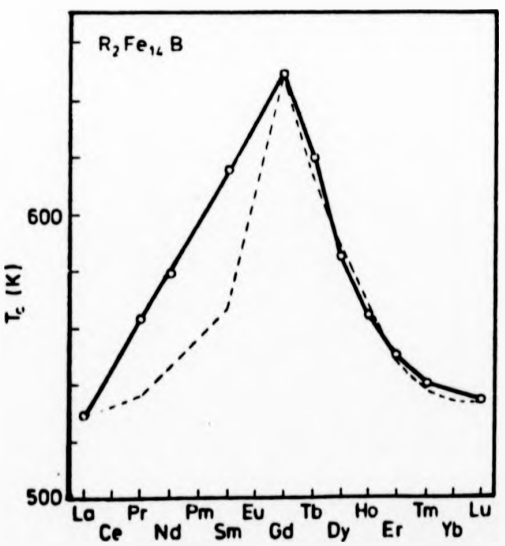


Figure (7.4) Curie temperatures of $R_2Fe_{14}B$ compounds. The broken line represents model calculations (after Sinnema *et al* 1984).

Fe(2), Fe(5) and Fe(6), in $Nd_2Fe_{14}B$ relative to $Y_2Fe_{14}B$. The increase of the 3d moment is due to an "enhanced" 4f-3d exchange interaction which is a consequence of the very short distances between R(II), Fe(2) and Fe(6). The increased 3d moments can thus account for the larger t.h.f. at site II. The increases in $B_{hf}$ do not, however, display any systematic variation across the series. This fact will prove to be of considerable nuisance value in the interpretation of nmr data as one is unable to calculate the shift of the resonant frequencies due to the t.h.f.

### 7.2.1 SPIN REORIENTATION BEHAVIOUR

The $R_2Fe_{14}B$ compounds display temperature-dependent, spin-reorientation behaviour which can conveniently be divided into two categories. The direction of magnetization of $Y_2Fe_{14}B$, where the Y is non-magnetic, shows that the Fe sublattice has an easy c-axis as do the R sublattices for R = Pr, Nd, Tb, Dy and Ho. For R = Sm, Er, and Tm, the R sublattice easy direction of magnetization is perpendicular to the c-axis. (The preferred direction of the rare-earth sublattice is determined, to lowest order, by the sign of $B_2^0$, which in turn is determined by the sign of $\alpha_J$ for a given $A_2^0$. Values of $\alpha_J$ are given in table (7.1). The spin reorientations observed in $Sm_2Fe_{14}B$, $Er_2Fe_{14}B$, and $Tm_2Fe_{14}B$ (see figure (7.5b)) are a consequence of the competing anisotropies of the two sublattices. At high temperatures the Fe-Fe interaction is dominant and moments are c-axis aligned. As the temperature is reduced, however, the R sublattice anisotropy begins to gain importance and eventually dominates, causing a spin reorientation from the c-axis into the basal plane.

A second type of spin reorientation (see figure (7.5a)) is thought to occur in $Nd_2Fe_{14}B$ and $Ho_2Fe_{14}B$. There is great confusion in the literature, not only about the mechanism of this phenomenon, but also

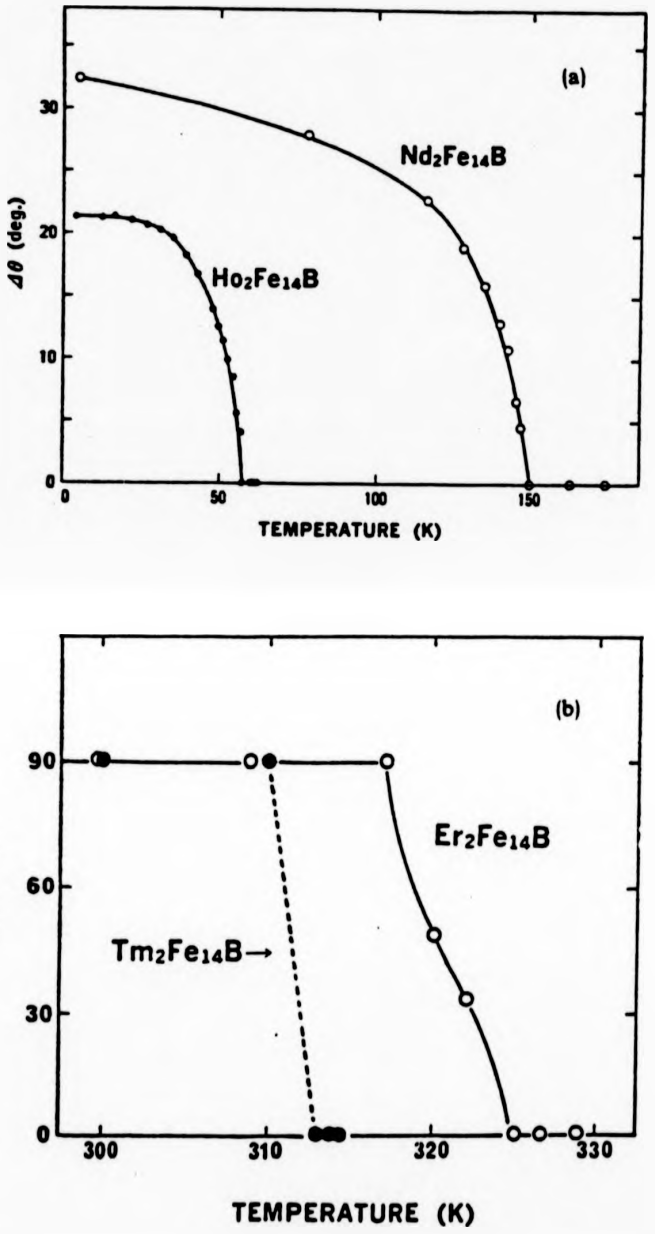


Figure (7.5) Temperature dependence of the magnetization angle from the c-axis, $\Delta\theta$, in (a) $Nd_2Fe_{14}B$ and $Ho_2Fe_{14}B$ deduced from magnetization results and (b) $Er_2Fe_{14}B$ and $Tm_2Fe_{14}B$ deduced from torque results. (Hirosawa *et al* 1986)

about its existence. It is generally agreed that, at room temperature, the moments lie along the c-axis. Whether or not the magnetization rotates away from this direction as the temperature is lowered is a matter for debate. Spin reorientations are supported by magnetization and torque measurements on single crystals (Hirosawa *et al* 1986), $^{57}$Fe Mössbauer in single crystal $Nd_2Fe_{14}B$ (Koon *et al* 1986) and differential scanning calorimetry (Fuerst *et al* 1986). The conclusion reached from magnetization measurements on $Nd_2Fe_{14}B$ is that the moments leave the c-axis at 150 K and tilt at an angle of 32$^0$ from this direction at 4.2 K, lying in a (110) plane; in $Ho_2Fe_{14}B$ the moments leave the c-axis at 60 K and lie in a (110) plane at an angle of 22$^0$ to the c-axis at 4.2 K. The results of neutron diffraction experiments, which should be the most direct and sensitive, are not all in agreement with this picture. Herbst *et al* (1985) have found no evidence for spin reorientation or canting from neutron powder diffraction experiments on $Nd_2Fe_{14}B$. The magnetic moments were found to lie along the c-axis at temperatures of 273 K and 77 K, well above and below the proposed spin reorientation temperature of 150 K. Givord *et al* (1985), on the other hand, conclude from polarized neutron diffraction, that the low values of the components of the Nd moments along the direction of magnetization at 4.2 K suggest a non-collinear structure for $Nd_2Fe_{14}B$. High field magnetization measurements on $Nd_2Fe_{14}B$ in fields of up to 25 T have been interpreted in terms of an orbital quenching and the lack of a unique value of the Nd moment (Miyajima *et al* 1986). $^{165}$Ho nmr data in $Ho_2Fe_{14}B$ are presented in section (7.4.1), which strongly indicate a quenching of the R moment at site II. A spin reorientation is supported on the basis of nuclear quadrupole measurements.

The latter type of spin reorientation, namely that said to be observed in $Nd_2Fe_{14}B$ and $Ho_2Fe_{14}B$, has been explained by different authors in contrasting ways. A non-collinear arrangement of the magnetic

moments in $Nd_2Fe_{14}B$ is thought to be a consequence of competing anisotropies at the two structurally distinct Nd sites (Givord *et al* 1984). The differing behaviour of the two sites was attributed to the dominance of the $B_2^2$ term over the $B_2^0$ for one of the sites. The fact that $B_2^2$ dominates $B_2^0$ has since been confirmed by Mössbauer spectroscopy in $Gd_2Fe_{14}B$ (Bogé *et al* 1986) although why $Nd_2Fe_{14}B$ undergoes a spin reorientation and $Pr_2Fe_{14}B$ does not (the second order Stevens' coefficient, $\alpha_J$, is the same for both Nd and Pr) is not explained. The approach followed by Boltich and Wallace (1985) is to adopt a Hamiltonian of the form

$$H = H_{cf} + H_{ex} \tag{7.1}$$

where
$$H_{cf} = B_2^0 O_2^0 + B_4^0 O_4^0 \tag{7.2}$$

and
$$H_{ex} = 2(g-1)\mu_B \underline{J}.\underline{B}_{ex} \tag{7.3}$$

Since the crystal field has been assumed to be axially symmetric it is possible, without loss of generality, to rewrite the exchange Hamiltonian as follows:

$$H_{ex} = -2(g-1)\mu_B(J_z|B|\cos\theta + J_x|B|\sin\theta) \tag{7.4}$$

where $\theta$ is the angle between the exchange field and the c-axis. Using this Hamiltonian they have calculated the angular dependence of the ground state energy for fixed values of $B_4^0/B_2^0$, and the ground state energy dependence, as a function of $B_4^0/B_2^0$, for various values of $\theta$. The ground state energy, as a function of $\theta$, which is relatively insensitive to the value of $B_4^0/B_2^0$, displays a broad minimum around $\theta = 45^0$ in $Nd_2Fe_{14}B$, whereas in $Pr_2Fe_{14}B$ no such minimum is observed. The ratio

$B_4^0/B_2^0$ was fixed in so far as the point charge model was used to determine the sign of these parameters ($B_2^0$ is negative and $B_4^0$ is positive).

In the work described here, three compounds from the $R_2Fe_{14}B$ series have been chosen for study; $Ho_2Fe_{14}B$, $Tb_2Fe_{14}B$ and $Pr_2Fe_{14}B$. Limitations were imposed by the frequency range of the nmr spectrometer but fortunately one of the heavy rare-earths chosen is reported to undergo a spin reorientation while the other remains c-axis aligned throughout its ordered temperature range. Both heavy rare-earth compositons are ferrimagnetic. The remaining sample is a light rare-earth compound and is ferromagnetic.

## 7.3 SAMPLE PREPARATION

The samples used in this study have been prepared by Sumitomo Special Metals Co. in ingot form. Ingots were prepared in two forms: magnetically aligned and non-aligned. Non-aligned ingots were simply produced by induction melts of the appropriate composition followed by annealing at 900 °C for a period of two weeks. Induction melts of the off-stoichiometric compositon (i.e. slightly rich in R) were made in an alumina crucible under an argon gas atmosphere and annealed for a suitable length of time. The ingots were then crushed to a particle size of approximately 1 mm diameter by a jaw crusher, to roughly 100 $\mu$m by a disk mill, and then pulverized in a suitable solvent to about 3 $\mu$m by a ball mill. The powder was aligned in a magnetic field of 800 kA/m and pressed at a pressure of 200 MPa. The compacts were then sintered in an argon atmosphere for one hour and cooled rapidly. The sintered samples were then given a post-sintering heat treatment for one hour at 400-1400 K and cooled rapidly (Sagawa *et al* 1984).

The mounting of the samples on the central conductor of a microwave cavity was dependent on the ingot preparation method. Non-aligned ingots were simply ground into a powder, mixed with epoxy resin and painted

onto the stainless steel central conductor. (For $Ho_2Fe_{14}B$ experimental results indicated the need to produce domain size particles and consequently grinding time was approximately two hours.) Thin rods were cut by spark erosion from the magnetically aligned ingots and glued onto the central conductor using a conducting epoxy resin; the axis of alignment was parallel to the major axis of the stainless steel rod which forms part of the central conductor (McCausland and Mackenzie 1979).

## 7.4 EXPERIMENTAL PROCEDURE & RESULTS

The experimental considerations involved in obtaining the nmr spectra from the $R_2Fe_{14}B$ compounds, where R = Ho, Tb, and Pr have been discussed in chapter 4. In each instance the priority of the experiment was to obtain spectroscopic information. Therefore, detailed information concerning relaxation or signal power is not presented but only mentioned in passing. It is sufficient to note that the spectrometer was optimized for maximum signal strength.

### 7.4.1 $Ho_2Fe_{14}B$

Initially the nmr experiments were carried out on a fairly coarse powder filed from a polycrystalline ingot. The spectrum is shown in figure (7.6). It was suspected that the signal arose from a mixture of domains and domain walls. This suspicion was confirmed by an investigation of the r.f. power dependence of the signal. Low power and high power maxima were noted; the low power maximum being attributable to domain walls. On the basis of this, the coarse polycrystlline powder was ground under acetone for an hour in a successful attempt to produce quasi-single domain particles.

The field dependence of the spectral lines, for both fine and coarse powders, was examined in various fields. Temperature dependence of the relaxation was also investigated by examining the general structural features at 1.3 K. The results obtained from the coarse powder clearly

show that the signal arises from a number of sites. Applied field causes a reduction in $a_t$ indicating a ferrimagnetic alignment of the R-Fe moments. As mentioned earlier, two maxima were observed in the signal strength as a function of r.f. excitation power indicating a mixture of domain and domain wall signal. The application of a 4 T field, which was not enough to sweep out domain walls to any significant extent, did not produce a better resolved spectrum. Indeed, due to inhomogeneous broadening, closely separated lines are actually smeared into each other (see figure (7.6)).

Given that an applied field had failed to remove the domain wall signal, single-domain particles offered some hope of being able to obtain relatively "clean" spectra. The results of nmr in finely powdered $Ho_2Fe_{14}B$ (Shah *et al* 1987) are shown in figure (7.7). Comparing the coarse and fine powder spectra, it is clear that many of the spectral lines present in the coarse powder spectrum are absent in the fine powder results. This observation, together with the fact that signal strength increases on the application of a field indicates that the fine powder spectrum is predominantly from domains as opposed to domain walls.

The results may be interpreted in the scheme developed in chapter 2, where the resonant frequency is given by:

$$\nu_{m,m-1} = a_t + (2m - 1)P_t \qquad (2.48)$$

Given that I = 7/2 for Ho, it is clear that a given pair of values for $a_t$ and $P_t$ ($a_t \gg P_t$), which can be associated with a single site, will produce a seven line spectrum centred about $a_t$ with a line separation of $2|P_t|$. The parameters $a_t$ and $P_t$ have been obtained by a least-squares fit of the observed resonant frequencies to equation (2.48). Both $a_t$ and $P_t$ may be separated into intra-ionic (dependent on $\langle J_z \rangle$ and $\langle J_z^2 \rangle$

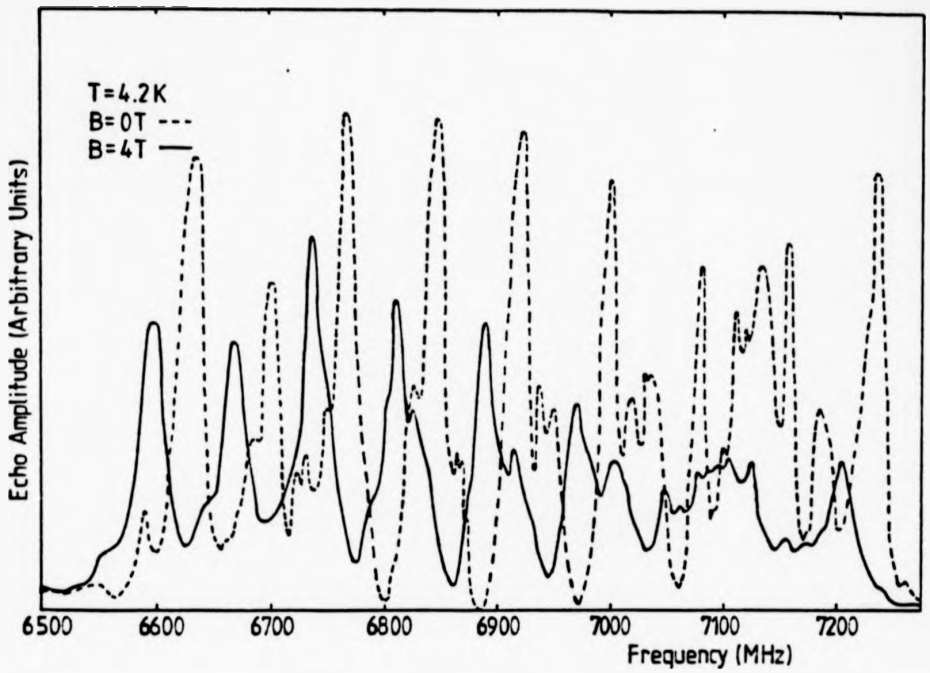


Figure (7.6) Nmr spectrum of $^{165}$Ho from coarsely ground $Ho_2Fe_{14}B$, showing field dependence at 4.2 K.

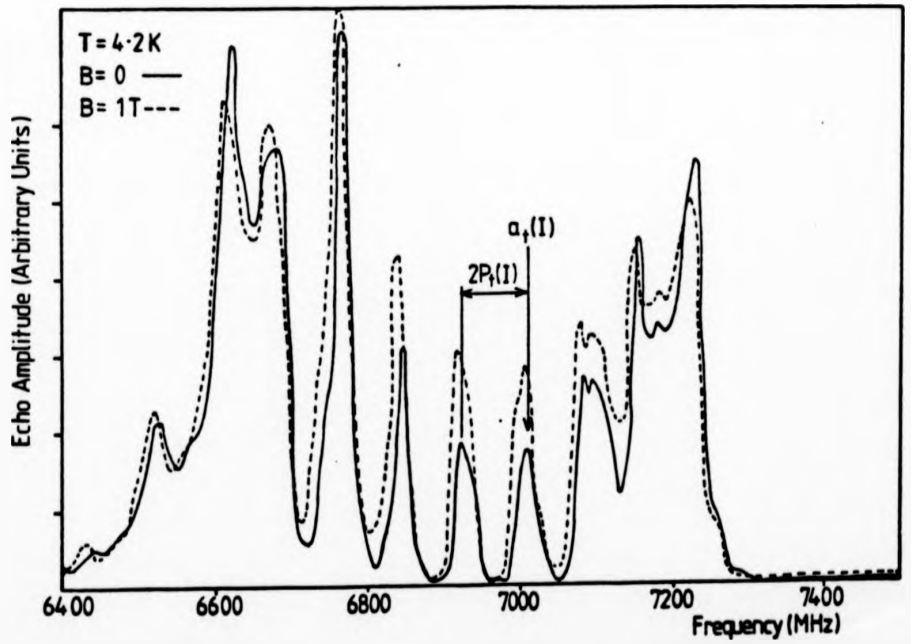


Figure (7.7) Nmr spectrum of $^{165}$Ho from finely ground $Ho_2Fe_{14}B$ at 4.2 K, showing field dependence (Shah *et al* 1987).

respectively) and extra-ionic contributions, denoted by a single prime and double prime, respectively.

Following the site labelling scheme of Bogé *et al* (1986) (site I has a negative extra-ionic electric field gradient) it has been found that when R is non-magnetic, the transferred hyperfine field (t.h.f) at both sites I and II is the same (Berthier *et al* 1986) and is due entirely to the Fe sublattice. However, when R is a heavy, magnetic rare-earth then the t.h.f. at site II is larger than at site I (Berthier *et al* 1986), although in the case of $Ho_2Fe_{14}B$ how much larger is not known. The value of the t.h.f. in $Lu_2Fe_{14}B$ is known (Berthier *et al* 1986) and can be scaled in the ratio of the outer electron hyperfine coupling constants (Campbell 1969) to obtain a value for the t.h.f. in $Ho_2Fe_{14}B$; this procedure is appropriate for site I only since the presence of a magnetic R ion increases the t.h.f. at site II. The t.h.f. at site I in $Ho_2Fe_{14}B$ is calculated to be 58 ±10 T. Using the gyromagnetic ratio, 8.9 MHz/T, for holmium, the shift of the seven-line spectrum associated with site I, due to the t.h.f. is 510 ±90 MHz. If the R ions are assumed to be in a fully polarized state $|J, J_z = \pm J\rangle$ (Sinnema *et al* 1984) the intra-ionic contributions to $a_t$ and $P_t$ ($a_0'$ and $P_0'$) can be obtained from Bleaney (1972) and previous measurements. A value for $a_t$ can therefore be calculated.(See table 7.2).

The extra-ionic contribution to $P_t$, $P''$, may be calculated, for both sites, using

$$hP'' = \frac{3eQ_nV_{zz}''}{4I(2I-1)} \qquad (2.40)$$

where e is the charge on the proton, $Q_n$ is the nuclear quadrupole moment and $V_{zz}''$ is the extra-ionic contribution to the electric field gradient (e.f.g.). The value for $V_{zz}$ at the $^{155}Gd$ nucleus

| | $*P_o'$ | $£P''$ | $2P_t$ | $*a_o'$ | $\$a''$ | $a_t$ | Width of spectrum |
|---|---|---|---|---|---|---|---|
| | calc. | +63 (3) | -15.6 (0.3) [-13.0] | 94.6 (6.6) [100] | 6497 (8) | 513 (89) | 7010 (89) | 568 [600] |
| Site I | | | | | | | |
| | meas. | - | - | 80 (5) | - | 511 | 7008 (5) | 460 |
| | calc. | +63 (3) | 23.6 (1.9) [-10.4] | 173.2 (9.8) [105] | 6497 (8) | >513 (89) | >7010 | 1039 [631] |
| Site II | | | | | | | | |
| | meas. | - | - | <80 (10) | - | <528 | <7025 | <460 |

**TABLE 7.2** Spectral parameters for $^{165}Ho$ in $Ho_2Fe_{14}B$ in MHz. Values in square parentheses calculated for spin tipping of 22° from the c-axis. Errors are given in parentheses
£ Calculated using $V''_{zz}$ derived by Bogé *et al* (1986).(see text)
$ Calculated using value for t.h.f. in $Lu_2Fe_{14}B$ (Berthier *et al*1986).
* Fully polarized free ion parameters from Bleaney (1972).

in $Gd_2Fe_{14}B$ is due to the lattice only, since $^{155}Gd$ is an S-state ion. Values for $V''_{zz}$ have been obtained from $^{155}Gd$ Mössbauer spectroscopy in single crystal $Gd_2Fe_{14}B$ (Bogé *et al* 1986). Assuming that the Sternheimer antishielding factor is approximately constant for the lanthanides, the values of $V''_{zz}$ can be used to calculate $P''_t$ using equation (2.40). The calculations are summarized in table (7.2).

The proposed spin reorientation behaviour of $Ho_2Fe_{14}B$ will lead to four magnetically inequivalent sites I, I', II and II'. It is not possible to say, *a priori*, what the consequence of a tilted magnetization will be on $a_t$ for a given site. However, if we assume that the R-ions remain almost fully polarized, as suggested by magnetization measurements, then the effects will be small.

Spin reorientation will modify $P_t$ in a way which can be readily understood. The a-b plane is a mirror plane in the point symmetry group for both R sites and therefore the c-axis is one of the principal axes, x, y and z, of the e.f.g. tensor. Similarly, the other two principal axes are [110] and $[\bar{1}10]$. Symmetry arguments are insufficient to ascribe the labels x, y and z to the principal axes. ($|V_{xx}| \leq |V_{yy}| |V_{zz}|$, where $V_{xx}$ is the second derivative of the electric potential in the direction of the x-axis). However, best fits to $^{155}Gd$ Mössbauer spectra in $Gd_2Fe_{14}B$ (Bogé *et al* 1986) have been obtained with polar angles $(\theta,\phi)$, of the direction of the c-axis aligned Gd moment with respect to the e.f.g. coordinate systems, as (0,0) and (90,90) for site I and II respectively. In $Ho_2Fe_{14}B$, allowing for a proposed spin tipping of 22° (Hirosawa *et al* 1986) from the c-axis in the (110) plane, the polar angles become (22,0) and (68,90) for sites I and II respectively. If symmetry at the site of interest is orthorhombic then (McCausland 1986)

$$V_{<J>} = \frac{V_{zz}}{2}\left|3\cos^2\theta - 1 + \eta \sin^2\theta\cos 2\phi\right| \qquad (7.5)$$

where $V_{<J>}$ is the e.f.g. along the direction of the moment, $V_{zz}$ is the e.f.g. along the principal z-axis of the e.f.g. tensor and $\eta$ is the asymmetry parameter defined by

$$\eta = \frac{V_{xx} - V_{yy}}{V_{zz}} \qquad (7.6)$$

for which values have been obtained by Bogé *et al* (1986). Equation (2) can now be used to calculate $P''$, replacing $V_{zz}$ by $V_{<J>}$.

Within a subset of sites I, $V''_{zz}$ will be the same and $V'_{zz}$ (the intra-ionic contribution to the e.f.g) will depend on $<J_z(I)>$ and $<J_z(I')>$ and similarly for sites II and II'. On these assumptions, the proposed spin-canted structure for $Ho_2Fe_{14}B$ will result in four seven-line spectra. However, if quenching effects are small, then within each subset of sites I and II, $a_t$ will differ only slightly, i.e

$$|a_t(I) - a_t(I')| \ll |a_t(I) - a_t(II)| \qquad (7.7)$$

From the nmr results (see figure 7.7) site I can be easily identified. There is excellent agreement between calculated and measured values of $a_t$, given that the extra-ionic dipolar field has been neglected and the hyperfine coupling constants have been scaled linearly. The application of a 1 T field causes a reduction of ≈8 MHz in the value of $a_t$ indicating a ferrimagnetic alignment of the R and Fe moments as expected. Agreement between calculated and measured values of $P_t$ at site I, however, is not as good; there is a difference of approximately 15 %. Second order contributions have not been considered but are only be appreciable if the energy separation of the crystal field ground state and the first excited state is small. The long relaxation times observed indicate that the energy separation between the ground state and first excited state is considerable (Waind *et al*

1983) and consequently second order effects have been neglected.

Calculations show that if the R moments are c-axis aligned then the top line of the site II spectrum should have a frequency of at least 7530 MHz ($a_t$ (II) plus half spectrum width) and $2P_t$ should be 173 MHz (see table 7.2). This is in conflict with experiment; no evidence was found for lines associated with site II in the frequency range 7250 to 7500 MHz, either at 4.2 K or at 1.3 K in zero or applied fields up to 8 T. Pulse separation time was reduced to a minimum value of 200 ns at 1.3 K. The reduction in temperature together with a reduction in the pulse separation and the application of a field are extremely favourable conditions for the detection of a signal in this material. Bearing in mind that the application of a 1 T field required the gain of the spectrometer to be reduced to avoid saturation, it may be asserted with relative confidence that there are no resonances above 7225 MHz. The frequency range 6000 to 6400 MHz has also been scanned for other resonances but none were found.

If a spin reorientation is assumed then the calculated value of $P_t$ is significantly reduced (see table 7.2) and consequently so is the expected frequency of the top resonance line. The frequency of the highest resonance is calculated to be 7325 MHz and $2P_t$ is calculated to be 105 MHz, if the moment at site II is fully polarized. The discrepancy between calculated and measured values of $P_t$(II) and $a_t$(II) can be attributed to quenching. Given the uncertainty in the calculation of the t.h.f (due to the "enhanced" t.h.f at site II) there is satisfactory agreement between the calculated and measured parameters for site II, if we assume a spin reorientation. The identification of only two sites as opposed to four can be understood if $|a_t(I) - a_t(I')|$ is so small that it cannot be resolved by nmr. In this case the corresponding spectra would overlap and appear as one. If the same were true for site II then there would only be two apparent sites instead of four.

Summarizing, then, the spectral parameters for $^{165}Ho$ in $Ho_2Fe_{14}B$ for the two crystallographically inequivalent sites have been calculated. The calculations have been performed on the following assumptions: (a) the R ions are fully polarized (Sinnema *et al* 1984), (b) the hyperfine field at the nucleus of a holmium ion occupying site II will be larger than at site I (Berthier *et al* 1986) and (c) the extra-ionic e.f.g measured in $Gd_2Fe_{14}B$ (Bogé *et al* 1986) can be used to obtain the extra-ionic contribution to the nuclear quadrupole splitting. The generally accepted spin-canted structure for $Ho_2Fe_{14}B$ leads to four magnetically inequivalent sites. We have been able to identify site I clearly and have found strong evidence that at site II the Ho moment is quenched since both $\langle J_z^2(II)\rangle$ and $\langle J_z(II)\rangle$ are reduced from the fully polarized values. The concurrent quenching of $\langle J_z^2(II)\rangle$ and $\langle J_z(II)\rangle$ rules out the possibility that the reduced frequency of site II may be due to an anomalously small t.h.f at that site. The identification of just two magnetically inequivalent sites does not, at first, favour the spin reorientation interpretation but on closer examination of the calculated nuclear quadrupole splittings, a c-axis aligned structure is found to be in conflict with our experimental results. On the basis of this a spin reorientation gives closer agreement.

7.4.2 $Tb_2Fe_{14}B$

Sample preparation was carried out in the same way as that described for $Ho_2Fe_{14}B$. A coarse powder was produced and nmr experiments were carried out at 4.2 K and 1.3 K, in zero and applied fields. The spectrometer was optimized for a sample $Tb_2Fe_{14}B$. A thorough search was carried out for a signal in the frequency range 3100 to 5000 MHz. A very small signal was noted at 4325 MHz at 1.3 K. Pulse separation was reduced to a minimum of 200 ns and the frequency range was scanned again. No increase in the signal at 4325 MHz was noted and no additional lines were found.

Doubting the Tb content of the sample, a small piece of the "$Tb_2Fe_{14}B$" was taken and arc-melted. Without subsequent annealing, it was powdered and nmr measurements were made at 4.2 K in zero field on the spectrometer which had been optimized for $TbFe_2$. Large Tb resonances were found that were indicative of a multiphase Tb-Fe compound. It was possible to closely identify one set of resonances with $TbFe_2$ (Azevedo *et al* 1985). It was thus evident that the notional $Tb_2Fe_{14}B$ did in fact contain Tb as the rare-earth and thereby eliminating one very obvious interpretation of the results, i.e. that "$Tb_2Fe_{14}B$" did not contain Tb.

Suspecting rapid relaxation, the $Tb_2Fe_{14}B$ sample was investigated by means of CW nmr. The search was limited to the frequency range 4000 - 5000 MHz. Calculations performed on the basis of a fully polarized R ion and a scaled t.h.f indicated that two lines (top line of each site) should fall in this range. No hint of a signal was detected. The lack of a signal from $Tb_2Fe_{14}B$ provides some consolation in that one can assume that the material was almost single phase i.e no $TbFe_2$ or $TbFe_3$ were present.

7.4.3 $Pr_2Fe_{14}B$

The $Pr_2Fe_{14}B$ alloy is very hard and consequently it was not possible to grind the material into powder form using a pestle and mortar. Two types of samples were investigated; a filed powder and an extended rod of dimensions 5 x 1 x 0.5 mm.

The filed powder produced a small signal at 4.2 K in zero field. The application of a 1 T field caused a decrease in the size of the signal after an initial increase. It was possible to identify one site clearly but a second site was not evident. It was thus decided to measure at 1.4 K. Again, one site was very clear (see figure (7.8)) but now a second site could also be identified. The application of a 0.5 T field enhanced the signal; the second site became much clearer.

In an effort to avoid possible strain-induced effects that may

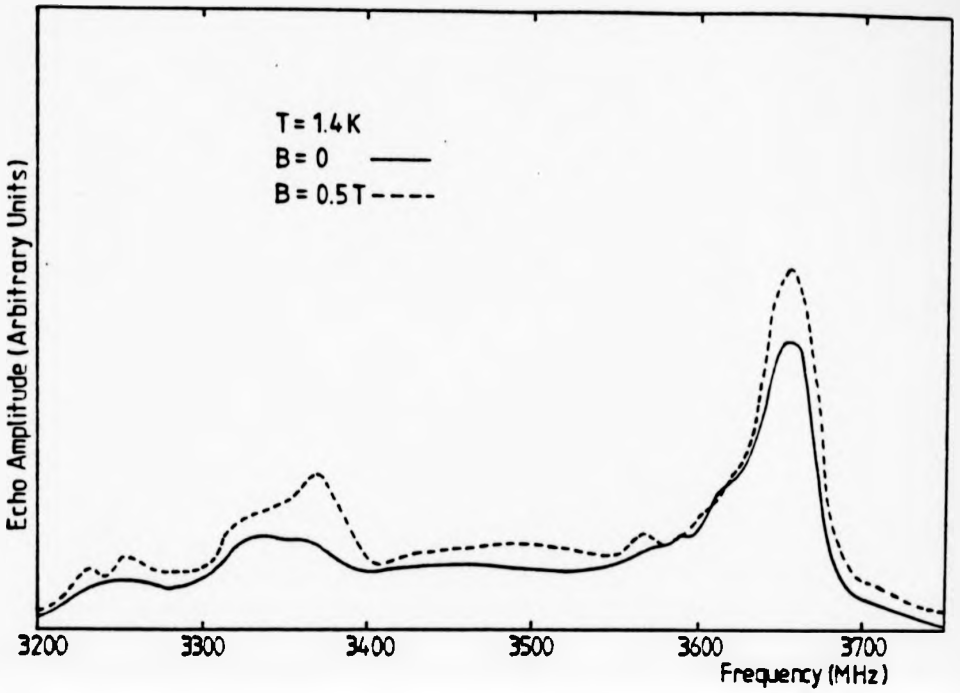


Figure (7.8) Nmr spectra of $^{141}Pr$ from a powdered sample of $Pr_2Fe_{14}B$ at 1.4 K

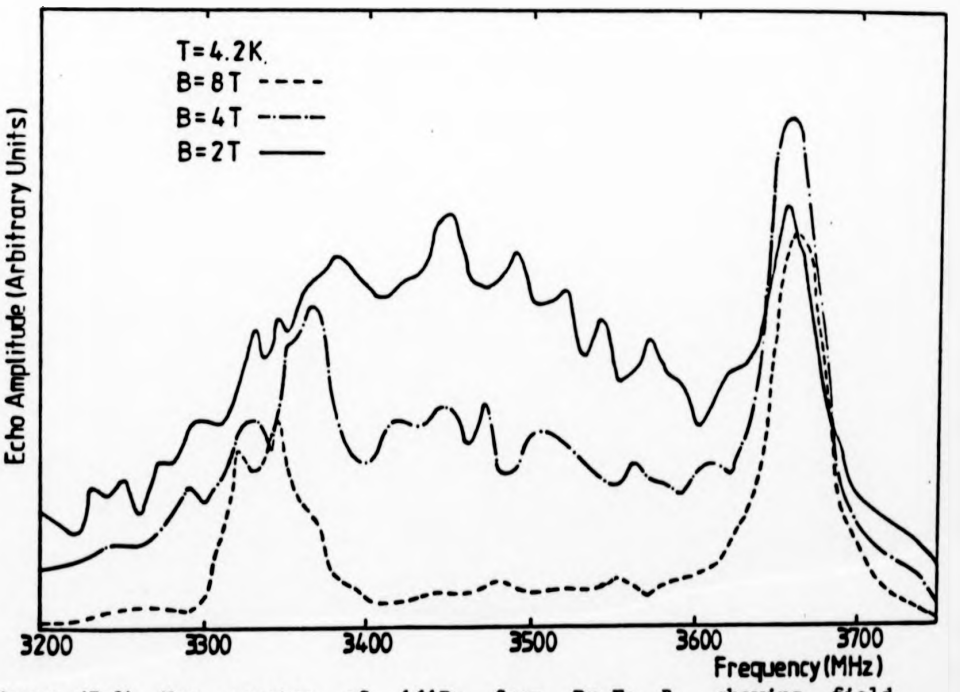


Figure (7.9) Nmr spectra of $^{141}Pr$ from $Pr_2Fe_{14}B$, showing field dependence at 4.2 K; rod-shaped sample.

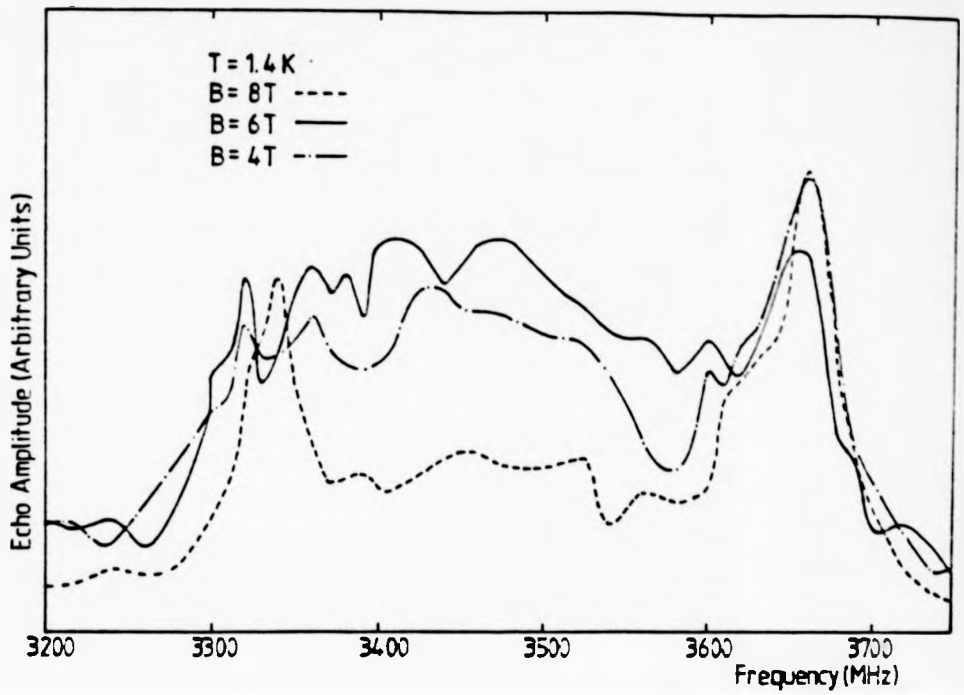


Figure (7.10) Nmr spectra of $^{141}Pr$ from $Pr_2Fe_{14}B$ showing field dependence at 1.4 K; rod-shaped sample.

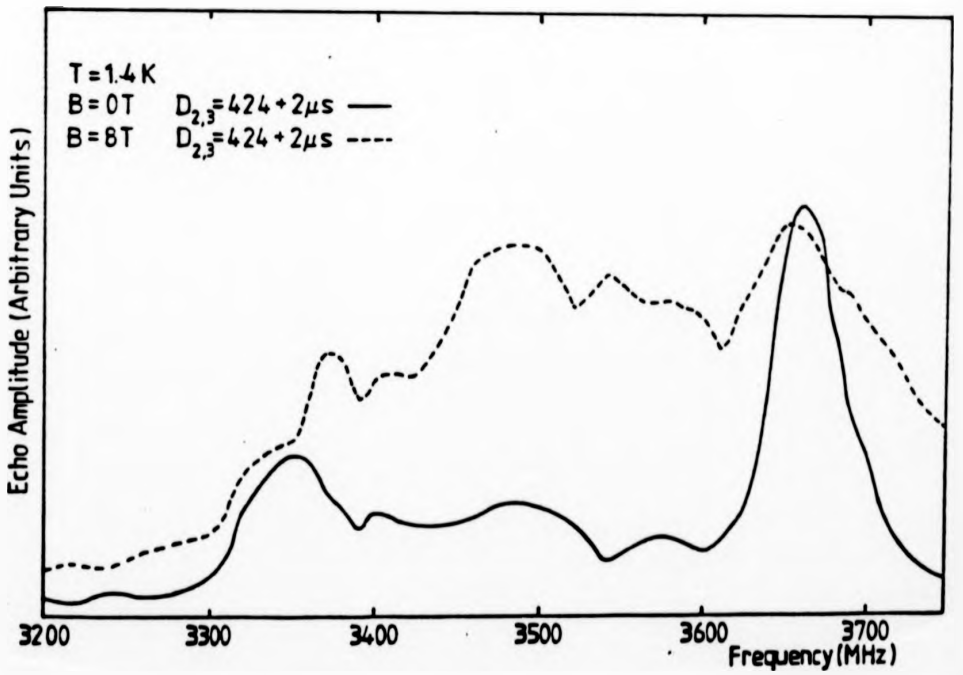


Figure (7.11) Influence of increased excitation pulse separation on the nmr spectra of $^{141}Pr$ from $Pr_2Fe_{14}B$; rod-shaped sample.

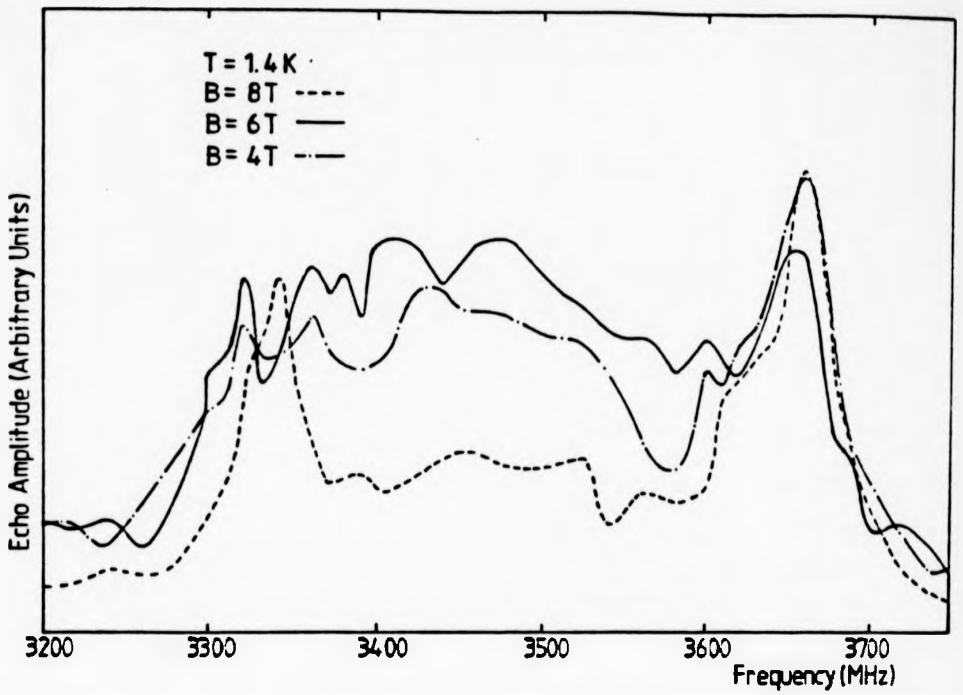


Figure (7.10) Nmr spectra of $^{141}Pr$ from $Pr_2Fe_{14}B$ showing field dependence at 1.4 K; rod-shaped sample.

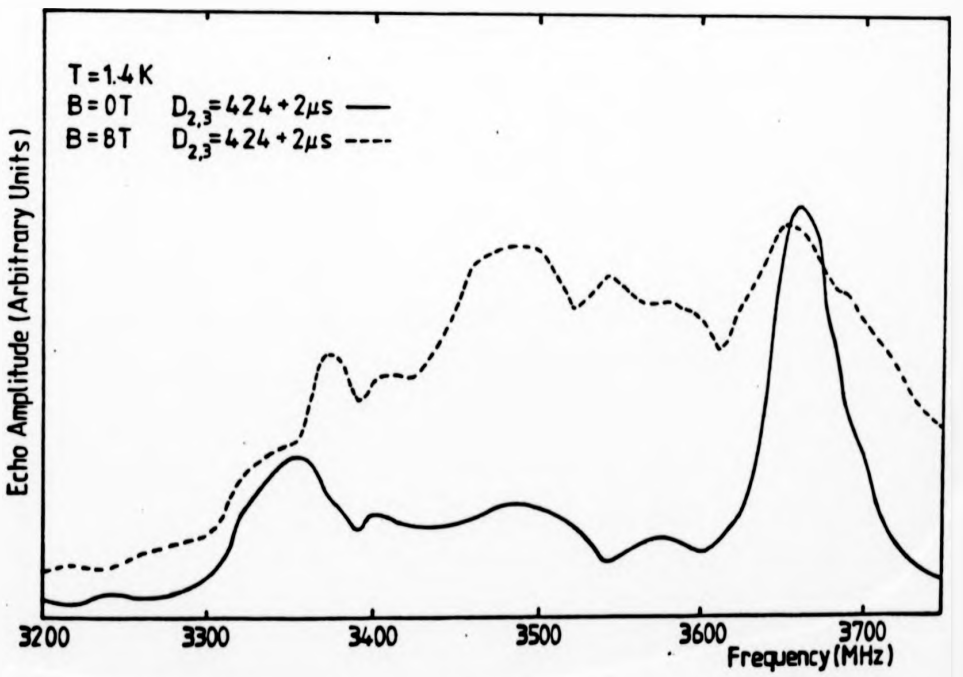


Figure (7.11) Influence of increased excitation pulse separation on the nmr spectra of $^{141}Pr$ from $Pr_2Fe_{14}B$; rod-shaped sample.

result from filing $Pr_2Fe_{14}B$ to produce a powder, a rod was spark-cut and glued to the central conductor using conducting epoxy resin. The nmr experiments were carried out in the usual way at 4.2 K, initially, and then at 1.4 K, in zero and various applied fields. The results are shown in figures (7.9) and (7.10), respectively.

Once again relaxation effects were investigated for the sole purpose of improving spectroscopic information. Even so, useful diagnostic information has been obtained from relaxation measurements. The small nuclear quadrupole moment of Pr means that quadrupole structure is not resolved in the frequency domain; a small $P_t$ and inhomogeneous broadening conspire to smear the lines into each other. The information can, nevertheless, be accessed in the time domain by measuring the oscillatory decay of the echo amplitude (Abe *et al* 1966). This was possible only for the higher frequency site. (The signal from the lower frequency site was small and therefore prevented a reliable measurement of oscillatory behaviour.)

The spectra obtained indicate two inequivalent sites, regardless of sample preparation. It is interesting to note that neither site shows a gyromagnetic shift due to an applied field of up to 8 T. (If one compares data obtained for site I from figures (7.8) and (7.9), then it is clear that an applied field of 8 T does not shift the peak by the expected gyromagnetic contribution of 104 MHz.) The resonance from the low frequency site, site II, is clearly resolved in an external field of 8 T but merges with domain wall signal as the field is reduced. The lack of a gyromagnetic shift prevents comment concerning the alignment of the Pr and Fe spins. There is little doubt, however, that alignment is ferromagnetic; calculations of line position strongly support this. Analysis of the results may be carried out as for $Ho_2Fe_{14}B$. The situation is somewhat easier in the sense that no spin reorientation behaviour is predicted.

Qualitative statements may be made about the relaxation behaviour by examination of the various spectra. General spectral features (ratio of peak signal to background) remain unaltered as a function of temperature (see figures (7.9) and (7.10)). This indicates that there is a similar temperature dependence of the relaxation at both sites. The domain wall signal increases slightly at the lower temperature but the difference is minimal.

By altering the pulse separation, spin-spin relaxation effects can be studied. An increase of 2 $\mu$s leaves the spectral features essentially unaltered, indicating long spin-spin relaxation times of similar magnitudes for both sites I and II (see figure (7.11)). Results and calculations are summarized in table (7.3).

There is a difference of approximately 4 % between the calculated and measured values of $a_t(I)$. In terms of the resolution of the spectrometer, the difference is enormous and its origin is not readily obvious. It is possible that the value of $B_n$ used in the calculation of $a_t(I)$ is too small. It is more likely, however, that the parent ion polarization term, which is totally neglected by use of the hyperfine coupling constants, is responsible. This proposition is examined in more detail in the following paragraph.

The magnetic ordering temperature of $Pr_2Fe_{14}B$ (figure (7.4)) is higher than that predicted on the basis of a simple mean-field model (Sinnema *et al* 1984). This has been explained by noting that the total coupling strength of the R and Fe moments depends on the polarizability of the 5d electrons i.e. on the 5d band width which varies as $r^{-5}$, where r is the inter-atomic separation of the R ions (Heine 1967). Polarization of the 5d electrons is predicted to be greater for LRE ions in $R_2Fe_{14}B$ than for HRE ions given that the R-R separation is somewhat larger for LRE alloys than for HRE alloys. A larger self-polarization of the parent ion can thus be expected. If the total hyperfine field at

| | $*P_o'$ | $£P''$ | $2P_t$ | $*a_o'$ | $\$a''$ | $a_t$ |
|---|---|---|---|---|---|---|
| calc. | -2.62(0.13) | +0.81(0.02) | -3.62(0.15) | 4372(40) | -578(130) | 3794(170) |
| Site I | | | | | | |
| meas. | - | - | $\|2P_t\| = 2.0$ | - | -712(50) | 3660(10) |
| calc | -2.62(0.13) | -1.22(0.13) | -7.68(0.26) | 4372(40) | <-578(130) | <3794(170) |
| Site II | | | | | | |
| meas. | - | - | - | - | -1032(50) | 3340(10) |

**TABLE 7.3** Spectral parameters for $^{141}Pr$ in $Pr_2Fe_{14}B$ in MHz. Errors are given in parentheses.
£ Calculated using $V''_{ZZ}$ derived by Bogé *et al* (1986).(see text)
$ Calculated using value for t.h.f. in $Lu_2Fe_{14}B$ (Berthier *et al* 1986).
* Fully polarized free ion parameters from Bleaney (1972).

the Pr nucleus is expressed as

$$B_{hf} = B_{4f} + B_{sp} + B_n \qquad (7.7)$$

where $B_n$ for Pr in $Pr_2Fe_{14}B$ is obtained from scaling the value of $B_n$ for Lu in $Lu_2Fe_{14}B$, $B_{sp}$ is then calculated to be -10.5 T. This will cause a reduction in the resonant frequency of 135.5 MHz, which is in excellent agreement with the observed reduction of 134 MHz.

Partial quenching of the Pr ions could, in principle, explain the discrepancy between the calculated and measured values of $a_t(I)$ but this possibility is excluded on the grounds of field-dependent behaviour (see below).

Examination of figures (7.8) and (7.9) reveals that neither site shows the full gyromagnetic shift of approximately 104 MHz in an applied field of 8 T. Even 10 % of the expected shift could easily be resolved. Particularly at the higher frequency site, this is not happening. Two obvious interpretations of this effect can be readily dismissed (see below).

In $Pr_2Fe_{14}B$ the hyperfine field is in the same direction as the applied field (if any) and therefore the unquenching of Pr ions due to an applied field will result in a positive contribution to the resonant frequency. The gyromagnetic shift resulting from an applied field, which is also positive, would therefore not be compensated by a possible unquenching of the Pr ion. Quite to the contrary, unquenching would "enhance" the gyromagnetic shift.

The relationship between the t.h.f. and the 3d moment is not obvious given the diffuse nature of the latter; an increase in the t.h.f. is not necessarily indicative of a growth of the 3d moment and vice versa. An explanation of the lack of a gyromagnetic shift based on the growth of the 3d moment in an applied field resulting in an increased t.h.f. may

be discounted on other grounds, namely that in $Lu_2Fe_{14}B$ the magnetization as a function of field saturates in a field of approximately 1 T. The magnetization in this composition is solely attributable to the iron sublattice; saturation of the magnetization in a small field indicates no further growth of the 3d moment.

The t.h.f. is mediated via polarization of the conduction electrons; it is highly unlikely that the application of an 8 T field could further polarize the conduction electrons to an extent whereby the net result is to cancel the gyromagnetic contribution due to the applied field. Following the notation used in McCausland and Mackenzie (1979), the extra-ionic hyperfine field $B''$ is given by

$$B'' = (1 + K)B_a \qquad (7.8)$$

where K is the Knight shift and is usually $<10^{-2}$. Equation (7.8) is only strictly valid for a Pauli paramagnet; it is assumed here that all other contributions to $B''$ are constant in field and can temporarily be neglected. To produce a cancellation, K is required to be -1. Together with the fact that K is almost always positive (see, for example, Slichter 1978), it seems unreasonable to invoke this mechanism as being reponsible for the lack of a gyromagnetic shift in $Pr_2Fe_{14}B$. Having eliminated the obvious mechanisms, the lack of a gyromagnetic shift in $Pr_2Fe_{14}B$ remains a puzzling feature of the results presented here.

The reduction of the measured value of $P_t$ as compared to its calculated value can be analysed in a straightforward manner. In general, $P_t$ (see chapter 2) is given by

$$P_t = P' + P'' + P_{cond} \qquad (2.45)$$

Plausible arguments have been presented which indicate that quenching of the rare-earth ions is negligible. The reduced value of $P_t$ must therefore originate in $P''$ or $P_{cond}$; $P_{cond}$ has been neglected in the

calculation of $P_t$. Although $P_{cond}$ is usually small, it is dependent on the polarization of the 5d electrons, through the 4f-5d interaction, and therefore may be significant in $Pr_2Fe_{14}B$. It is not straightforward, however, to quantify this term but a significant contribution may be expected given that the 5d electrons are well polarized.

$P''$ has been calculated using the value of $V''_{zz}$, measured by Bogé *et al* (1986), in a single crystal sample of $Gd_2Fe_{14}B$. It is unlikely, therefore, that errors associated with the calculation of $P''$ will be large.

Experiments conducted on single-crystal specimens generally yield more precise information than those conducted on polycrystalline samples. Single crystals of $Pr_2Fe_{14}B$ of the dimensions required for spin-echo nmr using the Manchester spectrometer are not available at present. Notwithstanding this limitation, an attempt to obtain accurate information was carried out on magnetically aligned, sintered powder specimens of $Pr_2Fe_{14}B$ (quasi-single crystals for the purposes of nmr).

The results are presented in figure (7.12) and, in keeping with the unwritten laws of experimental physics, provide no extra information but only raise further questions. Only the zero-field spectrum is shown; a quick examination of the spectrum in an applied field of 8 T showed it to be similar to the zero-field data.

The reasons for the "failure" of this experiment are not clear, but it is possible that the sintering and aligning process has resulted in the introduction of defects into the structures as well as grain boundaries. It is conjectured that in such a situation, an 8 T field may well be insufficient to sweep out domain walls.

## 7.5 DISCUSSION AND CONCLUSIONS

$R_2Fe_{14}B$ compounds, where R = Ho, Tb and Pr have been studied by spin-echo and CW nmr at 4.2 and 1.3 K in various fields ranging from 0 to 8 T. Signals were seen in $Ho_2Fe_{14}B$ and $Pr_2Fe_{14}B$

but no nmr signal from the rare-earth site, either spin-echo or CW, was detected in $Tb_2Fe_{14}B$. $Ho_2Fe_{14}B$ was found to have at least two magnetically inequivalent sites; one of which has a substantially quenched moment whereas the other is nearly fu lly polarized. Nuclear quadrupole measurements compare favourably with calculations based on a spin-reorientated structure at 4.2 K. The Ho and Fe sublattices are found to be ferrimagnetically coupled, as expected from magnetization and other measurements.

In $Pr_2Fe_{14}B$, two inequivalent sites have been identified. An enhanced t.h.f at site I, together with a small amount of quenching may be inferred from the data with some degree of certainty. The lack of a gyromagnetic shift in this material prevents deductions about the alignment of the component sublattices, although calculations performed on the basis of ferromagnetic alignment are in reasonable agreement with experiment and published magnetization measurements (Hirosawa *et al* 1986).

The absence of a signal from $Tb_2Fe_{14}B$ is difficult to attribute to any particular factor without further experimentation. Fast spin-spin relaxation is probably not responsible given that CW nmr failed to show a signal. The anisotropy field in $Tb_2Fe_{14}B$ is large (approximately 30 T) but is comparable to that in $Pr_2Fe_{14}B$. The nmr enhancement factor needs to be investigated to ascertain its effect on the signal; accurately known crystal field parameters are required.

Useful information could be obtained by neutron scattering and $^{57}Fe$ Mössbauer in $Ho_2Fe_{14}B$ and $Pr_2Fe_{14}B$. Mössbauer spectroscopy in zero and applied fields would yield the magnitude of the various moments, as would neutron scattering. Above all, progress in the analysis of the experiments detailed herein has been hindered by the lack of accurately determined crystal field parameters.

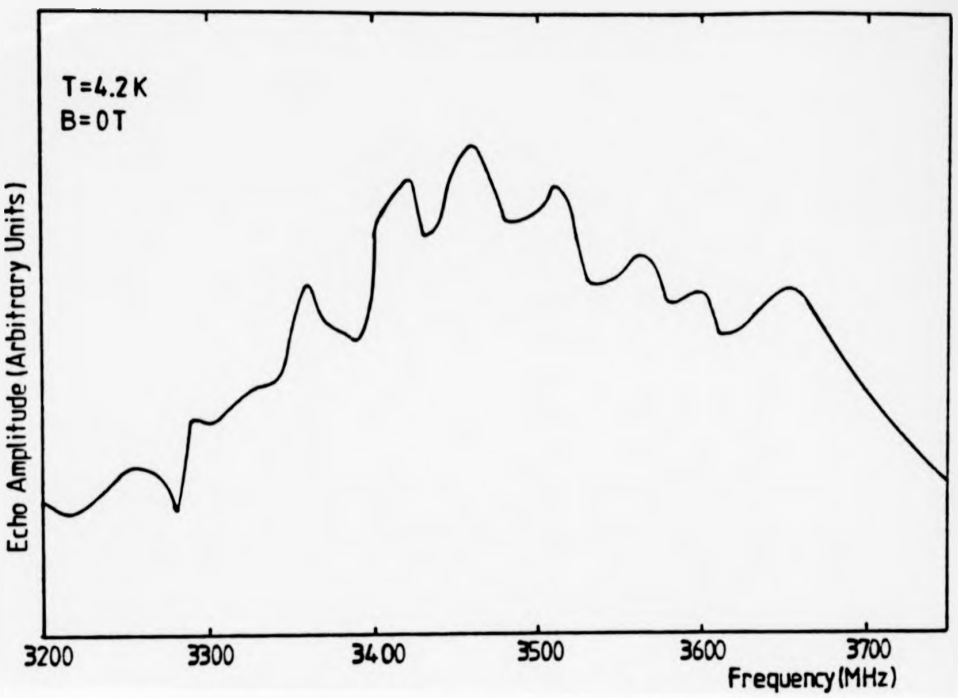


Figure (7.12) Zero-field nmr spectrum of $^{141}Pr$ from $Pr_2Fe_{14}B$; magnetically aligned, rod-shaped sample.

## REFERENCES


Abe H, Yasouka H and Hiria A (1966) *J Phys Soc Japan* 21 77

Alben R, Becker J J and Chi M C (1978) *J Appl Phys* 49 1653

Alperin H A, Cullen J R, Clarke A E and Callen E (1977) *Physica* 86-88B 767

de Azevedo W M, Mackenzie I S and Berthier Y (1985) *J Phys F* 15 L243

Begum R J, Cornelius C A, Lee E W and Samadian V (1984) *J Phys F* 14 2739

Berthier Y, Bogé M, Czjzek G, Givord D, Jeandey C, Li H S, and Oddou J L (1986) *J Mag Mag Mat* 54-57 589

Bleaney B, (1972) *Magnetic Properties of Rare Earth Metals* ed R J Elliott (London: Plenum) p383-420

Boltich E B and Wallace W E (1985) *Solid State Commun* 55 529

Bogé M, Czjzek G, Givord D, Jeandey C, Li H S and Oddou J L (1986) *J Phys F* 16 L67

Boucher B (1976) *J Phys (Paris) Letts* 37 L-345

Boucher B (1977) *IEEE Trans Mag MAG* 13 1601

Brenner A, Couch D and Williams E K (1950) *J Res Natn Bur Stand* 44 109

Buschow K H J (1984) *Handbook on the Physics and Chemistry of Rare Earths* ed K A Gischneidner and L Eyring (London: Elsevier Publications)

Butler D and Greenough R (1986) *Unpublished Results*

Cadogan J M and Coey J M D (1984) *Phys Rev B* 30 7326

Campbell I A (1969) *J Phys* C2 1338

Chappert J (1979) *J Physique Colloq* 40 C2-107

Charles S W, Popplewell J and Bates P A (1973) *J Phys F* 3 664

Chaudhry M A (1983) *Ph D Thesis* University of Manchester, Manchester U K

Chi G C and Cargill G S (1976) *Mater Sci Eng* 23 155

Chudnovsky M and Serota R A (1983) *J Phys C* 16 4181

Clarke A and Belson H (1972) *AIP Conference Proceedings* 5 1498

Cochrane R W, Harris R and Plischke M (1974) *J Non-Cryst Solids* 15 239

Cochrane R W, Harris R, Plischke M, Zobin D and Zuckermann M J (1975) *J Phys F* 5 763

Croat J J, Herbst J F, Lee R W and Pinkerton F E (1984) *Appl Phys Letts* 55 2078

Chappert J, Coey J M D, Liénard A and Rebouillat (1981) *J Phys F* 11 2727

Czjzek G, Fink J, Gotz F, Schmidt M, Coey J M D, Rebouillat J P and Lienard A (1981) *Phys Rev B* 23 2513

Duwez P, Willens R H and Klement W (1960) *J Appl Phys* 31 1136

Dzyloshinkii I (1958) *J Chem Solid* 4 241

Edmonds A R (1957) *Angular Momentum in Quantum Mechanics* (Princetown: Princetown University Press)

Edwards S F and Anderson P W (1975) *J Phys F* 5 965

Egami T, Flanders P J and Graham C D (1975) *AIP Conf Proc* 24 697

Fert A and Campbell I A (1978) *J Phys F* 8 L57

Freeman A J (1972) *Magnetic Properties of Rare Earth Metals* ed. R J Elliott (London: Plenum Press)

Freeman A J and Watson R E (1965) *Magnetism vol IIA* ed. G T Rado and H Suhl (London: Academic Press)

Fuerst C D, Herbst J F and Alson E A (1986) *J Mag Mag Mat* 54-57 567

Fujimori H, Yoshimoto H and Masumoto T (1981) *J Appl Phys* 52 1893

Fujimori H, Kikuchi M, Obi Y and Masumoto T (1975) *Japan J Appl Phys* 14 1077

de Gennes P G (1962) *J Phys Radium* 23 1962

Geohagen J A, Koon N C and Das B N (1982) *J Appl Phys* 53 7816

Givord D, Li H S, Moreau J M (1984) *Solid State Commun* 50 497

Givord D, Li H S and Tasset F (1985) *J Appl Phys* 57 4100

Goebel and Dormann (1979) *J Mag Mag Mat* 13 219

Greenwood N N and Gibb T C (1971) *Mössbauer Spectroscopy* (London: Chapman and Hall Ltd)

Gubanov I A (1960) *Fiz Tver Tel* 2 502

Hadjipanayis G C, Hazelton R C and Lawless K R (1982) *Appl Phys Letts* 43 797

Harris R, Plischke M and Zuckerman M J (1973) *Phys Rev Lett* 31 160

Hauser J J (1975) *Phys Rev B* 125 160

Heine V (1967) *Phys Rev* 153 673

Herbst J F, Croat J J, Pinkerton F E and Yelon W B (1984) *Phys Rev B* 29 4176

Herbst J F, Croat J J, Yelon W B (1985) *J Appl Phys* 57 4086

Hirosawa S, Matsuura Y, Yamamoto H, Fujimura S and Sagawa M (1986) *J Appl Phys* 59 873

Czjzek G, Fink J, Gotz F, Schmidt M, Coey J M D, Rebouillat J P and Lienard A (1981) *Phys Rev B* 23 2513

Duwez P, Willens R H and Klement W (1960) *J Appl Phys* 31 1136

Dzyloshinkii I (1958) *J Chem Solid* 4 241

Edmonds A R (1957) *Angular Momentum in Quantum Mechanics* (Princetown: Princetown University Press)

Edwards S F and Anderson P W (1975) *J Phys F* 5 965

Egami T, Flanders P J and Graham C D (1975) *AIP Conf Proc* 24 697

Fert A and Campbell I A (1978) *J Phys F* 8 L57

Freeman A J (1972) *Magnetic Properties of Rare Earth Metals* ed. R J Elliott (London: Plenum Press)

Freeman A J and Watson R E (1965) *Magnetism vol IIA* ed. G T Rado and H Suhl (London: Academic Press)

Fuerst C D, Herbst J F and Alson E A (1986) *J Mag Mag Mat* 54-57 567

Fujimori H, Yoshimoto H and Masumoto T (1981) *J Appl Phys* 52 1893

Fujimori H, Kikuchi M, Obi Y and Masumoto T (1975) *Japan J Appl Phys* 14 1077

de Gennes P G (1962) *J Phys Radium* 23 1962

Geohagen J A, Koon N C and Das B N (1982) *J Appl Phys* 53 7816

Givord D, Li H S, Moreau J M (1984) *Solid State Commun* 50 497

Givord D, Li H S and Tasset F (1985) *J Appl Phys* 57 4100

Goebel and Dormann (1979) *J Mag Mag Mat* 13 219

Greenwood N N and Gibb T C (1971) *Mössbauer Spectroscopy* (London: Chapman and Hall Ltd)

Gubanov I A (1960) *Fiz Tver Tel* 2 502

Hadjipanayis G C, Hazelton R C and Lawless K R (1982) *Appl Phys Letts* 43 797

Harris R, Plischke M and Zuckerman M J (1973) *Phys Rev Lett* 31 160

Hauser J J (1975) *Phys Rev B* 125 160

Heine V (1967) *Phys Rev* 153 673

Herbst J F, Croat J J, Pinkerton F E and Yelon W B (1984) *Phys Rev B* 29 4176

Herbst J F, Croat J J, Yelon W B (1985) *J Appl Phys* 57 4086

Hirosawa S, Matsuura Y, Yamamoto H, Fujimura S and Sagawa M (1986) *J Appl Phys* 59 873

Hutchings M T (1964) *Solid State Physics* 16 ed. F Seitz (London: Academic Press)

Imry Y and Ma S (1975) *Phys Rev Lett* 35 1399

Jeandey C, Czizek G and Tomala K (1986) *J Mag Mag Mat* 54-57 257

Kasuya T (1956) *Prog Theor Phys (Kyoto)* 16 45

Klement W, Willens R H and Duwez P (1960) *Nature* 187 869

Köbler U, Kinzel W and Zinn W (1981) *J Mag Mag Mat* 25 124

Koon N C and Das B N (1981) *Appl Phys Letts* 39 840

Koon N C and Das B N (1984) *J Appl Phys* 55 2063

Koon N C, Abe M, Callen E, Das B N, Liou S H, Martinez A and Segnan R (1986) *J Mag Mag Mat* 54-57 593

Koon N C, Schindler A, Carter F (1971) *Phys Letts* 37A 413

Kramer J (1934) *Annln Phys* 19 37

Kramer J (1937) *Z Phys* 106 675

Lee E W *et al* (1987) To be published

Liebermann H H and Graham C D Jr. (1976) *IEEE Trans Magn MAG* 12 929

Luborsky F E, Becker J J and McCary R O (1975) *IEEE Trans Magn* MAG-11 1644

Luborsky F E (1983) *Amorphous Metallic Alloys*: London: Butterworths

Mackenzie I S (1969) *PhD Thesis* University of Manchester, Manchester U K

Mader S and Norwick A S (1965) *Appl Phys Lett* 7 57

Margulies S and Erhman J R (1961) *Nuc Inst Methods* 12 131

Mattis D C (1965) *Theory of Magnetism* (New York: Harper and Row)

McCausland M A H (1986) *Private communication*

McCausland M A H and Mackenzie I S (1979) *Adv Phys* 28 305

McMorrow D F (1987) *PhD Thesis* University of Manchester, Manchester U K

Miyajima H, Otani Y, Chikazumi S, Hirosawa S and Sagawa M (1986) *J Mag Mag Mat* 54-57 587

Mohammed K A and Lanchester P C (1986) *J Mag Mag Mat* 60 275

Moorjani K and Coey J M D (1984) *Magnetic Glasses* (Amsterdam: Elsevier Publications)

Moriya T (1960) *Phys Rev* 91 120

Panissod P, Aliaga-Guerra D, Amamou A, Durand J, Johnson W L, Carter W L and Poon S J (1980) *Phys Rev Lett* 44 1465

Pelcovits R A, Pytte E and Rudnick J (1978) *Phys Rev Lett.* 40 476

Poon J J and Durand J (1977) *Solid State Commun* 21 793

Prakash Om (1985) *Unpublished Results*

Rainford B D, Samadian V, Begum R J, Lee E W and Burke S K (1982) *J Appl Phys* 53 7725

Rhyne J J, Pickart S J, and Alperin H A (1974) *AIP Conf Proc* 18 563 and references therein.

Rudermann M A and Kittel C (1954) *Phys Rev* 96 99

Sagawa M, Fujimura S, Togawa M, Yamamoto H and Matsurra Y (1984) *J Appl Phys* 55, 2083

Shah N J, Prakash Om, Ross J W and Mohammed K A (1986) *J Mag Mag Mat* 54-57 235

Shah N J, Ross J W and Yamamoto H (1987) To be published *J Phys F*

Simpson A W and Brambley D R (1971) *Phys Stat Sol (b)* 43 291

Simpson A W (1974) *Wiss Z Tech Univ Dresden 23 1027*

Sinnema S, Radwanski R J, Franse J J M, de Mooij D B and Buschow K H J (1984) *J Mag Mag Mat* 44 333

Slichter C P (1978) *Priniples of Magnetic Resonance* (New York:Springer Verlag)

Smart J S (1966) *Effective Field Theories of Magnetism* (London: W B Saunders Co)

Smith F W (1978) *Solid State Commun* 25 341

Soukoulis C M (1978) *Phys Rev B* 18 3757

Stevens K W H (1952) *Proc Phys Soc (London)* A65 209

Stevens J G and Stevens V E (1976) *Mössbauer Effect Data Index* (London: Plenum Press)

Toulouse G (1977) *Commun Phys* 2 115

Wagg A R (1974) *PhD Thesis* University of Manchester, Manchester U K

Waind P R (1983) *PhD Thesis* University of Manchester, Manchester U K

Waind P R, Mackenzie I S and McCausland M A H (1983) *J Phys F* 13 1041

Yosida K (1957) *Phys Rev* 106 893